UNIVERSITÀ DEGLI STUDI DI PADOVA

DIPARTIMENTO DI INGEGNERIA INDUSTRIALE

CORSO DI LAUREA MAGISTRALE IN INGEGNERIA CHIMICA E DEI PROCESSI INDUSTRIALI

Tesi di Laurea Magistrale in
Ingegneria Chimica e dei Processi Industriali

EXPERIMENTAL ANALYSIS AND MODELLING OF A DRY GRANULATION PROCESS

Relatore: Prof. Andrea Claudio Santomaso
Correlatore: Prof. Lian X. Liu

Laureando: Giovanni Bizzotto

ANNO ACCADEMICO 2019 – 2020

Virtus et fortuna optimi
sodales somniorum sunt

Abstract

One of the most widespread pharmaceutical tablets manufacturing process is the dry granulation using roll compaction followed by milling, which is particularly suitable to treat the moisture and heat sensitive drugs. The granule size distribution represents the main parameter to analyse and control, and it is affected by the material properties of powders and the operating conditions, which include the roll compaction conditions and the milling ones. Accurate prediction of the granule size distribution from milling of ribbons with different properties is crucial for ensuring tablet quality in the final compaction stage. In this study, ribbons with precisely controlled porosity, thickness and moisture content were produced in a die, through the compression of the excipient MCC Avicel® PH-102. The ribbons were, then, milled at different impeller speeds with a conical mill and the granule size distributions were measured by QicPic SYMPATEC. A population balance model (PBM) with a newly developed breakage function was implemented to model the granule size reduction. Experimental results showed that the granule size distribution was bi-modal and the fines produced increased with the impeller speed, the levels of porosity and with dryer raw powder. For ribbons with the same porosity value, thicker ones led to more fines in the milling product, which may be caused by the increased chance of attrition/shear in the mill. The PBM developed can successfully predict the effect of ribbon porosity and impeller speed on the granule size reduction. In conclusion, the targets of the project were achieved, and the excellent results can represent a good base on which more deeper studies can be performed.

Riassunto

Uno dei processi maggiormente impiegati nella produzione di compresse farmaceutiche è la granulazione a secco mediante compattazione e successiva macinazione. Tale processo è particolarmente indicato per il trattamento dei principi attivi sensibili all'umidità ed al calore. La distribuzione granulometrica rappresenta il principale parametro da monitorare ed analizzare ed è influenzata dalle proprietà delle polveri lavorate e dalle condizioni operative impostate, relative ai processi di compattazione e di macinazione. La previsione della distribuzione granulometrica delle particelle derivanti dalla macinazione di nastri con proprietà differenti è fondamentale per garantire la produzione di pastiglie di qualità nel processo finale di compressione dei granuli stessi. Nel presente studio, dei nastri con porosità, spessore e contenuto d'acqua accuratamente controllati sono stati prodotti mediante la compressione uniassiale, in uno stampo, della polvere dell'eccipiente MCC Avicel® PH-102. I nastri sono stati, quindi, macinati in un mulino conico impostando differenti velocità della girante e le distribuzioni granulometriche sono state misurate mediante l'uso di un QicPic SYMPATEC. Un bilancio di popolazione (PBM) è stato successivamente implementato per modellare la distribuzione granulometrica mediante l'ausilio di una funzione di rottura delle particelle recentemente sviluppata. I risultati sperimentali evidenziano come la distribuzione granulometrica sia bimodale e la quantità di fini prodotti sia maggiore all'aumentare della porosità dei nastri, della velocità della girante del mulino ed al diminuire del contenuto d'acqua della polvere iniziale. Inoltre, i nastri con lo stesso livello di porosità ma con uno spessore maggiore presentano una produzione di fini superiore nei campioni di granuli analizzati. Ciò può essere dovuto ad un incremento dell'impatto dei fenomeni di taglio ed attrito nel processo di macinazione dei ribbon. Nella fase finale di modellazione, il bilancio di popolazione sviluppato è stato in grado di predire con successo gli effetti della porosità dei nastri e della velocità della girante sul processo di macinazione. In sintesi, gli obiettivi del progetto sono stati raggiunti e gli ottimi risultati possono rappresentare una buona base sulla quale condurre ulteriori approfondimenti.

Table of Contents

Introduction 1

Chapter 1. **Literature Review and Background** 3

1.1 Pharmaceutical Market 3
1.2 Pharmaceutical Tablets 4
1.3 Manufacturing Processes for Pharmaceutical Tablets 6
1.3.1 Direct Compression 7
1.3.2 Wet Granulation 8
1.3.3 Dry Granulation 9
1.4 Dry Granulation Using Roll Compaction 10
1.4.1 Main Features and Problems of Dry Granulation 13
1.4.2 Moisture Effects 17
1.5 Modelling 20
1.5.1 Discrete Element Method 21
1.5.2 Population Balance Model 24

Chapter 2. **Materials and Methods** 29

2.1 Excipient: Microcrystalline Cellulose 29
2.2 Equipment 32
2.2.1 Instron 1175 and Die Compactor 33
2.2.2 Conical Mill 34
2.2.3 QicPic Sympatec 35
2.2.4 Humidity Chamber 38
2.2.5 Moisture Analyser 39
2.3 Structure of the Experiments 40
2.4 Methodology of Different Experiments 41
2.4.1 Ribbons Production 41
2.4.2 Milling 45
2.4.3 Particle Size Distribution (PSD) 47

Chapter 3. **Experimental Results** 49

3.1 Ribbon Characterization 49

3.1.1 Statistical Analysis 54

3.2 Kinetic of Milling 58

3.3 PSD from QicPic 62

3.3.1 Final PSD 62

3.3.2 Time Comparisons 64

3.4 Effect of the Operating Conditions 65

3.4.1 Porosity 65

3.4.2 Impeller Speed 67

3.4.3 Thickness 69

3.4.4 Moisture Content 73

3.5 Determination of Fines 76

3.6 Shape Analysis 79

3.7 Experimental Results Considerations 82

Chapter 4. **Modelling** 85

4.1 Purpose 85

4.2 Structure of the Model 86

4.3 Method to Determine the Model Parameters 88

4.4 Model Results 91

4.4.1 Model for the Prediction of the Final PSD 91

4.4.2 Model for the Time Prediction 95

4.5 Final Model 97

4.5.1 Influence of the Operating Conditions of the PBM Parameters 97

4.5.2 Prediction at Different Conditions 101

4.6 Validation of the Model 103

Conclusions 107

List of Figures 109

List of Tables 113

Symbols 114

Acknowledgments 119

Appendix 121

Appendix 1: Ribbons Characterization and Fines 121

Appendix 2: PSD of the Experiments 127

Appendix 3: Matlab Code of the PBM Model 133

References 137

Introduction

A pharmaceutical tablet is a solid dosage form of a drug, which ensures the oral administration of a medicament. It is the preferred and most common dosage form of a drug, and it covers roughly the 70% of the ethical pharmaceuticals dispensed in the world, thanks to the main advantages that it offers, especially the easy and effective administration of a drug by the patient. The three industrial manufacturing processes of the pharmaceutical tablets are the direct compression of the powder, the wet granulation and the dry granulation. In particular, the latter is the main one used to process the heat and moisture sensitive materials, as it does not affect the chemical-physical properties of the drugs. This process is characterized mainly by four steps. First, the blending of all the components of the final tablet is performed. They include primarily the excipient and the Active Pharmaceutical Ingredients (APIs). Then, flat structure called ribbons are produced by compression between two rotating rolls, in order to compact the powder into solid intermediate tablets. These ribbons are, then, grinded into a mill, in order to produce the granules with suitable sizes, which are fed to the following compression and form the final pharmaceutical tablets.

The main target of the dry granulation is the enlargement of the sizes of the raw powders and so, the improvement of the compactability of the material to produce high quality tablets. A deep study of the different steps of the process is necessary in order to achieve a better understanding of the best design and operating conditions to set. Many studies have been performed on the dry granulation, in order to deepen the main features of the process. The most important problem to overcome is characterized by the Particle Size Distribution (PSD) of the granules, which must be narrow and suitable for the compression into tablets. The fines represent the main issue concerning the achievement of a good PSD, as they must be minimized in order to improve the compaction and the quality of the final product. Many studies in literature deepen the negative effects of the fines and the conditions that contribute or prevent their production. The generation of fines depends on the properties of the material processed, which changes for different powders, the design of the process, which includes the kind of mill selected, and the operating conditions set in the process, which goes from the roll compaction speed and force to the impeller speed set in the mill.

By considering the literature results already achieved, this work analyses the effects of different operating conditions of a dry granulation process, in order to get a better understanding of a process of dry granulation. The project will focus on the influences that the level of porosity of the ribbons produced have on the determination of the PSD of the granules after the milling step and on the number of fines produced. This kind of analysis

will be performed thanks to a process of production of ribbons by a batch uniaxial compression, which is different from the usual step of the dry granulation and from the other literature studies. Nevertheless, it ensures a low variability in the porosity among the ribbons and allows to study its effect with a high precision. Besides, the impeller speed set in the mill selected will be studied to understand the influence on the PSD and the generation of fines. The last part of the experimental phase will concern the analysis of the environmental relative humidity of the warehouse of the powder, in order to get possible effects in the process. This kind of analysis aims to understand one underestimated factor, but that can affect the quality of the production. Indeed, its management can lead to an improvement of the process efficiency. The last part of the work will concern the modelling of the milling step through the implementation of a PBM with a newly developed breakage function. The purpose is the design of the model and the research of its parameters and their dependences on the operating conditions, in order to predict the granule size reduction of the ribbons. The material chosen to perform all the experiments is the Microcrystalline Cellulose Avicel® PH-102 (MCC 102), which represents one of the most widely used excipient to produce pharmaceutical tablets, covering mostly the function of a binder.

Therefore, the main targets of this work can be outlined and summarized in the following points:

- Deep experimental study of the effects of different process parameters on the PSD of the granules used to be compressed into the final pharmaceutical tablets;
- Search of the best operating conditions in order to minimize the undesired generation of fines and to improve the PSD of the milled granules;
- Design of a model, based on the PBM, suitable to predict the PSD of the milled granules as function of the different operating conditions deepened in the experimental phase.

The structure of the thesis is divided into four main chapters. The first one regards a deep analysis of the results already achieved in literature, starting from an overview of the pharmaceutical market, then, the manufacturing of tablets and the models' achievements will be rigorously studied. In chapter 2 the methods followed in the different experimental procedure will be explained in depth, in addition to the description of the main equipment used. The chapter 3 reports all the experimental results achieved in this work, focusing on the main outcomes and the influences of the operating conditions on the process. Lastly, in chapter 4 the model design, the search of its parameters and the validation of the model itself, through experimental data, are performed and deeply descripted.

Chapter 1

Literature Review and Background

This chapter aims to present an overview of the main features involved in this work, through a critical analysis of the state of art and the literature. The main purpose is the development of a deep background, useful for a better comprehension of the topics studied in this thesis and for the explanation of different issues arose during the project. Therefore, starting with the description of the pharmaceutical tablets, then, their manufacturing processes will be discussed, focusing on the dry granulation through roller compaction, which represents the specific process studied in this work.

1.1 Pharmaceutical Market

The pharmaceutical manufacturing industry represents one of the largest and most profitable economic sectors in the world. It reaches revenues greater than 1,2 trillion of US dollars in 2019, with an average growth in the last five years (period 2014-2019) equal to 1,6%, involving more than 16.000 businesses and 3 million of employers in the world. The development of the emerging countries and the growing aging of the population are leading the increase of the customer base of this market, fostering its expansion and growth.[1-W] The R&D represents the engine of this sector and the expense for the research amounts to more than 150 billion of US dollars per year. As proof of this propensity for the research, 5 of the 11 leading R&D companies in the world belong to the pharmaceutical sector, in 2016. Besides, the annual spending in the R&D is 5 times greater than the ones of aerospace, defence or chemical industry, while it is 1.5 greater than the growing software and computer industry. Figure 1.1 underlines this predominance, showing how much considerable this division is in the overall sector, especially compared to the other sectors. Besides, according to 2016 EU Industrial R&D Investment Scoreboard, the Pharmaceutical and Biotechnology sector covers the 19,1% of the total business R&D worldwide investments and expenditure. In 2014, the gross value added of the pharmaceutical industry covered the 3,8% of the worldwide manufacturing one.[1]

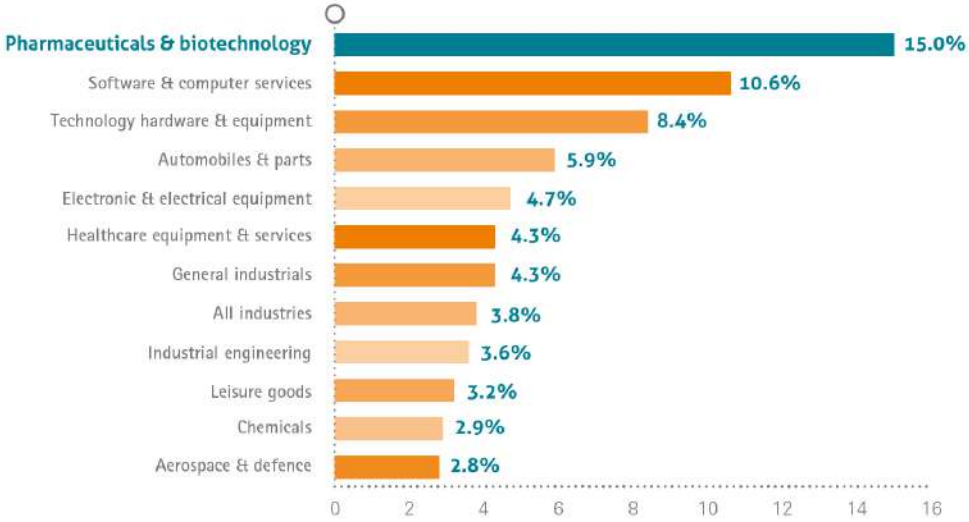

Figure 1.1. *Ranking of industrial sectors distinguished by the overall R&D contribute as percentage of the net sales in 2016* [4]

European Union market represents the 18% of the global one and its leading country is Italy, which produced goods for 31.2 billion of US dollars in the pharmaceutical manufacturing, in 2018. Even during the last years, strongly affected by the economic crisis, the pharmaceutical industry has been witnessed of an increase in contrast with the drop of the Italian Gross Domestic Product GDP. This countercurrent trend was highlighted by the 10% of growth of the sector in the interval 2010-2015, while the national GDP was falling of 3% during the same period. This underlines the great importance of this manufacturing for the Italian economy and the prosperity and flourishing opportunity that this sector can offer.[2] Besides, it has proved its considerable role for the high qualified employment. Indeed, the quality of the human resources is pointed out by the percentage of graduated employees, which reaches the value of 90% of the total, much greater than the average of the overall manufacturing percentage, which amounts to almost 60% of total. This represents the main competitive advantage of the Italian pharmaceutical industry and an excellent incentive for the investments which have increased more and more in the last years, indicating a growth of 22% in the period 2012-2017.[2]

1.2 Pharmaceutical Tablets

A pharmaceutical tablet is an oral solid dosage form and it has become the most popular way of dosage of drugs, since last century. It is a compacted solid which can be ingested to release the contained drug along the gastrointestinal tract. Nowadays, tablets represent roughly the 70% of all ethical pharmaceuticals dispensed in the world. This status has been gained thanks to the many advantages offered by this kind of dosage form. First, tablets' success is

founded on the simplicity and convenience of production, delivery and storage. Besides, an accurate stability and homogeneity of the product can be ensured for most of the drugs used. Indeed, tablets represent an excellent product, able to offer to the costumer a great dose precision and stability of content and a comfortable and quick dosage form. They can be easily handled and taken by the patients and their lighter and more compact shape allows them a simple shipment and package. Tablets may be different in shape, size, thickness and dissolution characteristic. Some of the main products are compressed, film coated, effervescent and dispersible tablets. Moreover, tablets' manufacturing costs are the lowest ones among all the oral dosage forms and the production is suitable for large scale. Unfortunately, they are characterized by some disadvantages, which consists mainly in the difficulty of swallow that some patients can have. Besides, some drugs could not be suitable for this kind of formulation, since they could have a poor wetting property or made by powders with a low flowability.[3]

Tablets are divided in two main groups, the molded tablets and the compressed ones. The first type is prepared by a molding process where the moisten material is forced into moulds of different shapes. Then the product is pulled out and dried to get the final tablets. The molded tablets represent a small part of all the tablets produced, which are manufactured by compression processes. Indeed, these are widely used, since the final properties can usually satisfy all the physical requirements in terms of hardness, friability, size and weight homogeneity.[2-W] There are three main processes used for this kind of tablets:

- Direct compression;
- Wet granulation;
- Dry granulation.

These processes are used to produce tablets different in the final properties and targets and they involve different steps, as blending, compaction, milling, mixing and tabletting in the manufacturing path of the ultimate product. The physicochemical characteristics of each drug and excipient used require a different way of manufacturing, and the choice represents a critical factor to achieve a good quality and effective product.[4].

Usually the drug is not compressed alone, since it is a valuable product, which performs its medical function at small quantities and often it has not suitable physical properties to produce a handleable tablet, so it is used along with an excipient, which can have many properties, depending on the final application of the medicine. The study of the compatibility of the mixture drug-excipient is fundamental to develop a valid product, able to perform its function in the most effective way. Therefore, the choice of different excipients covers an

important role in the design of the tablet. The excipient is defined as an ingredient in the formulation, active or inactive, which is not the drug and it is used to prepare a drug substance into a final solid dosage form.[5] Their main task is the variation the physicochemical properties of the drug. Some of the most important functions the excipients can hold are the dispersion, the absorption, the dilution and the binding. It is clear how the amount and the typology of excipient selected are strongly dependent on the final dosage forms, since they determine the primary features of the tablet.[5] The excipient studied in this work has typically the function of a binder, so it allows the formation of granules and preserve the integrity of the final product.

1.3 Manufacturing Processes for Pharmaceutical Tablets

As mentioned above, the processes of production of tablets are divided into three well known methods: direct compression, wet granulation and dry granulation. While the first one is conceptually different from the other two processes, these ones have a common conceptual basis, which consists in the phenomena of the granulation.[6] In the pharmaceutical industry, granulation consists in a process where the raw powder particles are forced to adhere each other to produce larger forms called granules. Granules are supported by the bonds between the primary particles. These bonds can be created by compression (dry granulation) or through the help of binding agents (wet granulation). These granules have particle size in the range of 0.2 - 4.0 mm in the pharmaceutical industry, although they are mainly produced with a particle size range of 0.2 - 0.5 mm. Besides, the ideal properties of the granules include spherical shape to improve the flowability of the powder, a minimum level of moisture and hardness to prevent the possibility of the breakage or the pulverization and a narrow PSD which leads to homogeneity in the content and properties of the final tablets.[7] Moreover, the density of the granules must be optimal in order to ensure the best quality in the final product.[8]

The granulation is widely used in tableting, because it allows a better control of the process conditions and it helps to produce better tablets. Indeed, granulation can prevent undesirable phenomena of segregation of the ingredient of the powder mixture and it helps to improve its flowability and compaction properties.[6,9] The quality of the final product is related to the compressibility and compactability of the components used in the powder mixture. While the first property represents the ability to decrease the volume under compression, the compactability can be defined as the ability of the powder to be compressed into a tablet of a specific tensile strength.[10]

1.3.1 *Direct Compression*

Direct compression represents the simplest process, able to produce tablets from a powder mixture made by the Active Pharmaceutical Ingredient (API) and suitable excipients. As it does not require any kind of pre-treatment, this process is efficient and it includes just two main steps: dry blending of the powders and compaction of the mixture. It can reduce the labour time and costs and it eliminates the use and impact of heat and moisture, improving the stability of thermo and moisture sensitive API.[6] Figure 1.2 summarizes the main steps of this process. The Mannitol represents an example of the excipient that can be added to the powder mixture. This last one is collected and sent to the tablet press, which represents an automatic device able to produce a huge number of tablets. In this step pressure is applied to the powder held in a die cavity. This device is responsible for the compression stage, which is typically divided in four distinct steps: filling, metering, compressing and ejection.[12] The compressibility of the materials is extremely important to ensure efficiency to the process. It depends on the material properties such as surface energy and deformation. An estimation of the compressibility of the powder mixture can be achieved from a relationships between the porosity of the final tablet and the applied pressure.[13] Generally, this kind of process is used for medium- to high-potency compounds where the drug content is less than 30% of the total amount of formulation. The main advantage of the direct compression is the low number of unit operations required. Besides, usually, fewer excipients may be added in a formulation of this kind of tablets and some compounds direct compressed point out a faster dissolution rate compared with the granulation processes.[14]

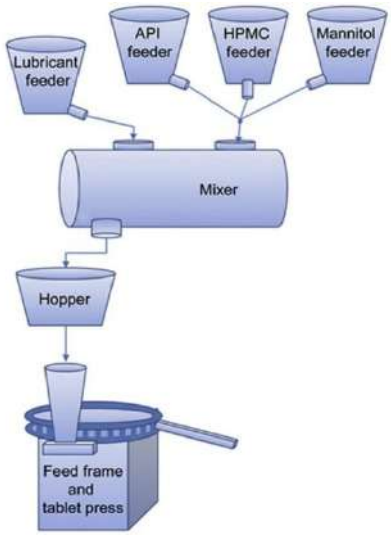

***Figure 1.2** – Illustration of a direct compression process [11]*

1.3.2 Wet Granulation

Wet granulation is the most complex and used process for the manufacturing of pharmaceutical tablets. It represents roughly the 70% of the tablets production industry, since it can cover a wide range of capabilities, from light to very dense granules.[15] The main advantage is the capability to control the flow properties of the powder mixture ingredients. It is widely used when the flowability and compressibility of the primary components are poor. The granulation process increases these properties and ensures a uniform distribution of the drug in the final tablet and a controllable release of the API. The stability of the product can be improved through the addition of stabilising agents to the powder mixture. During the compression stage, the potential segregation of the components is removed thanks to the granulation step.[16] In the wet granulation a liquid binder is combined with a powder mixture to agglomerate effectively the small particles into larger granules, which are sieved, dried and, eventually, milled to achieve the desired granule size distribution. The wetting of the powder mixture is highlighted by Figure 1.3, which shows how the binder creates physical bonds among the single solid particles to produce a large agglomerate that represents the granule. The liquid binders can be aqueous based, or organic solvent based.[17] Their task is promoting size enlargement to produce larger granules and providing a suitable cohesiveness to the powder mixture. There are three main different kinds of wet granulation processes: low shear, high shear and fluid bed granulation. They are characterized by different equipments for each step and present advantages and limitations which make them suitable for different kind of products.[16] Even if this process is very flexible and effective, it has some disadvantages. The main one is related to the high number of different steps and units involved in the process, which implies higher costs for the equipment and a longer labour time. One more significant problem of the wet granulation concerns the APIs sensitive to the moisture and heat, which represents the conditions typical of the environment of this process. Indeed, there are some types of drugs that can be easily

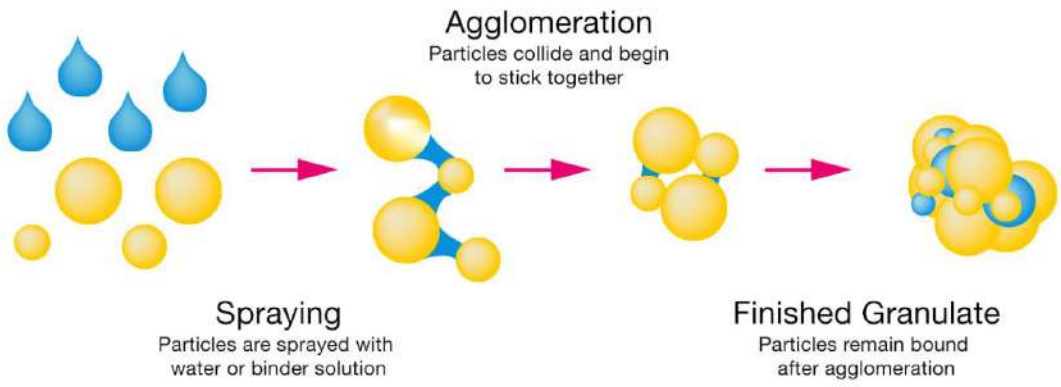

Figure 1.3 *- Steps of wetting of powder mixture with the liquid binder* [3-W]

degraded in these critical conditions. Besides, while the aqueous solutions used could limit the stability of the mixture to granulate, some organic solvents can increase the risk of the development of an explosive or hazardous environment. For these reasons, many types of drugs need other production processes, like direct compression or, mostly, dry granulation.[6]

1.3.3 *Dry Granulation*

Dry granulation is used to produce granules, without using a liquid binder. This process can be used successfully if the components of the mixture have enough inherent cohesive properties to ensure the agglomeration. The main advantage of dry granulation is the elimination of the influence of moisture and heat to the APIs, which makes this process competitive and suitable for the sensitive types of drugs.[16] In this granulation the powder particles are aggregated under high pressure. This compaction can be performed through two different processes: slugging and roller compaction. In the slugging the material is first compressed typically by using a tablet press with large flat-faced tooling, then, these compressed slugs are comminuted through a mesh screen inside a suitable mill. Hence, the material can be combined with a lubricant and it is sent to the tablet press which compresses the granules into the final product. This process has many disadvantages, which includes a poor control and economies of scales, low manufacturing throughput and a larger amount of energy and time required with respect to the roller compaction.[6]

Dry granulation performed by roller compaction represents the best process of tabletting for drugs sensitive to the heat and moisture effect. It is better than the slugging method, since it can handle a larger amount of material in a short period of time and the energy required is lower. This process represents the target analysed in this work and it will be described more in depth in §1.4 of this chapter. Figure 1.4 shows the schemes of the wet and dry granulation processes in the tabletting manufacturing. While the final stages dedicated to the production of the tablet are in common, the differences between the two processes are represented by the granulation method adopted. In the dry granulation, after a dry mixing of the components, the agglomeration of granules is achieved in a simple step (via slugging method or roller compaction) without the addition of liquid binder or the transition to the drying operation. Compared to the wet granulation, this one is faster and cheaper, since the units involved are low and the entire chain requires less labour time.[18]

Dry granulation used in industry started in the late 1940s and its popularity has increased more and more in the last 25 years thanks to the development of new efficacious API characterized by chemical fragility and sensitivity.[16] Besides, the progress of dry

granulation technique has been developing with a recent innovation: The Pneumatic Dry Granulation. This process utilizes a combination of roller compaction and a patented air classification method which can produce granules of a high level of flowability and compressibility, although it presents some limits in the recycle of the fines produced.[7]

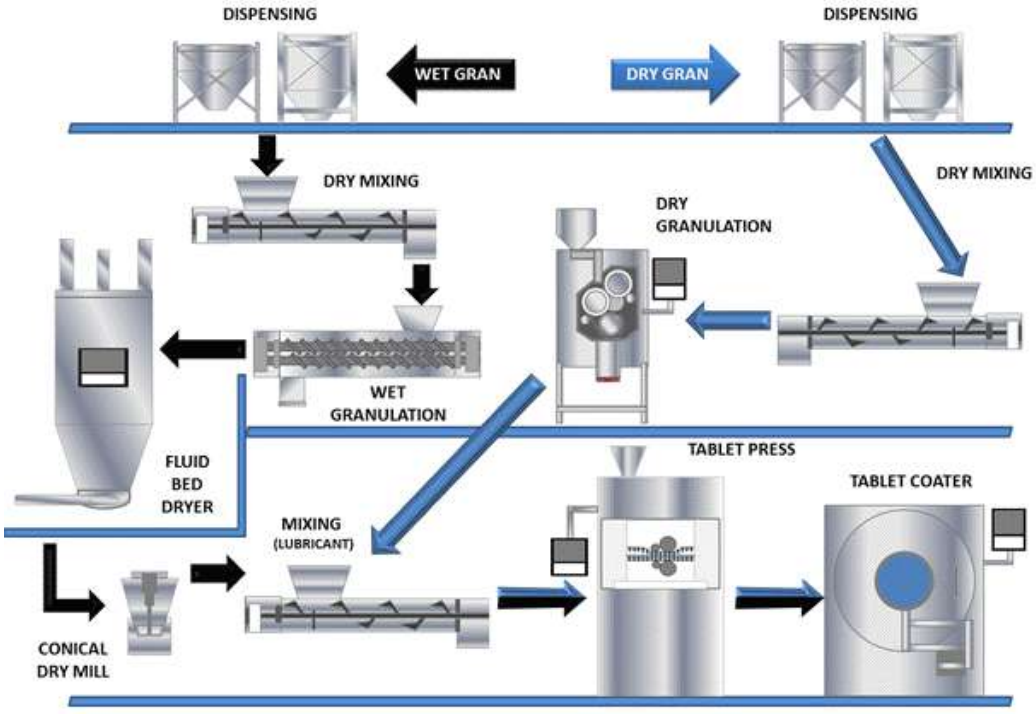

Figure 1.4 *- Schemes of the tablets manufacturing processes by wet granulation and dry granulation* [4-W]

1.4 Dry Granulation Using Roll Compaction

While slugging process is an old technique used in the past of the pharmaceutical manufacturing, the dry granulation using roll compaction has been a key technology for the last years and it will be widely used in the future of the tablets manufacturing. Thanks to the growing scale of manufacturing pharmaceutical worldwide and the increasing need for faster processing, this kind of dry granulation has been developed to speed up the production, enhancing the quality of the final tablet. Indeed, this process can facilitate the processing, preventing particle segregation and improving the drug dosage weight control and the content uniformity. It is also profitable, since the uses of energy and raw materials are limited, compared to the slugging method. Besides, as a dry process, it has the advantages of eliminating aqueous and solvent binders and so, eliminating the need of explosion proof room and equipment. Therefore, this represents the best process for APIs sensitive to the heat or moisture.[17]

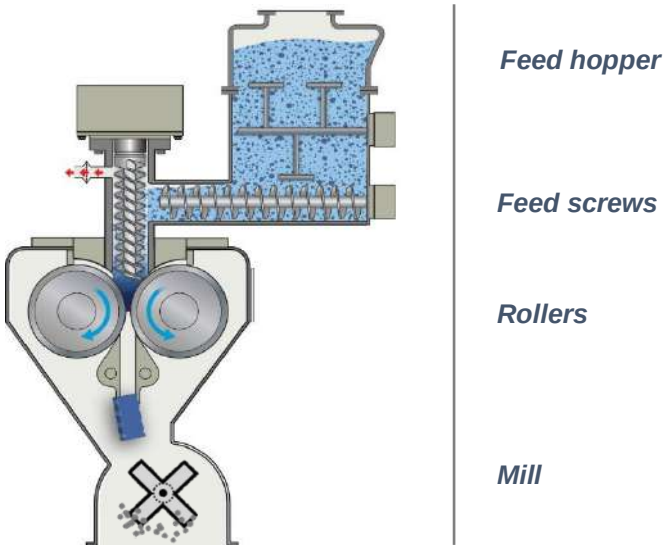

Figure 1.5 *- Dry Granulation process using roller compaction* [5-W]

Figure 1.5 highlights the structure of the process of dry granulation using roller compaction, underlining the steps sequentially. This process involves two main stages: the roll compaction in which the powder mixture is compressed through two counter-rotating rolls to produce long flat ribbons or flakes and the following milling of the ribbons into granules, performed in a suitable mill.[18] The first part consists in the feeding of the raw material and the compaction in the narrow space between the two rolls. As Figure 1.6 shows, this space is divided in three different zones. The first one is the slip region where the mixture enters. In this part the stresses are quite small and the densification of the powder is dominated by the rearrangements of the particles. The second area is the nip region where the compaction force dominates, and the particles deform plastically and eventually break. The third and last zone is the release region, where the ribbons are not subjected to compression forces anymore.

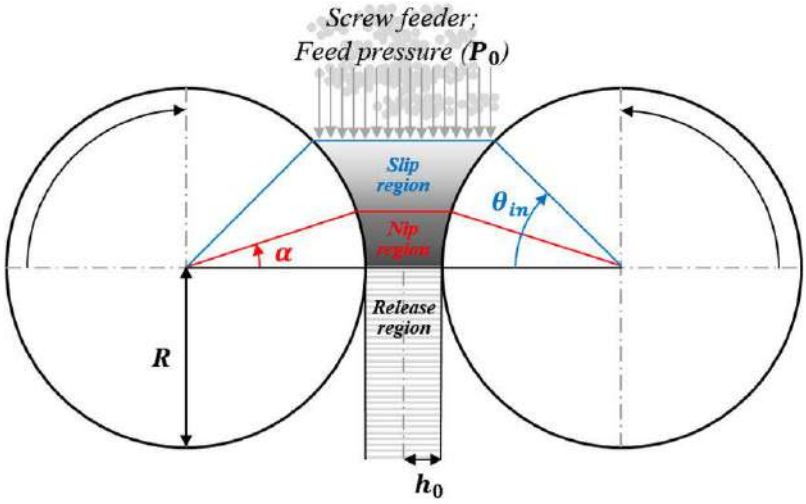

Figure 1.6 *- Different regions of the roll compactor* [18]

The angle α of Figure 1.6 is called nip or gripping angle and it marks the transition between the slip and the nip regions. Instead, the angle θ_{in} marks the beginning of the slip, or feeding, region.[20] The major advantages of this process are the environmentally friendly characteristic and the continous production of granules.[21] The roller compaction equipment can vary, as there is a wide range of pressure and roll types to achieve the desired compaction level of the ribbons. Usually the design of the roll compactor and the choice of the operating conditions depends on the type of drug and the properties of the excipients used in each process.[17] Indeed, the characteristics of the ribbons produced are directly affected by the operating conditions of the roll compaction stage and they influence the size distribution of the granules achieved through the milling process.[21] Besides, the properties of the ribbons strongly affect the particle size distribution (PSD) of the product of milling. According to many studies, the roll-compaction pressure has been found to be the most important parameter to control.[22, 23, 24] Indeed, it represents a factor which is responsible for minimizing the production of undesired fines during the milling step of the granulation process and which controls the tensile strength of the final tablets. The conclusions achieved by the literature reports the need of a compromise between the generation of fines, which are minimized if the compression force is high, and the phenomena known as the loss of reworkability that explains how the higher is the roll-compaction pressure, the lower is the tablet tensile strength.[22]

Even if dry granulation using a roll compaction represents a profitable process for the manufacturing of pharmaceutical tablets, it is affected by some problems that limited its performance and its use. These disadvantages will be discussed more in depth in §1.4.1. The second main stage of this kind of dry granulation is the milling of the ribbons, which allows to generate the granules suitable for the following production of the final pharmaceutical tablets in the tablet press. The operating conditions of the milling process are fundamental to control the size of the granules and then to achieve a better quality in the final tablets. In this step many different variables affect the PSD of the granules, as the type and design of mill and the type and size of the screen used. The size reduction in milling is driven by different contributions of impact, shear and compression, based on the mill type, material properties and operating conditions.[9] Besides, there are two main different mechanical mechanisms in the process of milling of ribbons: breakage of ribbon which is responsible for the reduction of the size of the ribbons and the surface chipping/abrasion, which leads to the production of fines.[25] The fines can be described as the smallest class size of the particles' distribution. Tough a general definition is not expressed, usually, for the general pharmaceutical excipients and powder mixtures the upper limit of their sizes can be assumed between 125 μm and 250 μm.[25, 26]

The types of mills are classified according to the way of application of the forces, which are the impact, the attrition and the shear-compression. Many types of mills are normally used in the pharmaceutical industry for the grinding of the ribbons in the dry granulation process, and the choice is driven by the properties of the feed material and the desired specification of the final product. The jet mills and ball mills are quite used in this industry and they are characterized by attrition and a double contribution of impact and attrition mechanisms, respectively.[27] Nevertheless, the two most commonly used mills in dry granulation processes are the hammer mill and the conical mill.[28] The first one is a high impact grinding equipment and it can reach a significant reduction of the original size of the particles and a narrow PSD, though the particles' shape is quite irregular.[27] Instead, the conical mill represents the mill used in this work and its primary mechanism for the granule breakage has been found to be the impact,[29, 30] even if the compression forces gives a significant contribution to the size reduction.[27] Many single impact experiments proved this theory and the way of impact breakage of the agglomerate was determined to be a combination of localised disintegration and multiple fragmentation originated thanks to the cracks propagation.[29]

1.4.1 Main Features and Problems of Dry Granulation

The dry granulation using roller compaction has many advantages with respect to the direct compression and slugging, since it has more robustness, uniformity and scalability with respect to wet granulation, because it is economical and suitable for sensitive APIs.[31] Nevertheless, it is affected by some problems and disadvantages that can lead to a poor quality of the final tablet. The main ones are discussed in the present work and are summarized in Table 1.1. Raw powder with a narrow PSD can remedy complications in downstream processing steps and improve the drug dosage performance.[28] Therefore, the main complication in the dry granulation process is given by the undesired production of fines in the milling step. The fines are responsible for the reduction of the flowability properties of the granules that leads to problems of the segregation of the different sizes of particles and components.[32] Besides, a great amount of fines brings to a high variability of the weight and a heterogeneity of the final tablets due to the separation of the fines from the larger granules. The segregation leads also to the separation of the drug from the excipients and so to a heterogeneity of API in the tablets produced. Indeed, the amount of fines is directly related to the quality of the tablet and they affects also its strength and hardness.[29] In order to minimize all these disadvantages, in industry a recycle step of the fines produced during the milling is developed, though it is not always able to adjust the problem.[33]

Table 1.1 *- Problems of dry granulation process*

Problems	Causes	Consequences
Fines	• Larger and coarse raw particles • Low compression forces • High impeller speed	• Reduction of flowability • Segregation of components • Heterogeneity in final tablet properties
Low tablet tensile strength	• Too High compression forces • Raw powder too dried	• Fragile tablets
Sticking and picking	• Leak of powder in the logo seal • Tooling defects	• Tablets damages and not suitable for the costumers
Capping	• High concavity of the mould • Air trapping in the die • Granules too dried	• Breakage of the cap of tablets
Scaling-up of the process	• Proportion of different regions of roll compaction step	• Difference in the quality and quantity of products between laboratory and industrial plant

It has been proved how the size of the raw material used can affect the production of fines. Indeed, for a conical mill, larger and coarser primary materials bring to an increase in the amount of fines. So, smaller input particles can help to achieve a better PSD in the granules. This seems a paradox, but it can be explained by considering the mechanism of breakage, which is led by the impacts. Indeed, with a larger raw material the particles need more time to be milled to the suitable size given by the screen holes. This leads to more impacts which produce a greater amount of fines.[29] The properties of the granules and the following tablet are strictly dependent by the roller compactor step. Indeed, less fines are produced if the pressure used is greater, because the density of the ribbon is higher.[22] If the density increases the porosity decreases, since they are related by the following equation:

$$\varepsilon(\%) = 100\left(1 - \frac{\rho_b}{\rho_t}\right) \tag{1.1}$$

Where ε represents the percentage level of porosity, while ρ_b (g/cm^3) and ρ_t (g/cm^3) are the bulk density and the true density of the powder, respectively. The bulk density can be easily calculated as the ratio between the mass and the volume of the ribbon. Instead, the true density is a property of the material or the powder mixture used. The use of the porosity, instead of density is preferable, since the density can vary considerably among the materials, while the porosity, calculated through the equation 1.1, allows a better comparison among different materials.[25]

The effect of the roll compaction dominates over milling process in the determination of the PSD. Therefore, attention must be paid in the choice of the compression force, because the higher is the pressure and the lower is the tensile strength of the final tablet. So, a compromise must be chosen between a good flowability, given by a higher roll compression which takes to a low amount of fines, and a good strength of the tablets, which is not ensured when the pressure used is too great. Besides, a lower compaction force leads to a rougher surface and an irregular shape of the ribbons which are responsible for the improvement of the compactability. Moreover, the choice of the type of roller affects the production of fines. It has been found that the rimmed-roll can eliminate the effect of the friction between the particles of the raw powder and the side seal of the compactor.[22] Besides, rimmed-roll can apply a uniform stress and consequently a homogeneous density of the ribbon along its width.[34] Other common problems in this manufacturing process affects the tablets, like sticking or capping, but they are mostly produced in the granulation step, rather than the final compression. The sticking phenomena represents the loss of powder, which remains stuck to the walls and the punches of the die during the compression. It is generally due to tooling's defects, like steel heterogeneity or roughness, or to an excess of moisture in the raw powder and it causes considerable problems to the production line, as the tablet press needs a stop for maintenance to be cleaned and restore. Another similar problem is the picking, in which the loss of powder is related to tooling's embossing and occurs typically within the logo of the product. The capping represents another common defect that could affects the tablet manufacturing. It consists in the separation of the upper section of the tablet and it is typically due to a high concavity of the mould, air trapped in the die, granules too dried after the milling step or a large amount of fines after the granulation process.[35] Regarding the operating conditions of the milling step, the impeller speed affects the PSD and the production of fines in the conical mill, while in the hammer its influence can be neglected.[9] The efficiency of this step is greater if the milling chamber is full. In particular for the conical mill the noise is reduced and the PSD is narrower compared to other similar mills.[26] Moreover, the mill speed seems to decrease the time of grinding, while an increase of the roll compaction force leads to an extension of the milling time.[30] Nevertheless, a study has discovered that there is a strong correlation between the impeller speed and the production of fines, whose amount can be defined through a function of the square of the speed.[30] The screen aperture size has a great impact on the time and work of this process, as the impeller shape has on the overall performance of the milling. Besides, the type of the screen has a significant impact on the PSD, since, with the same holes' dimensions, scratching screens have been proved to produce granules larger than the smooth ones at equal operating conditions. The fines can be further minimized through a multiple step milling, which reduces the level of the size reduction, but, on the other hand, decreases the efficiency

of the entire process.[26] Moreover, the mixing step needs to be designed carefully, since the segregation of components could occur and affect the quality of the final tablet. A good number of solutions have been developed to manage this kind of problem, specifically to prevent the separation of the excipients from the API, which can cause considerable heterogeneity in the quantitative dosage of the drug to the patient.[36] The last but not least problem of the granulation processes is the scaling-up of the system firstly designed in laboratory and that needs to be adapted for the industrial production. Although one of the main advantages of the dry granulation with respect to the wet one is an easier scaling-up step, this procedure has some obstacles to overcome. One of this is the proportion of different regions of the roller compactor, shown in Figure 1.5, which changes by simply enlarging the laboratory tool to an industrial plant and so, the compaction step conditions are modified. Many different methods have been developed to design an industrial scale plant of roller compaction and milling, nevertheless, the strategy by trial and error is quite used in industry in order to set the best configuration.[37]

Therefore, dry granulation using roller compaction (DGRC) has a great number of parameters that can be set to achieve the desired specifications on the product and the process management. Indeed, under an industrial point of view, the control of the manufacturing time and the energy consumption is fundamental in order to develop a performing process. Hence, the milling rate represents a parameter to minimize the costs, which are affected by the mill type and the process parameters such as the impeller type and speed and the screen used. It can be defined as the total mass milled over the time of processing, as highlighted in equation 1.2:

$$Milling\ Rate\ (g/s) = \frac{mass\ of\ ribbons\ milled\ (g)}{time\ for\ milling\ (s)} \tag{1.2}$$

In a study of the conical mill performance, the milling rate has been proved to be faster with scraping impellers, teethed round sidearm and scratching screen surface profile.[26] This specific configuration allows to decrease the residence time of the powder and, at steady state conditions of the process, it takes to a smaller amount of fines, because the material needs less time and, so, it is less affected by the attrition phenomena. To keep the operating condition at steady state 40% of the volume of the milling chamber, should be kept full of ribbons. In order to minimize the energy costs, the effective specific energy must be calculated, as shown in the equation 1.3.

$$E_e\ (J/g) = \int_0^t \frac{\Delta P_t}{m} \partial t \tag{1.3}$$

Where ΔP_t (W) is the effective power consumption, t (s) is the time of milling and m (g) is the total mass milled during the time t. Although the specific energy outlines the efficiency of the milling process, in order to find out the best setting of the operation both the milling rate and the energy must be improved. Therefore, the overall performance of the configuration of the milling step can be highlighted by the variable P (g^2/Js) in equation 1.4, which represents the ratio between the milling rate and the effective specific energy.

$$P = \frac{Milling\ rate}{E_e} \tag{1.4}$$

This variable can easily describe the quality of the performance of the configuration used, as the higher is its value better is the setting of the milling step. Clearly, different configurations must be studied, by keeping the compaction step and materials properties constant. It has been proved that in a conical mill with scratching screen and higher impeller speed (at steady-state conditions), the configuration is more efficient and suitable to minimize both the energy consumption and the milling time.[26]

1.4.2 Moisture Effects

Moisture content of drugs and excipients plays an important role in tablets manufacturing, since the water affects the chemical, microbiological and physical properties of the final product and the control of humidity represents a fundamental step in the pharmaceutical industry.[38] But first, moisture affects the characteristics of the raw powder. Many studies have been carried out to deepen the behaviour of powders with different water contents. For example, the Microcrystalline Cellulose (MCC), which represents one of the most widely used pharmaceutical excipients, has been analysed and some results proved that its specific volume and the water diffusion coefficient increase, by rising the moisture content, while the Young's module decreases, proving that the stiffness of MCC decreases. The microscopical evidences of the phenomena belong to the decrease of the number of hydrogen bonds among the cellulose chains with the water content. It leads to the expansion of the volume of MCC and to a better molecular mobility of the polymeric chains, since the intermolecular forces decrease. The macroscopic effect consists in the alteration of the polymer chain from a brittle structure to a softer and more elastic one.[39] The understanding of these effects is fundamental in the roller compaction, as this step needs to bond the powder particles to create a suitable agglomerate. The bonding depends on some properties of the material, such as the compressibility, and deformability, and the type of bonds includes the Van Der Waals forces, solid bridges and hydrogen bonds, which are affected by the water

content.[40] The moisture content in a powder can belong to adsorbed water and/or to the water of crystallization, which is represented by water molecules that are settled inside the crystalline structure of the material. The most significant macroscopic effect of a high moisture content in an excipient like MCC is a poor flowability and the increase in cohesion.[41] This leads, inevitably, to some problems in the roller compaction, since the flow of feed is not enough uniform to ensure homogeneous ribbons. Indeed, it has been found that the ribbons created with a higher moisture content in the raw powder presents different density along the flat structure, as the porosity at the centre was lower than the edges one.[40] The cohesion increases, as the water content produces liquid bridges among the particles, but if the moisture content becomes too high the caking phenomena may occur and it will drastically reduce the flowability of the powder, damaging dramatically the performances of the roller compaction steps. Nevertheless, a further increase of the water, until the complete cover of the surface of the material, can increase again the flowability, because the water starts playing the role of lubricant. Although the moisture can severely affect the homogeneity of the roller compacted ribbons, in the die compaction, where the compression is uniaxial, the water has been found to ease the force transmission between the two punches of the die and so it can reduce the variability of the density in the tablets produced.[42] This result is the consequence of the rearrangement and deformation of the particles, favoured by the moisture content.

The final tablets quality is affected by the water content of the raw powder used. Indeed, the tensile strength of compacts decreases with the moisture, even if an optimal level is necessary to produce ribbons and then tablets more resistant.[41] According to a study on a direct compression process, for the MCC this level is equal to 4-5% of moisture content and it ensures good compression behaviour and hardness of the final tablets. This water content is also excellent for the direct compression of MCC into tablets, as the hardness is good and the friability of the tablet is minimum.[38] The effect of moisture on the MCC powder can be summarized in two consequences at different water contents:

- The water makes the powder more cohesive and less flowing due to the formation of liquid and solid bridges among the particles;
- The internal frictions among the particles are reduced when the water content is very high, due to the presence of liquid films, with a lubricant action, over the surface of the particles.

The study of the effects of moisture in the roller compaction performances highlights how more water can increase the pressure applied by the two rollers, as less powder can pass through the roll gap and so more material can be compressed in the compaction region. The

same study discovered that a high level of water content can break the ribbons in the half, as the free water, concentrated in the middle of the flat structure of the ribbon reduces the bonding strength, weakening the central region. Nevertheless, according to a study, although the moisture is an important parameter in the tablets manufacturing, the main properties of the excipient MCC, like cohesion and flowability, are not significantly affected by the water content if its level is below 10%.[41]

The effect of the moisture content has been studied for the dry granulation process, by analysing the particle size distribution of Lactose powders after the milling process. This allows to understand if the water can ensure good performance in the granulation process and so if it can produce agglomerates suitable for the following compaction into quality tablets. Therefore, the study focused on the analysis of the amount of fines produced during the milling of ribbons made by powders with different moisture content, achieved by storing the raw material in an environment of different relative humidity level, from 10% to 80%. This procedure allows to understand the direct effect of the environmental condition of storage of the powder in the performance of the dry granulation process. The results highlight that at the highest moisture content (equivalent to 80% of relative environmental humidity) the largest amount of fines is produced, while the minimum one is achieved in the range of 20-40%. This has been attributed to the decrease in the flowability with the moisture content. It has been observed also that at the lowest water content, more fines are produced, with respect to 20-40% of environmental humidity, since the deformability in the dry powder is reduced, due to a reduction of the binding powder of the Lactose particles. The best deformability and compressibility, achieved in the range 20-40%, can ensure better bonds among the particles and so a lower production of fines. Another result achieved regards the width of the ribbons produced, which varies at different moisture content. Indeed, the powder stored at 80% of relative environmental humidity produces the thinnest ribbons, while the thickest ones are produced from the powder stored at 20-40% of humidity level. In the actual moisture content, there is a difference of the weight value, which does not follow the increase of the environmental humidity. In fact, in the range 10-40% the water content increases with the humidity level, while in the 40-80% it remains almost constant. This is attributed to the amorphous structures of the Lactose powder, which crystallize by increasing the humidity level, and so they desorb water compensating the effect of the increase of the environmental humidity. Besides, this desorption is responsible for the decrease of the flowability and the increase of the cohesion of the powder. All these results underline how the optimum conditions of storage for roller compaction of lactose powders are in the range of 20-40% of relative environmental humidity.[43] The procedure followed in the present work to study the effect of the moisture content of the MCC in the dry

granulation performances will focus in the observation of the production of fines after the milling step, aiming to analyse the features that can characterize the MCC and the influence of the environment on its properties.

1.5 Modelling

In order to predict the operation of dry granulation and the behaviour of the processed powder, the modelling of the different steps plays a fundamental role. It is mostly used to simulate the process and find the best operating condition for the manufacturing systems. A great number of models have been developed to represent with reliability the performance of the process during the various steps. For instance, in order to predict the powder behaviour between rolls during the roll compaction Johanson proposed in 1965 a continuous model characterized by a semi-analytic description of the basic properties of the granular materials and the roll compaction variables. It was one of the first good models in this process, even if many limitations emerged during the years, mostly correlated with discrepancies between the calculated and experimental results.[44] Many other models have been developed to ensure a better prediction of the ribbon properties, and some of them were successfully used in pharmaceutical applications. Besides, for a better understanding of the particle technology and of the solid behaviours, many experiments and studies have been carried out thanks to the progress of instrumentation and they have become the strong base of the modelling approach, which needs a deep theoretical background to be implemented efficiently. Indeed, the experimental results were predicted by the models with difficult and the laboratory studies helped to understand some features of the operating conditions and the materials properties.[45] For instance, during the roll compaction step the heterogeneity of the applied pressure has been discovered and the studies highlights how it is greater in the centre of the nip region, while in the edges a great variability of the values has been observed.[46] This variability, however has been found to be damped by increasing the pressure, leading to a better homogeneity along the width of the compaction region.[47] Moreover, the air trapped in the powder has been discovered to be a significant problem for the development of suitable models. Indeed, the air flows generated from the slip and, mostly, nip regions during the roll compaction can remove away the incoming powder and, then, totally disturb the press feeding. In extreme cases, the air can lead to the fluidization of the particles.[45] This problem was managed thanks to an implementation of the model which adopts a multiphase material, made by a solid and a gas phases and the possible interaction between the two phases. Therefore, some progresses have been achieved and a better reliability of the model representative power of the compaction process has been successfully reached.[48] One more fundamental challenge in the modelling of dry granulation is the development of a

model suitable for the scalability of the process from the laboratory scale to an industrial plant. The importance of this step can be easily understood, as the best operating conditions achieved during the preliminary study can ensure to save energy, materials and money and to reach the best quality in the final product, if the laboratory plant is successfully scaled into the industrial one. Usually pharmaceutical industry adopts trial and error techniques, but some models are implemented to minimize operating costs and time, especially when the materials and the quality product are more valuable.[45] Except for the compaction step, the main modelling methods used in the dry granulation concern the milling process, where the ribbons are size-reduced into granules. Indeed, the milling is an energy-intensive and costly process and its efficiency is quite low. Therefore, mathematical modelling is widely used for the design of milling system and for the process simulation to find out the best configuration and operating conditions. The approaches used for the modelling could be divided into five main families, classified for their theoretical bases:[49]

- Purely data-driven models and empirical models, which are based on the experimental data and results and on correlations among specific energy and time of process and particle size milling;
- Particle-scale mechanistic models which include materials properties to define and describe the particle breakage;
- Mechanistic models such as the finite element method (FEM), in which the behaviour of the particles is modelled as a continuum phase, and especially the discrete element method (DEM), which considers each particles interaction and deformation. Combinations of both can be used, with consequent advantages;
- Population balance models (PBM), which are used to describe the temporal and spatial variation and reduction of the PSD during the milling step;
- Models based on computational fluid dynamics, which can describe multiphase system, by considering the gas contribution to the process and they usually consists in a combination of PBM and DEM.

1.5.1 Discrete Element Method

The DEM represents a family of methods which includes all the numerical models able to simulate the movement of the particles and the effect of the interactions among the particles themselves. In particular, the DEM is widely used to model the dynamic of the particles in different type of mills, although it represents a computationally intensive method. It was proposed for the first time in 1979 by Cundal et al. [50] and since that time it has been largely

improved thanks to a deeper understanding of the interactions among particles. Now it can be successfully used to model many kinds of processes that involves solid particles, such as the mixing, milling, fluidization and filling. This last one covers an important role in the dry granulation, since it's fundamental to ensure a suitable feed of powder into the compaction region. Indeed, many progresses have been achieved in the study of the screw feeder and then in the DEM simulation of different mass flows and operating velocities of the screws.[45] Besides, DEM has been widely adopted in many processes of comminution, thanks to the capability of computation of the collisions among particles. Under the theoretical basis, the DEM represents a model that creates a great number of solid particles and then it simulates their motion in the process analysed. The movement of particles is directly related to the properties of the material and the conditions and type of system. Many forces, interactions and geometrical factors are implemented in this model to ensure a reliable simulation of the process, starting from the experimental observations. Basically, DEM solves Newton's laws of motion and the inter-particles contact equations.[51] It can be understood how much DEM can be expensive under a computational point of view. Indeed, usually the time required is too long and the device used needs great power and so its costs are considerable. Besides, it is limited by the number of particles, which cannot be too large to allow realistic achievement of the results, and the length of the simulation. Some facilitations are given by considering the particles as a continuum phase and using the FEM, which lets to find solutions to partial differential equation, which represents the structure of the problem, by solving algebraic equations. Many other simplifications and approximations can be included in the model, to lighten the calculation load and to speed up the performances. In practice, in the milling simulation DEM studies the particle-scale phenomena and micromechanical interactions which produces breakage of particles themselves. It's fundamental to understand the dynamic and micro-dynamic behaviour of the milling step, as it can simulate the translational and rotational motion of millions of particles, by integrating the physical laws and forces that affect each particle. Therefore, it can predict the milling performance, calculating the breakage rate and the impact energy distribution among the particles.[49]

The DEM has been applied in a wide number of studies of different kind of mills, from the tumbling mill [52] to cutting mill [53], stirred mill [54] and conical mill [29]. For instance, it was used to simulate the micro-dynamics and, mostly, to calculate the impact velocities and the stresses inside a rotary bar mill. The model was a bonded sphere DEM, where the ribbons where build as spheres and it allowed to determine also the size reduction of the compacted ribbons.[9] This reduction is generated by particle breakage and attrition and abrasion contributions, which are simulated by three main DEM models: Bonded Particle

Model, the Fragment Spawing and the Attrition Prediction. The principles of these models are highlighted in the Figure 1.7. The first one builds each grain, or ribbon, with many rigid particles connected to each other by bonds which can represent the material strength. This model can simulate successfully the internal stress distribution and the propagations of the breakage into the small particles created from the first grain, but it is limited by a finite number of smallest particles, and so the final PSD is narrowed by this constraint. This limit can be removed thanks to the Fragment Spawing where the grain can be broken into many smaller particles with sizes determined by a breakage function. The main problem of this model is the reliability and efficiency of the empirical breakage function developed. Instead, the Attrition Prediction considers the attrition phenomena which consists in the abrasion of a small amount of powders from the particles surface, without accounting the real breakage of grains into smaller size particles. Even in this model, an experimental correlation is used to simulate the mechanism of the attrition. As it has been developed for particles beds affected by a mild contribution of the attrition, it cannot be applied for the simulation of process with a high impact of the attrition (which would produce significant change of each particles size).[55] DEM can be used also for the calculation of the number of fragments and the fines fraction for each rupture. Nevertheless, its computational requirements make it unsuitable for industrial applications, even if it can give a detailed insight of the breakage mechanism.[30]

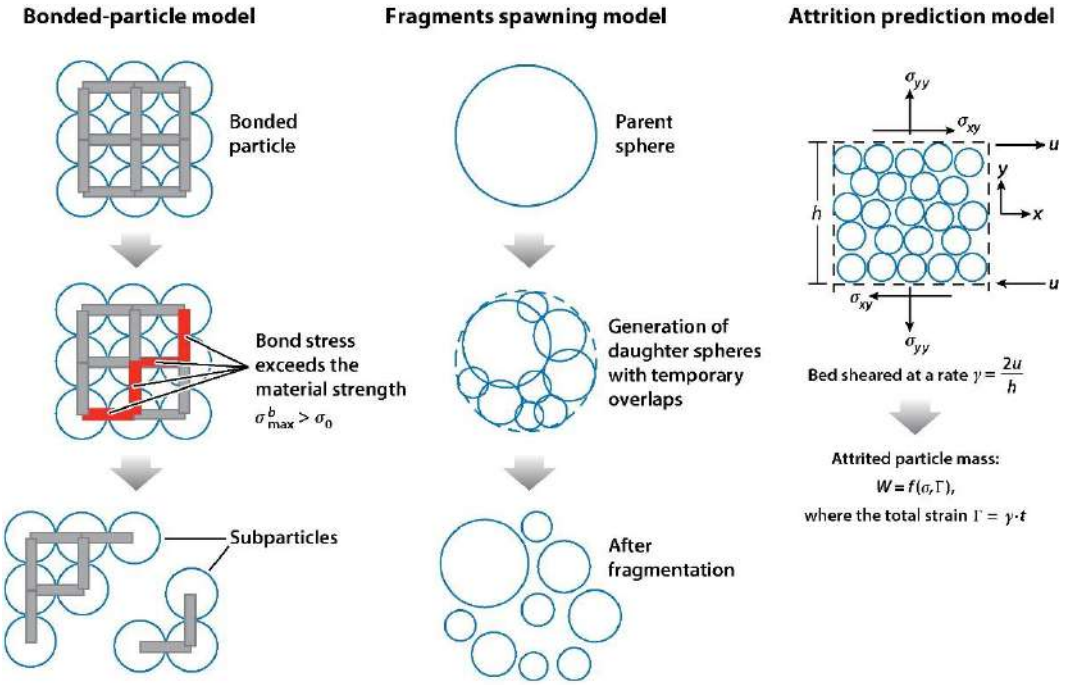

Figure 1.7 *- Illustration of the principles of the three main DEM models regarding the breakage of particles*[55]

During last years the DEM has been used successfully in a combination with the PBM model, which has allowed to improve the reliability of the simulation. The PBM consists in a mathematical model able to describe the evolution of the sizes of a population of particles, but it will be discussed more in depth in §1.5.2.[56] However, the PBM requires detailed information of the breakage in a microscopic scale and, in general, of mechanistic dynamic. It is semi-empiric and can be implemented together with DEM, as this one can provide a portion of the input of the PBM, like the impact energy distribution. The PBM usually needs experimental information, such as the broken mass at a given impact energy and energy-based breakage function, which will be described in next section. Therefore, PBM-DEM framework represents a powerful tool in order to predict the PSD and the breakage behaviour.[30] The structure that a DEM-PBM model can assume is quite complex. For instance, in a multiscale modelling framework, used to study a ball mill, the DEM has been adapted to calculate the impact energy spectra inside the milling chamber. These spectra are used to determine the time-dependent breakage rate involved in the PBM, which can, then, be solved to find the PSD at different milling times. At the end of the iterative cycle, this PSD is fed to the DEM, which can calculate the following breakage rate during the milling process. The specific breakage rate constants are, then, compared with the experimentally obtained ones in order to assess the predictive quality of the model.[57] The main advantage of this kind of models in the application in milling of dry granulation processes is the balanced compromise between the accuracy and the computational time. Indeed, a DEM-PBM model can predict the evolution of the PSD during the milling, without solving the DEM for the entire length of the process.[49] Many other examples of integration of the two models are reported in literature.[58, 59] Most of them were used to study milling conditions and particles properties of the dry granulation processes.[60]

1.5.2 Population Balance Model

The PBM is a mathematical tool useful to track the evolution of a population of particles. It can be used to describe dynamically the desired properties of the particles in a wide range of applications, which can include the grinding and milling processes or the polymerization or many others like the cellular growth, division and death.[56] It is defined by a general equation which can be modified in order to adapt it at each application:

$$\frac{\partial f(x,t)}{\partial t} + \frac{\partial \left(\dot{X}(x,t) f(x,t)\right)}{\partial x} = h(x,t) \tag{1.5}$$

where $f(x,t)$ is the density function, which represents the distribution of the distributed property x, while $\dot{X}(x, t)$ is the continuous growth term (g/s) of the internal coordinate x,

during the time *t.* The right term *h(x,t)* represents the PBM reaction term (s^{-1}), which usually consists in the process of aggregation or breakage of the materials in the system analysed. The first derivative term on the left side is the accumulation term and it underlines the change in the density function. The difference between the second left side term and the reaction one is the type of process which takes to a dynamic change of the function. Indeed, $\dot{X}(x, t)$ describes a continuous process of growth or of reduction, while the *h(x,t)* represents discrete processes, which are defined by mathematical functions called kernels. The nature of the coordinate *x*, which can be a scalar or a vector, defines the type of PBM, that can be one-dimensional or multi-dimensional. It is now clear that this general expression can be adapted to many different systems and applications, by manipulating the different terms. Some processes that use the PBM to study some dynamic size changes are the granulation, the flocculation or the waste-water treatment.[61] In the specific case of this work the PBM has been used to model a milling of pharmaceutical ribbons. This kind of work, in different ways, has been in part analysed in literature. These processes involve pure breakage mechanism and the model to be solved needs empirical results to define the necessary terms included in the equation. Therefore, the PBM contains a selection function or kernel that describes the rate of breakage and a breakage function that outlines the resultant fragment size distribution for the particles in each class size considered. Hence, the PBM continuous equation for a milling process can be reported as follows:

$$\frac{\partial n(v,t)}{\partial t} = \int_{v}^{\infty} b(v,u)S(u)n(u,t)du - S(v)n(v,t) \tag{1.6}$$

where *n(v,t)* is the numerical density function, *S* represents the Selection kernel (s^{-1}), while *b* is the breakage function. Instead, *v* (μm) is the granule size and *t* represents the time of milling.[30] In order to apply the model to an experimental study of milling, the equation is size-discretized, while the continuous time domain is preserved. The equation is then expressed by the following equation:

$$\frac{dM_i(t)}{dt} = \sum_{j=1}^{i-1} b_{ij}k_j(t)M_j(t) - k_i(t)M_i(t) \tag{1.7}$$

In this equation k_i (s^{-1}) is the size-discrete specific breakage kernel, while M_i is the mass fraction of the material in the class size *i* and b_{ij} is the size-discretized breakage function for the particle from size *j* to size *i*. The PBM in this case represents a mass balance of the material in the size intervals, at a time *t*. For the resolution of the differential equation, the

initial condition of mass is defined as the total mass of the class *i*, which characterizes the dimension of the ribbon at the initial time, that represents the moment just before the beginning of the milling of the roller compacted ribbon. The b_{ij} of the equation 1.7 can be defined with the use of the cumulative breakage distribution parameter B_{ij} in the following equations:

$$b_{ij} = B_{ij} - B_{i+1,j} \qquad b_{nj} = B_{Nj} \qquad b_{ii} = 0$$

These expressions are more convenient for a practical computational implementation of the model.[49] Literature reports many different definitions of the k_i and B_{ij} functions, as they depend on the type of mill and studied carried out.[62] Nevertheless, commonly in the milling literature, the cumulative breakage distribution function B_{ij} which represents the probability of a particle to pass from the size *j* to the size *i*, can be defined as follows:

$$B_{i,j} = \alpha\left(\frac{x_{i-1}}{x_j}\right)^{\gamma} + (1-\alpha)\left(\frac{x_{i-1}}{x_j}\right)^{\beta} \tag{1.8}$$

where α, β and γ are the breakage distribution function parameters and they represent the different sizes of the particles. Instead, the specific breakage kernel is defined as follows:

$$k_i = A\left(\frac{x_i}{x_0}\right)^{n} \tag{1.9}$$

Even in this equation *A* and *n* are the model parameters (the specific kernel parameters, in particular), while the x_0 (μm) is a normalizing particle size, which is usually assumed as the maximum particle size of the system.[49] By considering that the milling chamber usually needs a screen to select the right size for the outlet particles, the size reduction mechanism is dominated by the size of the screen aperture. This condition involves a residence time of the particles inside the milling chamber, as they need to be smaller than the screen size to pass. During that time, the particles are affected by the breakage mechanism, while, once their size is suitable to pass through the screen, they will leave the mill without further breakages. Therefore, a Heaviside function is added to the model, in order to describe the classification behaviour:

$$S(l) = S_o H(l - l_c) = \begin{cases} 0 & l < l_c \\ S_0 & l > l_c \end{cases} \tag{1.10}$$

where $S(l)$ is the selection kernel (s^{-1}) dependent by the dimension *l* (μm) of the particles, S_0 is the selection kernel part independent of *l* and *H* is the classification function which is

responsible for the selection of the smaller sizes of the outlet particles. Instead l_c is the critical size, which is dependent on the aperture screen size. The particles smaller than this value can exit the milling chamber.[29] However, for a better predictive capability of the model the classification function $H(l - l_c)$ needs a refinement near the value l_c. Indeed, there should be a further classification for the sizes between the real screen size and the critical one.[63] Although suitable approximations can be found in literature, this feature will be discussed more in the modelling chapter (chapter 4). All these expressions represent general definitions, but other forms are reported in literature, as other factors can be considered and affect the functions, such as the presence of fines which are responsible for the deceleration of the breakage rate. Besides, the effect of time can be negligible for the breakage kernel, as for most of the milling application $k_i(t)$ is assumed time independent. The breakage rate is, also, more sensitive to the processing conditions, with respect to the breakage function b_{ij}. This kind of model represent the traditional time-continuous PBM, which has been widely adopted in the last years. Nevertheless, literature highlights its limits, as it is a model restricted by a first-order breakage kinetics, which can be successfully used especially for short-time milling of ribbons fed with a narrow PSD. Therefore, during last period, many nonlinear breakage kinetics have been developed and used effectively for dense-phase milling processes. These models are characterized by multiparticle interactions evolving during time. In practice, the difference with the traditional PBM consists in the division of the breakage rate parameter in a first-order term and a population-dependent function. This last term can change and, so, it can describe different nonlinear breakage kinetics.[49] Once the PBM has been developed and set, the following step concerns the parameters estimation. Indeed, as their number is significant, a deep calibration of the model is necessary, and it is carried out thanks to the experimental data. Then, the model is used to simulate the process at different operating conditions and the calculated results are compared to an unused experimental dataset. Therefore, if the model is suitable to achieve good quality predictions of the real process, it can be used for the simulation of the PSD in the range of the conditions analysed in this specific study.[33] This procedure is known as the "inverse problem" which allows to calibrate the model via a parameter estimation. It is carried out through a back-calculation method, with the help of a nonlinear optimization technique. The fitting represents a minimization problem of the error among the results calculated with a specific set of parameters and the experimental ones.[49] The objective function used for this optimization process is usually the sum of the squared error (ER):

$$ER = \sum_{j=1}^{Z} \sum_{i=1}^{N} \left(Q_{ji}^{Exp} - Q_{ji}^{Cal}\right)^2 \tag{1.11}$$

Where Q_{ji}^{Exp} and Q_{ji}^{Cal} represent the experimental and calculated cumulative mass (g) undersize distribution, respectively, while *z* and *i* refer to the particle size distribution for a particular milling time and the size class, respectively.[33] However, the ER is good for the evaluation of the goodness of the model, in order to carry out a better comparison among different models the standard error of the residuals SER is used:

$$SER = \sqrt{\frac{ER}{D - K}} \tag{1.12}$$

where ER is the sum of the squared error, *D* represents the number of experimental data points and *K* is the number of the model parameters.[49] The elasticity of the model, given by the different expressions that each function can assume and the variable number of parameters the model can have, make the PBM a powerful tool for the prediction of the PSD for different kinds of processes. In chapter 4, starting from the theoretical basis analysed in these sections, the PBM suitable for this work will be developed and its functions will be described, in order to explain the choices adopted and the results expected by the following analysis.

Chapter 2

Materials and Methods

This chapter aims to be a technical introduction to the specific work of the thesis, by presenting the main tools and instrumentation that have been used in this project. The material used will be widely described in order to ensure a better connection between the present work and the pharmaceutical background. The choice of the equipment adopted in this work will be explained and the instrumentation deeply described. Besides, the methodology developed and followed in the project will be delineated in order to clarify the entire path exploited for the achievement of the final results. This chapter will focus more on the experimental part of the work, while the procedure used for the implementation of the PBM will be deeply described in the modelling section (Chapter 4).

2.1 Excipient: Microcrystalline Cellulose

The excipient used in the present work is the Microcrystalline Cellulose (MCC), which represents one of the excipients most used in the pharmaceutical tablets manufacturing. In particular, the project focuses on a study of the MCC Avicel® PH-102, which is a typology of MCC widely used in pharmaceutical industry. MCC is a depolymerized cellulose synthesized from α-cellulose precursor. This one is produced by a wooden pulp obtained from fibrous plant material. There are many different processes of synthesis, which goes from the reactive extrusion to the acid hydrolysis. The applications include the role of additive in pharmaceutical, food, cosmetics and other sectors, although the main one regards the use as a binder in tablets production. Indeed, the variable physicochemical properties that characterize it, allow different use and give different chemical composition and structural organization (crystallinity, molecular weight, …) to the material. The formula of MCC is $(C_6H_{10}O_5)_n$. The raw material that can be used in alternative to the pulp wood for the production are the cotton stalks, rags or cotton fabric waste or other vegetable materials like the oil palm, biomass residue or the grass fibres. The cellulose obtained by these materials is characterized by amorphous regions, which are converted into more crystalline fragments through the hydrolysis action of the acid.[64] Indeed, the acid hydrolysis is one of the most preferable process, thanks to a shorter time of manufacturing. The changing of the operating conditions allows to achieve the desired specifications for the MCC, like the

selected PSD. MCC is the most versatile inactive agent and it is also user friendly. It looks like a white and non-reactive powder with a good flowability. In the pharmaceutical industry, its properties make it suitable as excipient for direct compression and wet and dry granulation. Indeed, its main characteristics involve low bulk density, good stability, plasticity, insoluble properties, compactability, and a good flowability. Therefore, MCC ensures high quality tablets, characterized by mechanical strength, hardness and content uniformity.[6-W] The flowability of the powder represents a significant parameter to take into account to develop a performing tablet manufacturing process. The good value of flowability of the MCC, in general, but, mostly, of some of its typologies, allows this powder to be successfully used in tablets production and in faster processes, such as the high speed tableting.[65] The nominal particle size can go from 50 µm to 200 µm, depending on the properties desired for the product. Indeed, larger sizes present higher flowability and this allows to reduce the weight variation and to improve the content uniformity, while lower sizes are widely used for direct compression and, thanks to a low moisture content they are suitable for moisture-sensitive active pharmaceutical ingredients (APIs).[64] As specified above, the typology of MCC used in this work is MCC Avicel® PH-102, which is characterized by quite large particle sizes. The first part of the experimental analysis concerns the characterization of this powder. During this phase the PSD and the particles shape analyses have been carried out, in order to highlight the profile of the raw material used in the following experiment. The analysis has been carried out through the QicPic™, which will be described more in depth in the following sections, and the PSD has been plotted and reported in Figure 2.1. This shows the weight normalized frequency of particles along the different class of sizes, which represents an important parameter to evaluate the probability to find particles in a unit volume, although its significance will be discussed more in §2.4.3. Besides, the cumulative distribution of the particles is outlined, referring to the right vertical axis of the graph. It is useful to find different sizes relating to a cumulative percentage of the number of particles. The most important parameter for this analysis is the d_{50} which represents the 50th percentile of the PSD. The other important percentiles are reported in Table 2.1 in addition to other significant parameters useful for a deep development of the profile of the PSD. The description of these operators will be done in §2.4.3.

Table 2.1 *- PSD parameters of the MCC Avicel PH 102*

d_{10} (µm)	d_{50} (µm)	d_{90} (µm)	VMD (µm)	Span (-)
72.48	*161.06*	*274.19*	*168.61*	*1.25*

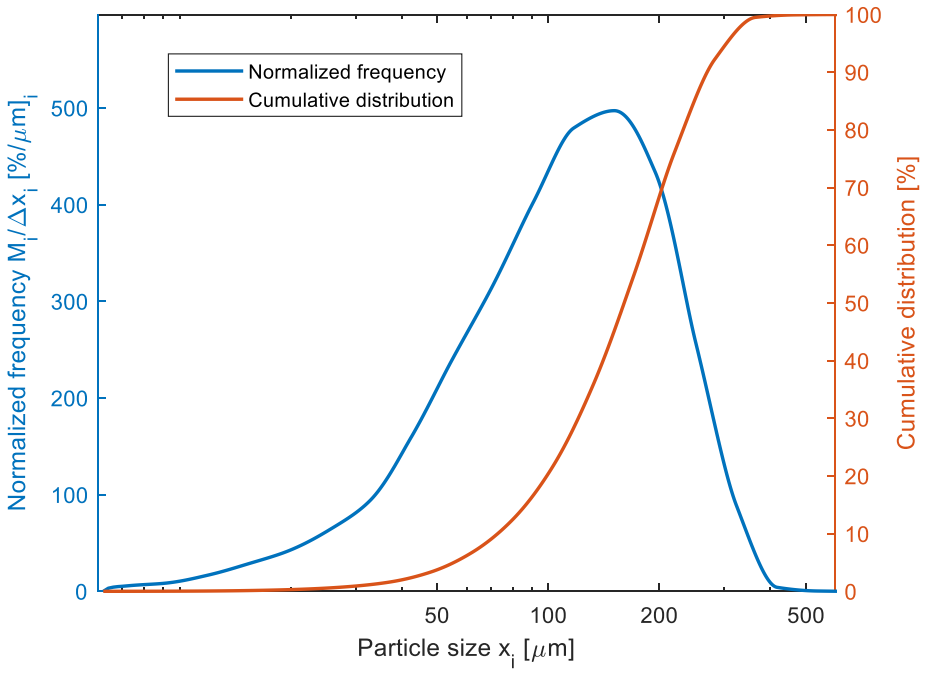

Figure 2.1 *- Normalized frequency and cumulative distribution of the PSD of MCC Avicel PH 102*

The difference between the volume mean diameter (VMD) and the d_{50} underlines the contribution of the volume of the particles in the determination of the mean of the diameter. Indeed, d_{50} is lower, because it considers the number of particles, and it highlights the size which separates the 50% of the small part of the population from the 50% of the greater one. Instead the VMD weights the volume of the particles in the calculation of the mean. By observing their values, the middle-class size of the population can be set around 165 µm. Besides, the cumulative distribution shows that the greatest sizes correspond to particle diameters equal to 300 µm, while the smallest ones are roughly 30 µm, although the interval of the distribution of the size is better described by the d_{10} and d_{90}, which are equal to 72 µm and 274 µm, respectively, according with Table 2.1. The span reported in the table is useful to describe the width of the distribution and its calculation will be better described in §2.4.3.

Regarding the shape analysis the aspect ratio and the circularity of the particle have been evaluated in order to outline the shape profile of the raw powder of MCC. The difference among them will be described in §2.2.3, nevertheless, the first one is related to the difference among the largest and smallest orthogonal diameter, underlining the elongation of the particles, while the circularity, represents the ratio between the area occupied by the particle's projection and its perimeter. Therefore, it is affected not only by the general shape of the particle, but also by the roughness of the surface. Figure 2.2 shows the trend of the aspect ratio AR and the circularity φ_p in the left and right y-axis, respectively. The result shows that the smaller particles are more similar to a sphere, while the shape deviates from

the spherical one, by increasing the size. The difference of the trend with the aspect ratio proves that the surface roughness is significant in the largest particles. The mean of the circularity of MCC Avicel® PH-102 can be estimated to be equal to almost 0.7-0.75. Instead, the aspect ratio does not show a clear relationship with the particles size, and the mean value can be assumed equal to almost 0.65. This result highlights that there is a difference between the similarity with a sphere and the proportion among the maximum and minimum diameter of the particles. Indeed, although the smaller particles show a higher circularity, there are significant discrepancies among those two diameters and these differences seem to be mitigated just a bit, by increasing the particles' sizes. However, for the largest part of the powder population found in the PSD analysis, the values of the two shape factors are similar and equal to almost 0.7.

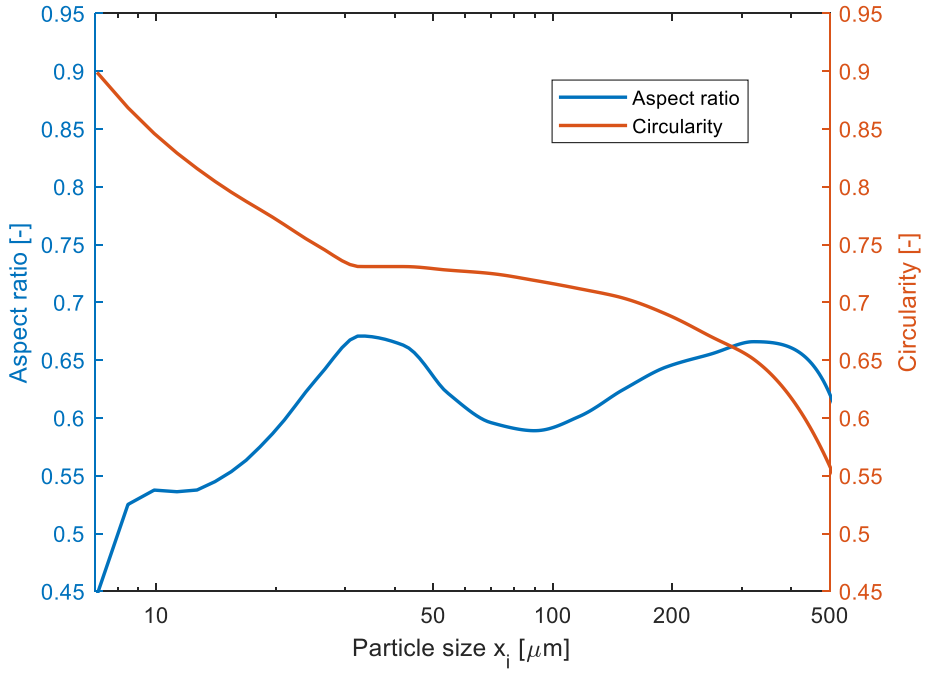

Figure 2.2 *– Shape analysis of the PSD of MCC Avicel PH 102*

The true density of the powder has been found in literature and it is equal to 1.57 g/cm^3.[66] This value will be useful for the calculation of the theoretical porosity of each ribbon, by using the equation 1.1.

2.2 Equipment

In this section the equipment used in the experimental analysis will be presented and described, in order to explain the function of each tool and its role in the procedure implemented in this study. The main features will be deepened and their characteristics in the laboratory simulation of the dry granulation process will be highlighted.

2.2.1 Instron 1175 and Die Compactor

Instron® 1175 is an electromechanical equipment for conducting compression and static tests with a load capacity range which goes from 10 N to 100 kN. It is coupled with a control and data acquisition software, which allows to collect live experimental data.[7-W] The machine represents a press which can be used both for compression and traction experiments. In this work Instron 1175 has been used to produce ribbons through a uniaxial compression of a set mass of powder in a die. This allows the production of fines with a more homogeneous distribution of the density, with respect to the industrial roll compaction step. All the tests have been performed in a room temperature controlled at 20°C. A 100 kN load cell has been used to transfer the compression from the machine to the die. The desired force of compression can be set in order to produce ribbons with different levels of porosity and thickness. The speed of compression has been set at 5 mm/min for all the experiments. Figure 2.3 shows the Instron 1175 and it highlights the detail of the press and the die compactor where the powder is filled and compressed to produce a circular ribbon. This last one is a Specac™ die with a max load of 45 tons and a nominal internal diameter of 32 mm. The dark grey press above the die is the 100 kN cell load used for the experiments.

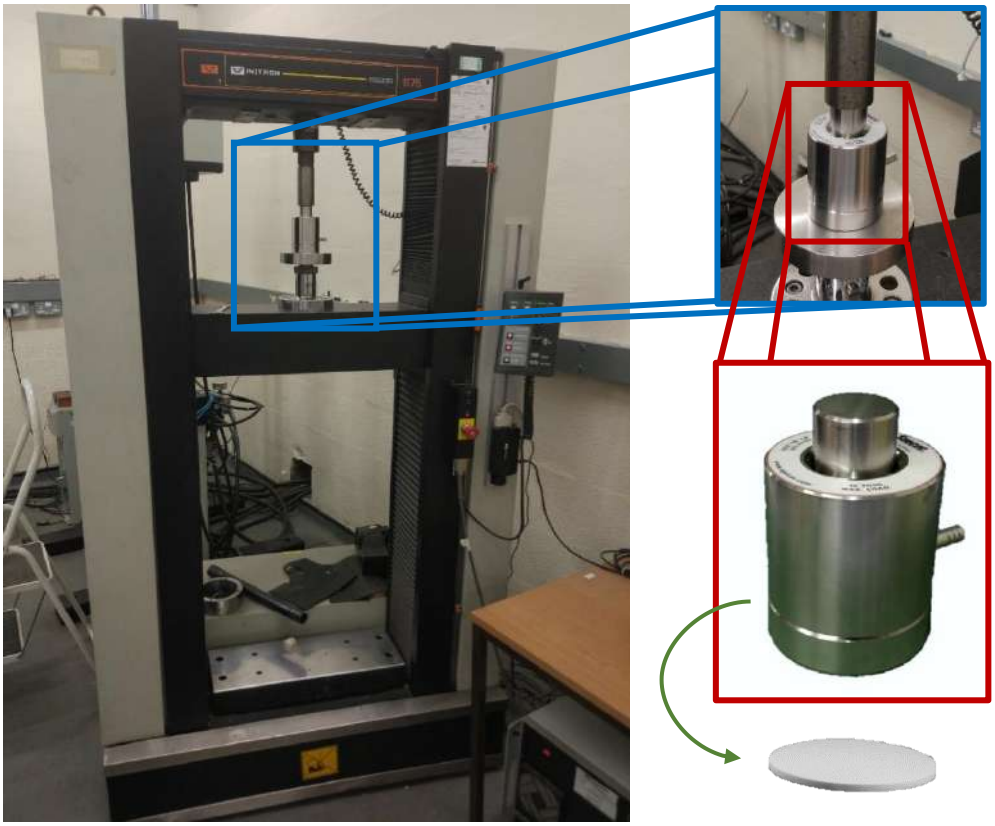

***Figure 2.3** - Instron® 1175 with highlighted details of the compression platform, of the die compactor (Specac™) and the ribbon produced*

2.2.2 Conical Mill

1. Hopper
2. Sieve housing with sieve insert and rotor
3. Motor cover
4. Gear box
5. Product tube with star knob screws
6. Safety sensor

Figure 2.4 *– ERWEKA® conical mill and marks of the most important components of its structure* [69]

The mill used in this work is a conical mill, which is one of the most used in the dry granulation processes.[28] The one used is an ERWEKA® conical mill type CM, which is a rotor sieve mill suitable to define the granules size. The milling chamber is set with a rotor linked to an impeller. Its name comes from the geometry of the milling chamber. The standard sieve gap with the impeller is set in the conic section at the value of 1.5 mm. The reduction of this gap increases the throughput but also the amount of fines produced. The rotational speed can be set from 20 to 400 rotations per minute.[67] Figure 2.4 highlights the conical mill structure and the most important parts. In the top the ribbons are fed in the hopper where the fall thanks to the effect of gravity to stop inside the milling chamber, where the motion of the impeller against the conical screen walls breaks the ribbons to produce the granules suitable for the following compression into tablets. As specified in Chapter 1, the main mechanism that characterizes the conical mill is the impact, although the attrition has a contribution in the overall process. Commons applications are related to the size reduction and the deagglomeration.[8-W] This device is widely used also in the wet granulation. In this type of mill, it has been found the size reduction paradox, whereby the coarser feed particles can increase the production of fines in the milled material. The key components of a conical mill are the impeller and the screen.[29] Indeed, the screen used ensure to control

the size of the granules produced, as the particles greater than the holes' dimensions do not pass through the screen and they remain into the milling chamber to be reduced more and more. Therefore, a maximum value of the size is set thanks to the design of the process. Consequently, the choice of the type of impeller and of screen is fundamental to achieve the desired specifications for the process. The variability of the choice allows to cover a wide range of applications, which goes from the pharmaceutical to the food industry. In this work a square impeller has been used, while a Glatt® scratching screen has been chosen with a nominal holes' diameter equal to 2.0 mm. This coupling ensures a fast and strong grinding of the ribbons. Figure 2.5 shows the section of the milling chamber to highlight the square impeller and the screen used to control the granules size, with the oval shape and dimensions of its holes. It can be noticed that, although the nominal size of the screen aperture is 2.0 mm, the real dimensions, which were measured through a caliper, are 2.6 mm for the long radius and 2.0 mm for the shortest one. The volume of the milling chamber was calculated through the geometrical dimensions of the truncated cone of the screen and the value was found to be equal to almost 320 cm^3. The volume allows to frame the amount of material that can be processed in this device.

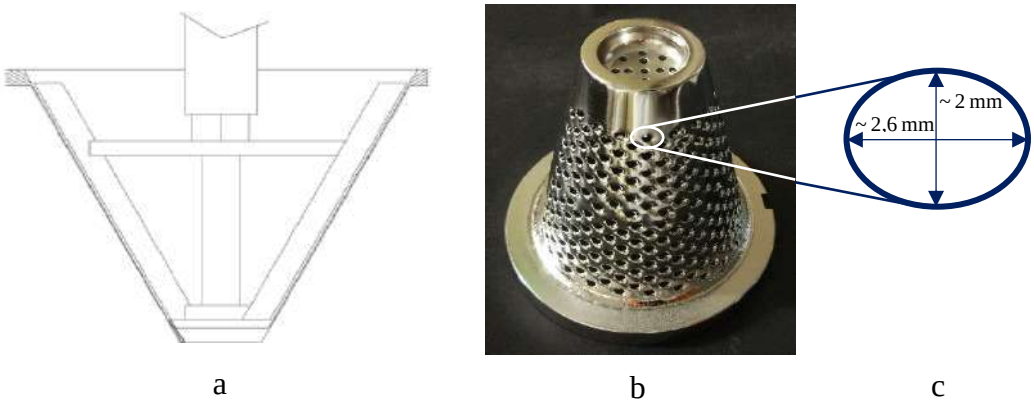

***Figure 2.5** - Vertical section of the milling chamber and structure of the impeller (a) and the Glatt® screen inserted in the milling chamber (b) with the detail of its holes dimensions (c)*

2.2.3 QicPic Sympatec

In this work a QicPic SYMPATEC™ has been used as device to determine the PSD and to perform the shape analysis by calculating the distribution of the shape factors already discussed in §2.1, which are the aspect ratio and the circularity. The machine performs the dynamic image analysis by measuring through a camera the volume of the particles, which are continuously flowing down in the camera tube. The structure of the QicPic can be observed in Figure 2.6 with the detail highlighted of the feed hopper where the particles to be analysed are loaded. At the top of the device, there is the vibratory feeder VIBRI, which

Figure 2.6 *- QicPic SYMPATEC™ machine and detail of the feed hopper* [68]

ensures a constant and optimized particle flow with a set feed-rate. The free movement of the particles leads to a random orientation and so, the actual shape and size of the particles of the sample can be precisely determined from different perspectives. The feed of particles is continuous and ensures reliable and representative results based on statistically significant number of particles. Roughly for general pharmaceutical powder 3 g is a consistent amount of material to feed to the QicPic. The high-quality image analysis is guaranteed by a high-resolution and high-speed camera able to capture up to 500 frames per second. Then the QicPic algorithm evaluates the millions of frames of the particles to determine the size and shape. Figure 2.7 shows the picture capture mechanism used during the flowing of the particles. The camera takes hundreds of frames per seconds of a part of the flow with an image angle highlighted in the figure. The GRADIS free-fall shaft controls the dispersion of compact particles and granules. The electrostatics particles can be easily dispersed by coating the GRADIS with a conductive surface. For the characterization of the particles, the evaluation regards the type of diameter analysed. The equivalent projection area of a circle (EQPC) is the transformation of the projection area of the particle into an equivalent circle (mm^2). The other important measure is the Feret diameter, which describes the particle through the distance of two parallel tangents. The two most important diameters are the maximum and minimum Feret diameter (F_{max} and F_{min}), which represent the longest and

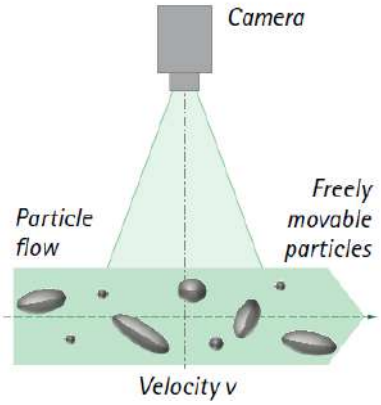

***Figure 2.7** - Scheme of the camera and the images capture of the QicPic [68]*

shortest extension of the granule, respectively. The aspect ratio AR is given by the ratio between these two diameters (μm), as follows:

$$AR = \frac{F_{max}}{F_{min}} \tag{2.1}$$

The evaluation of the PSD is performed through the EQCP and the charts, such as the one of Figure 2.1, show the cumulative distribution of the sizes in terms of fraction percentage of particles (based on the volume). The interval of particle sizes captured by the instrument goes from 5 μm to 4 mm. The other typical factor reported in PSD QicPic charts is the distribution density, which is the distribution of the particles in terms of volume and allows to understand which class sizes represents the main ones in the population of particles. The other shape parameter that is calculated and outlined in a chart by the QicPic is the circularity, which has been already presented in §2.1. It is defined as the circumference of the circle of equivalent area divided by the perimeter of the projected particle. The following expression can summarize the definition:

$$\varphi_p = \frac{\sqrt{(4\,\pi\,A_p)}}{P_p} \tag{2.2}$$

where A_p (mm^2) is the projected area of the particle and P_p (mm) is the perimeter of the projection of the particles. This value is automatically calculated by the QicPic software for each class of size and the distribution is outlined, as shown in Figure 2.2. The value of the circularity can vary from 0 to 1, where 1 corresponds to a particle with the shape of a perfect sphere and the lowest values represent much more irregular shapes.[68] Therefore, the SYMPATEC technology ensures the determination of the profiles of a population of particles, by evaluating and displaying graphically the most important powder characterization factors, such as the PSD, the AR and the circularity.

2.2.4 Humidity Chamber

In order to perform the experiments regarding the study of the effect that the humidity produces in the powder behaviour, a humidity chamber CLIMACELL^{TM} has been used. It represents a conditioned chamber where reproducing specific environment conditions inside. It is a useful device to keep constant different parameters, such as the temperature and the humidity level and to perform the desired tests. The working temperature goes from 0°C to 100°C in a dry environment and from 10°C to 95°C with humidity. The medium used to change values of the environmental humidity is demineralized water, and the range of humidity that can be set is 10%-98% of relative humidity. The refrigerant used in the machine is R134. The CLIMACELL is reported in Figure 2.8. The main applications of this machine regard the stability tests, research of germs and plant cultures, as many different natural climatic conditions can be easily reproduced in the CLIMACELL environment.[9-W] Besides, it is equipped with an internal lighting system, which can be coupled with the specific environmental conditions to guarantee the growth of the biological samples. In order to change the moisture content of a powder a thin layer of material is held in one of the shelves of the chamber for a set period, which changes in relation to many parameters, which involve the type of powder, the value of the humidity level of the environment of storage and the amount of material to treat.

Figure 2.8 *- Humidity chamber CLIMACEL^{TM} used to perform the experimental study of the humidity effect in the powder behaviour* [9-W]

2.2.5 Moisture Analyser

A moisture analyser has been used to determine the moisture content of the powder during the experiments. The main purpose was to ensure that the humidity level of the material has been kept constant during the entire experimental phase, in order to guarantee reliability to the results. Besides, it has been used to calculate the moisture content of the powder stored in environments at different humidity levels. This allows to relate the achieved results to the effect of water content of the MCC. The moisture analyser used is OHAUS® MB 35. It is characterized by a fast halogen heating system which ensures short time of measure. The readability performance of the weight is equal to 0.001 g, while the moisture sensitivity is equal to 0.01%. The system of measure requires a minimum weight of material which is equal to 0.5 g. Then the system is isolated, and the heat is provided at a set maximum temperature, which can go from 50°C to 160°C. The choice of the heating temperature requires the knowledge of the physicochemical properties of the material processed, as the purpose is to not degrade it or to change its state. Then, the moisture content is determined by weighing the powder until it becomes completely dried and the weight does not change anymore. The repeatability of the measure is equal to 0.10%.[69] Figure 2.9 illustrates the OHAUS MB 35 moisture analyser. The display shows the moisture content during the measurement and the final value determined by the analysis at the end of the heating time. The powder is added over a thin metal plate, suitable to a fast transfer of heat to the powder. The initial weighing needs to be done manually, by tare first the plate. Then, once the temperature has been set, the experiment carries on automatically and the display shows at the end the actual moisture content, the weight of the dry powder and the time required to perform the measurement.

***Figure 2.9** - OHAUS® MB 35 Moisture analyser used to determine the moisture content of the powder [69]*

2.3 Structure of the Experiments

The experiments performed in this works regard the simulation of the dry granulation process in a laboratory scale. The purpose of this project is the study of the effect of the change of different parameters in the PSD of the granules after the milling process and the following modelling of the milling step. Therefore, the method adopted first concerns the production of the ribbons from the raw material, which is the MCC Avicel® PH 102. Then, the ribbons are characterized and milled in the conical mill chosen and described in §2.2.2. The different milling conditions are tested and the effect of the impeller rotational speed is studied to determine its contribution in the production of fines and in the overall final PSD of the milled granules. The granules produced during the milling step are then analysed through the QicPic. The powder involved in all the experiments is the same, although the humidity of the environment of storage is tested at different values in order to study the effect of the moisture content in the powder behaviour during the dry granulation process. The scheme of the procedure followed in this work is highlighted in the scheme reported in Figure 2.10. The methods adopted starts from the production of ribbons from the raw powder of MCC 102 and it ends with the modelling of the results of the experimental phase, which were achieved by analysing the PSD of the granules generated through the milling of the ribbons in the conical mill.

Figure 2.10 *- Scheme of the procedure of study followed in this work*

Each step of the scheme showed in Figure 2.10 is characterized by different purposes and features studied. In order to achieve the target of this work, in the first step different batches of ribbons are produced at different levels of porosity and different thicknesses. Besides, more groups of ribbons are produced from MCC 102 powder stored in environments at different humidity levels, which takes to different moisture contents in the excipient powder. Then, the milling of all these batches of ribbons is performed in order to study the process at different rotational speeds. During each milling test two samples are collected, in order to study the PSD during the grinding. The final step of the experimental phase concerns the QicPic analysis of the granules, which aims to find the PSD of the population of particles. The results achieved are, then, used for the implementation of the PBM, in order to develop a model suitable to predict the PSD of the granules after the milling process, starting from batches of ribbons at different levels of porosity. Figure 2.11 shows the scheme of the procedure adopted and the conditions and parameters studied during each step of this work.

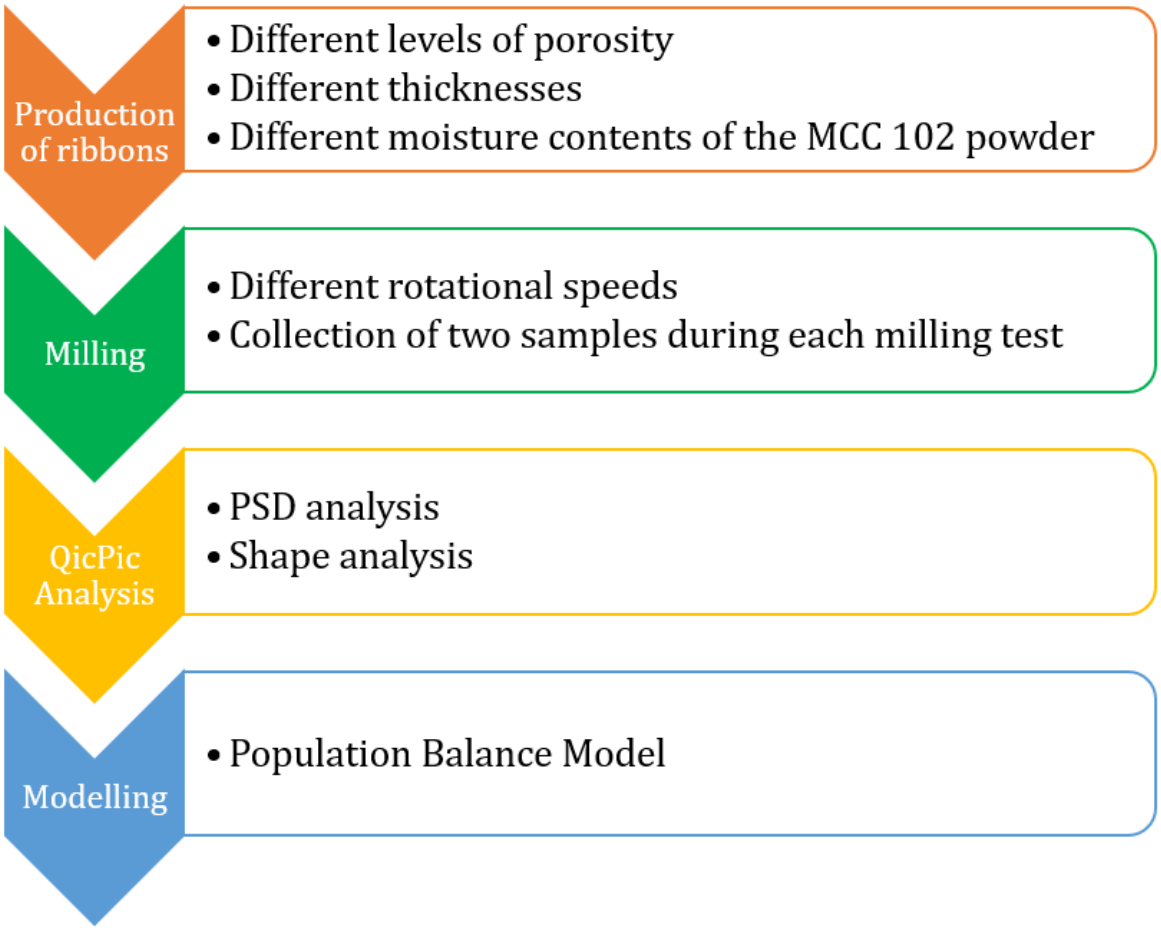

***Figure 2.11** - Scheme of the procedure followed and main parameters studied during each step of this work*

2.4 Methodology of Different Experiments

This section aims to present the methods followed in the experimental phase of this work. For each step the technical procedures used will be deeply described in order to explain the entire methodology adopted to simulate the dry granulation process and in order to ensure the reliability of the results achieved. Therefore, first, the ribbons production process will be presented, then the milling step and the PSD analysis will be outlined.

2.4.1 Ribbons Production

The production of ribbons is carried out using the Instron 1175 and the die described in §2.2.1. More batches are produced at different compression forces of the machine in order to produce ribbons with a wide range of porosities. Each ribbon is produced by adding a set mass of powder MCC 102 inside the cylindric cavity of the die, between two coin-shaped plugs, which transfer the compression and give the circular and cylindric shape to each

ribbon. The powder is measured by a suitable scale with the sensitivity equal to 0.01 g. Then, the die is placed in the Instron press platform, and the cell load is brought closer to the die. The desired compression force and speed is set through the software. As compression speed the same value has been set for all the tests and it is equal to 5 mm/min. Hence, the test is performed. During the compression the software collects the data of the force applied to the die as function of the length travelled. When the machine reaches the value of force desired it stops and it retires, moved by the relaxation traction of the compressed powder, until the sensors of the Instron do not detect forces form the die, anymore. Then, the ribbon is extracted from the cavity and it is characterized. Therefore, its weight is measured by a scale, in order to compare the mass added to the die and the weight of the ribbon. Its dimensions are measured through a caliper, which allows to find the diameter and the thickness of each ribbon. The sensitivity of the caliper used is equal to 0.01 mm. The characterization is fundamental in order to find the bulk density of the compressed powder. It can be calculated by dividing the weight by the volume of each ribbon. This is determined from its diameter and thickness, by using the formula for the volume of a cylinder. Then, the porosity of the

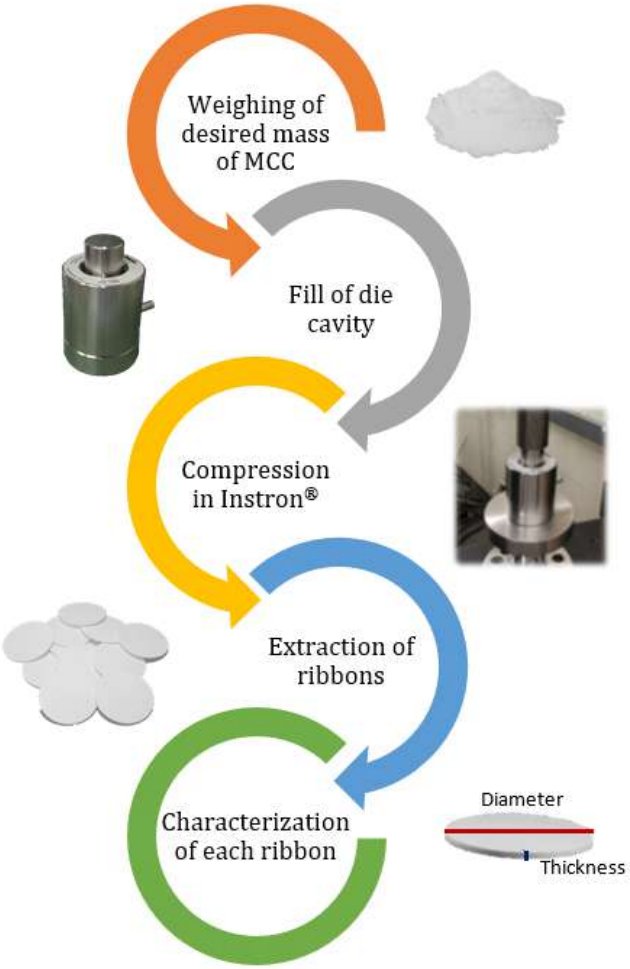

Figure 2.12 *- Scheme of the procedure for the production of ribbons*

ribbon is calculated from the equation 1.1. The scheme of the experimental steps that take part in the production of ribbons is highlighted in Figure 2.12. In order to achieve the first experimental target of this work, five different levels of porosities are chosen. The mass set for each ribbon is equal to 1 g of MCC 102 and it allows to produce a thin but handleable ribbon. The range of porosities goes from 50% to 20%, roughly, and the five averages of porosity of the produced batches for this part of experiment are: 48%, 40%, 36%, 28%, 25%. They were achieved by setting the following compression forces, respectively, to the Instron 1175: 15 kN, 22.5 kN, 30 kN, 45 kN, 60 kN. Each batch consists in 18 ribbons, which ensures to have, at least, 18 g per milling test. This amount of mass is sufficient for a good analysis of the PSD of the milled granules in the following measurement through the QicPic. The production of each batch of 1 g ribbons of a set level of porosity is repeated for three times, as the following milling step aims to study not only the effect of the porosity, but also the effect of the impeller speed in the grinding process, at the same ribbon properties. Indeed, three impeller speeds are set to find the effect of this factor in the final PSD, and they are equal to 100 rpm, 200 rpm and 350 rpm.

Then, the effect of the thickness is analysed, in order to find if it can affect the granules PSD at the same ribbon properties and the same operating conditions. In order to perform this kind of experiments, more than 1 g of mass is added to the die cavity and this increase differs according to the porosity desired and the compression force set. Therefore, more ribbon batches are produced at two set values of thickness: 1.60 mm and 2.00 mm. Regarding the thickness equal to 1.60 mm, five batches of ribbons are produced with the following level of porosities: 40%, 36%, 28%, 24% and 18%. The value 1.60 mm has been chosen because it represents, roughly, the thickness of the group of ribbons produced with 1 g at 15 kN, and, so, the comparison with this batch is also possible. While for the 2.00 mm of thickness just two more batches of ribbons are produced with 34% and 21% of porosity. These values differ from the other batches, nevertheless they are the closest levels reachable in order to keep constant the compression force and the thickness at 2.00 mm.

The following part of the experimental phase concerns the study of the effects of the environmental humidity to the PSD of the granules after the milling process. In order to perform these tests, three samples of raw powder of MCC 102 have been stored in the humidity chamber, described in §2.2.4, at three different levels of relative humidity and at the set temperature of 20°C. While the environmental humidity of the ordinary storage room of MCC 102 is equal to 30%-50%, roughly, the three levels set in the humidity chamber are: 20%, 50% and 80% of relative humidity. Each sample of powder is spread in large surface to create a thin layer of powder able to ensure a good contact of the powder with the environment. They are stored for 2 weeks, at least, and periodically the powder is mixed in

order to guarantee that all its parts are in contact with the environment. The moisture content is monitored through the moisture analyser, described in §2.2.5, during the two weeks and the powder is removed from the chamber, only when the values of the moisture reach an equilibrium and so, they show the same content, for at least 5 days in a row. Then, the powder is immediately compressed into ribbons. For each level of humidity, two batches of ribbons are produced at two set compression forces: 30 kN and 60 kN. Then, each group of ribbons with the same properties is milled at the impeller speed equal to 200 rpm. The last part of the experimental phase regards the modelling validation. Therefore, three more batches of ribbons are produced at different porosities values: 42%, 32% and 21%, by compression at the pressure values of: 19 kN, 37.5 kN and 90 kN, respectively. Then, they are milled at 300 rpm, 150 rpm and 200 rpm, respectively. All the batches of ribbons produced are reported in Table 2.1, which summarizes all the experiments performed. The table reported the mean of the percentage level of porosity of each batch of ribbons and the standard deviation of the group.

***Table 2.2** - Summary of all the batches of ribbons produced during the experimental phase. The values reported in the cells represent the mean of the porosity (%) of each batch ± the standard deviation of the group of ribbon*

Specification: 1 g of mass per ribbon						
Compression force (kN)		*15*	*22.5*	*30*	*45*	*60*
Impeller speed (rpm)	*100*	49.3 ± 1.2 %	-	35.4 ± 1.6 %	27.9 ± 1.2 %	25.4 ± 1.6 %
	200	48.5 ± 0.7 %	40.4 ± 0.5 %	36.4 ± 0.8 %	28.3 ± 0.8 %	25.6 ± 1.5 %
	350	48.3 ± 0.5 %	-	35.9 ± 1.1 %	28.0 ± 0.8 %	25.8 ± 1.3 %
Specification: 1.60 mm of thickness per ribbon						
Compression force (kN)		*22.5*	*30*	*45*	*60*	*90*
Impeller speed (rpm)	*200*	40.4 ± 0.6 %	35.4 ± 0.4 %	27.9 ± 0.6 %	24.1 ± 0.7 %	17.8 ± 0.7 %
Specification: 2.00 mm of thickness per ribbon						
Compression force (kN)		*30*			*60*	
Impeller speed (rpm)	*200*	33.7 ± 0.4 %			21.5 ± 0.4 %	

Specification: 1 g of mass per ribbon from MCC at 20 % of Humidity		
Compression force (kN)	*30*	*60*
200	40.1 ± 0.7 %	26.7 ± 1.3 %
Specification: 1 g of mass per ribbon from MCC at 50 % of Humidity		
Compression force (kN)	*30*	*60*
200	35.3 ± 1.5 %	24.0 ± 1.7 %
Specification: 1 g of mass per ribbon from MCC at 80 % of Humidity		
Compression force (kN)	*30*	*60*
200	27.6 ± 0.9 %	22.0 ± 1.2 %

Specification: Validation of the model, 1 g of mass per ribbon				
Compression force (kN)		*19*	*37.5*	*90*
Impeller speed (rpm)	*150*	-	31.0 ± 1.6 %	-
	200	-	-	21.5 ± 0.9 %
	300	42.3 ± 0.5 %	-	-

2.4.2 Milling

The milling is performed after the characterization of the ribbons. It represents a fundamental step in the dry granulation process, as it allows to produce the granules with size suitable for the following compression into the final tablets. It is a critical process due to the importance of the size of the granules, which represents one of the main factors that affect the quality of the pharmaceutical tablets. Therefore, the improvement of the effectiveness of milling and the study of its operating conditions are necessary to achieve the best performances of process and the best results. This represents the main purpose in the analysis of milling performed in this study. In particular, the impeller speed of the conical mill is deepened, in order to understand which conditions can improve the PSD of the granules. The analysis on the amount of fines related to the porosity and the impeller speed represents one of the path followed in this phase. Besides, the milling time and effectiveness will be studied as process

conditions change. The procedure of analysis has been developed during the first preliminary laboratory tests, whose purposes consisted in the setting up the best experimental configuration. As one of the purposes of this work was the dynamic study of the milling step, two samples have been collected during each test at different times, in order to analyse the PSD of the granules during the process. This allows to evaluate how the milling performances can change during the time. The first sample is collected after 10 seconds of milling, while the second one is collected at the end of the process. In order to evaluate the milling efficiency and time, a beaker is placed over a scale, which is used to measure the weight of the granules, live. Then, these tools are positioned with a funnel under the milling chamber, in order to collect all the milled products. The process is switched on one time per each sample to collect, so two times in the same test. The impeller speed range of the conical mill goes from 20 rpm to 400 rpm, but the conditions at the edges of the range are not considered in this study, as the device at 400 rpm does not show stable conditions during the rotation of the impeller. The speed analysed in the main part of the experiments are 100, 200 and 350 rpm, while 150 and 300 rpm are set in the final tests used to validate the model. The conditions of the impeller speeds of all the different tests are reported in Table 2.2, in the left columns. The conical mill used is suitable to this kind of analysis, which involves the collection of two samples during the same tests, as the start and stop setting up can be performed without disturbance from the impeller rotation. Indeed, this one stops immediately when the conical mill is switched off, instead of turning freely until the attrition forces stops it. So, the granules collected represents a reliable sample for the study of the PSD, as they are entirely produced at the milling speed set. The typical granules collected during the milling phase are reported in Figure 2.13, which shows the products of a test batch of ribbons with a mean porosity equal to 36.2%. Both larger granules and fines can be observed in the figure.

Figure 2.13 *- Granules produced after the milling of a test batch of ribbons with an average porosity equal to 36.2%*

2.4.3 Particle Size Distribution (PSD)

As already specified in the previous sections, in this work the PSD of the milled granules is the main parameter used to analyse the quality of the dry granulation process. It represents the weighed distribution of the particles as function of their class size. The determination of the PSD is performed through the QicPic SYMPATEC and it is then processed in order to outline the desired configuration of the results. The weight frequency has been chosen in order to show all the results regarding the PSD. In particular, the normalized frequency is performed in the charts of the experimental and modelling phase. The measure of the quantity of particles is given by the weight percentage of the particles of each class size (y-axis of the frequency plot), while the property of interest is the class size itself, which is the function along whom the distribution is outlined (x-axis of the frequency plot). So, the normalized frequency (%/μm) can be described by the following expression:[70]

$$f_N(x) = \frac{percentage\ of\ mass\ (\%)}{class\ size\ (\mu m)} \tag{2.3}$$

Besides, also the weight cumulative distribution is usually reported in the charts which regard the PSD of the granules and it helps to describe more in depth the results and to outline the overview of the distribution of the entire mass in the population of granules. This kind of distribution is plotted against the upper bond of each class size, while the normalized frequency $f_N(x)$ is plotted against the midpoint of each class size interval.

The other factors used in order to describe the PSD are represented by the d_{10}, d_{50} and d_{90} which represent the 10th, 50th and 90th percentiles of the PSD, respectively (μm). Besides, the volume mean diameter is widely used and it is represented by the following equation:

$$VMD\ (\mu m) = \frac{\sum_{i=1}^{n} D_i^4 v_i}{\sum_{i=1}^{n} D_i^3 v_i} \tag{2.4}$$

Where D_i (μm) is the geometric diameter of each class of size i. Instead v_i (%) is the percentage of that class size i. The variable n is the number of class size in the distribution. The other important factor used is the relative span (already reported in Table 2.1) which can be defined as:

$$Span = \frac{d_{90} - d_{10}}{d_{50}} \tag{2.5}$$

In order to calculate the percentage of mass the QicPic is used to analyse the samples collected during the milling. Each measure needs 1 g of granules, at least. The reliability of the results is ensured through three measures at the same sample. The milled granules are collected in a plastic bag after the process and they are mixed and dropped vertically on a blank sheet in order to create a stack of granules where the different sizes are distributed quite homogeneously in the radius of the base of the stack. Then, a slice of the stack is selected in order to take granules from the centre to the edges of the stack itself. This portion ensures a statistical reliability of each of the three measures. Now, the mass can be analysed in the QicPic. At the end, the three measures are averaged in order to get the cumulative PSD and the normalized frequency distribution of each sample. The same procedure is followed in order to find the shape profile of each sample collected.

Chapter 3

Experimental Results

In this chapter the results achieved during the experimental phase will be presented and discussed in depth. The first part will concern the characterization and the statistical analysis of the produced ribbons. Then, the milling kinetic will be discussed. The final and most important analysis is related to the description of the QicPic results and the comparisons between the PSD of the different batches in order to study how the operating conditions of the dry granulation process can affect the size of granules.

3.1 Ribbon Characterization

The ribbon produced during the die compaction step are characterized one by one, in order to find the mass, thickness and diameter of each tablet. These factors are fundamental to calculate the volume of each cylindrical ribbon and the porosity by using the equation 1.1. The batches of ribbons produced with their average porosity value have been already presented in §2.4.1. Each value of porosity, thickness, diameter and mass, which will be reported, represents the average of all the ribbons which constitute each batch produced. All these averages can be found in appendix. In the following pages the comparisons of the main values will be described, in order to understand the relationships and the influences between some factors, as the compression force and the moisture content and the values of those parameters (thickness and porosity).

By considering the tests carried out in this work, which have been summarized in Table 2.2, the first characterization to carry out concerns the study of the relationships among the porosity and the compression force used in the die compaction step. This one is reported in Figure 3.1, where the values of the porosity related to the set compression force represent the average of the three ribbon batches porosities produced with 1 g of mass per tablets and then milled at three different impeller speeds. The figure highlights that the increase of the compression force leads to the decrease of the level of porosity, as the compaction of the powder is better performed. The chart shows that the relationship is sharper at lower compression force, while the decrease is smoother at higher pressure, underlining that the compaction of the powder is already advanced at 45 kN and the porosity is approaching a limit. The value at 90 kN is related just to one batch of ribbon, produced with the aim of the

validation of the model, at the same conditions of the other ones. Between the lowest compression force, equal to 15 kN, and the highest one, equal to 90 kN, the porosity is more than halved, going from 48.7% to 21.5%. The values studied in this work include a wide range of porosities, allowing a good analysis and comprehension of the possible relationships between the porosity and the factors which will be deepened, especially the PSD.

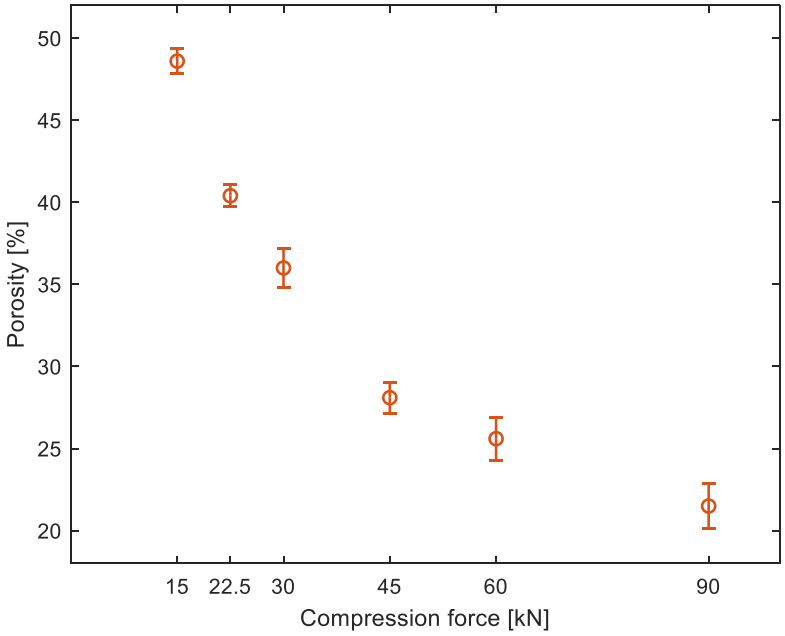

Figure 3.1 *- Porosity value with the standard deviation interval of the ribbon batches produced at the set compression force. Each ribbon has been made with 1 g of MCC 102*

As the thickness represents a parameter which will be studied to understand its influence in the production of fines and the PSD, in Figure 3.2 the relationship between the thickness of the same batches of ribbons of the previous chart and the porosity is reported. The porosity levels reported in the *x* axis represent the values of the *y* axis of Figure 3.1. So, through an easy comparison the relationship between the thickness and the compression force can be outlined qualitatively and it can be found to be very similar to the previous chart. Indeed, the trend found in Figure 3.2 highlights a linear relationship between the thickness and the porosity. The regression coefficient underlines a good linearity value as it is equal to 0.987, while the linear relationship is reported in the figure. The trend shows that the thickness of a ribbon increases by increasing the level of its porosity. This can be easily explained by considering that a better compaction, which represents a lower level of porosity, means that the tablet is thinner, as the compression force applied is greater. The standard deviation of all the groups of ribbons goes from 0.01 mm to 0.02 mm. Therefore, inaccuracies in the analysis could be neglected, as the value is smaller than 2% of the average thickness, although experiments have usually minimum imprecisions.

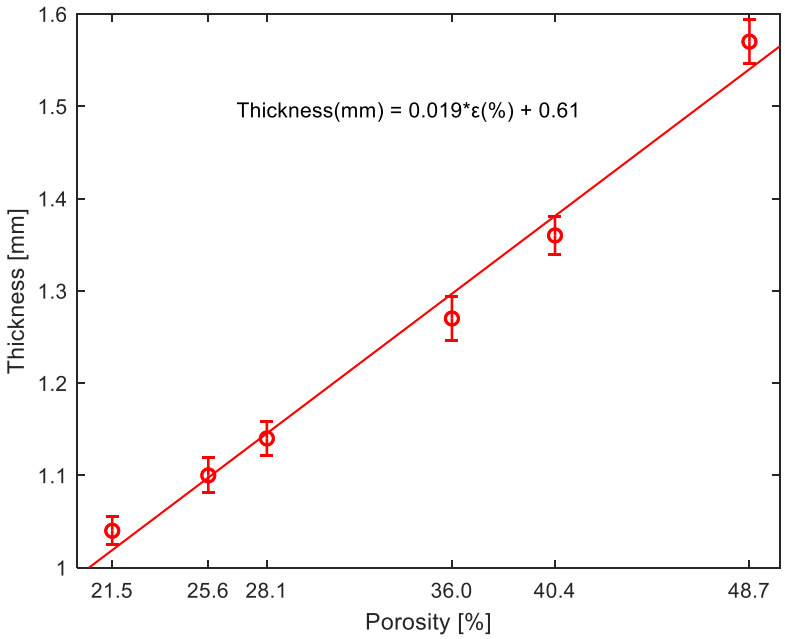

Figure 3.2 *- Thickness of the ribbon batches as function of the porosity. Each ribbon has been made with 1 g of MCC 102*

The experiments regarding the production of batches of ribbons at the same thickness, equal to 1.60 mm, and set compression forces, but with different mass per ribbons are performed and the relationships among the thickness used and the porosities are reported in Figure 3.3. The values of the compression forces and the diameters are reported in the Appendix, together with all the other groups of ribbons.

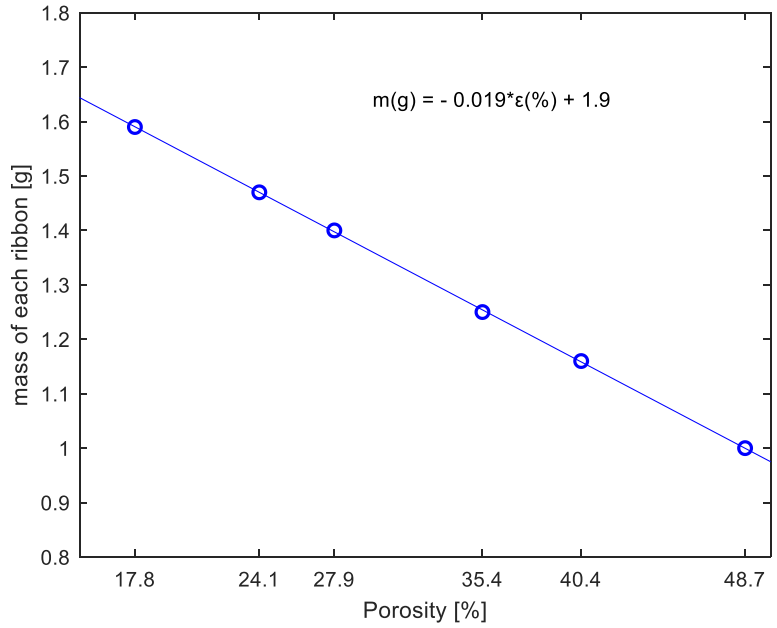

Figure 3.3 *- Mass of each ribbons used to produce tablets of a set thickness equal to 1.60 mm and different levels of porosity*

Figure 3.3 shows that there is a linear relationship between the mass used and the porosity achieved, by keeping roughly constant the thickness of ribbons. Indeed, the regression coefficient is equal to 0.999, indicating the high quality of the linear behaviour. Therefore, by increasing the compression force, and so decreasing the porosity, in order to produce a ribbon with a 1.60 mm of thickness, an increase of the mass to add is necessary. As Figure 3.2, this chart shows the experimental points highlighted by a circular mark and the fitting straight line, with its equation. By considering that the compression forces used are the same of the ones chosen for the experiments with 1 g of mass per ribbons, the porosity changes more by increasing the pressure. Indeed, with a compression of 90 kN, the porosity goes from 21.5% with 1 g of mass to 17.8% with 1.59 g of mass per ribbon. The deviation of the values of porosity decreases by increasing the porosity, and so by decreasing the compression forces used, until 22.5 kN, where both the groups of ribbons have the same porosity level, even if there is a small difference with the mass used per ribbon. This result underlines that the compaction of the powder is stronger if more mass is added to the die cavity and so, if the ribbons are heavier. Indeed, if the difference of mass used is larger and the compression force is greater the porosity level change is more pronounced.

The study of the effect of the moisture content in the thickness changes has been performed in order to understand how the humidity of the environment can affect qualitatively the compaction of the powder. The moisture contents measured through the moisture analyser for the powder stored at different humidity levels are reported in Table 3.1, where also the moisture content of the original powder is reported. The relative humidity of the environment of the powder in the Surrey particles laboratory can be set in the range of 35-50%.

Table 3.1 *- Moisture contents of the MCC 102 at different humidity levels of the storage environment*

Relative Humidity (%)	**20**	**50**	**80**	**(35-50)**
Moisture content (%)	*4.14*	*6.32*	*9.33*	*6.02*

The moisture content showed in Table 3.1 goes from roughly 4% to 9%. By considering the great range of humidity levels studied (20-80%), the difference of water content is quite small. Nevertheless, a variation is noticeable and so the storage conditions could affect the properties of the powder and they could represent a relevant factor in the overall dry granulation performances. The study of the moisture content influence in the compaction of the powder is summarized in Figure 3.4, where the thickness of the ribbons produced from the powder stored at different environmental humidity is related to the actual moisture content of the powder used to produce the ribbons and the compression force set in the die compaction step.

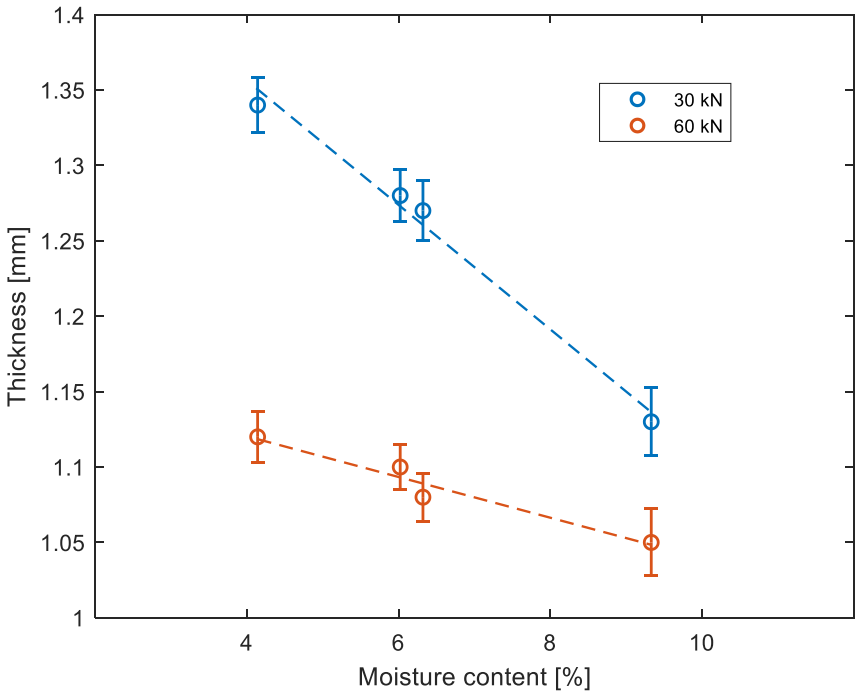

Figure 3.4 *- Thickness of the ribbons produced by powder with different moisture contents at two different compression forces: 30 kN and 60 kN*

Figure 3.4 shows that the thickness of ribbons decreases by increasing the moisture content of the powder, the relationships seem to be quite linear, even if the number of points is very low to prove that. Therefore, as expected, the water stored in the powder helps the compaction into ribbons. The difference in the thickness is more relevant for the lower compaction force, while for the group compressed at 60 kN the decrease is less sharp. Besides, for instance, it can be observed that the drier powder with 4.1% of moisture content needs double pressure to be compressed at the same thickness with respect to the wetter powder with a water content equal to 9.3%. So, the water content has a greater impact if the pressure used to produce the ribbons is lower. This result agrees with literature where the bonds among particles of powder have been studied in order to achieve a better understanding of the compaction behaviour. It has been found that with more water the formation of solid bridges among the particles occurs and it takes to more compacted tablets. This implies the production of stronger ribbons.[34] The following PSD of granules will be then studied in order to understand if the moisture content affects the distribution directly or if the differences in thickness, resulting from the different water contents, are responsible to possible variations of the PSD of milled granules.

3.1.1 Statistical Analysis

This paragraph regards the statistical analysis on the ribbons. The aim is the development of a study that can prove reliability to the results achieved during the experimental part. The analysis on the ribbons' porosity lets to understand if the comparisons between the different batches of ribbons are grounded on a solid base under a statistical point of view. The analysis has been performed through Minitab®.

The purpose is to carry out an ANOVA for the batches at the same level of porosity to understand if there is any kind of difference among the groups. This study shows if the averages of the samples are statistically different or not. The following figures show the boxplots of all the components which form a group of ribbons. This kind of charts allows to observe the four quartiles of the population, highlighting the two central ones, which represents the central 50% of the components. Besides, the average of each group is marked through a circle. These boxplots show the distribution of porosity in the population, in order to understand if all the ribbons produced at the same conditions have the same level of the property. The number reported below each distribution in the chart represents the impeller speed used to mill the group. The batches of ribbons analysed are the ones with 1 g of compressed MCC 102 and the ones with 1.60 mm of set thickness.

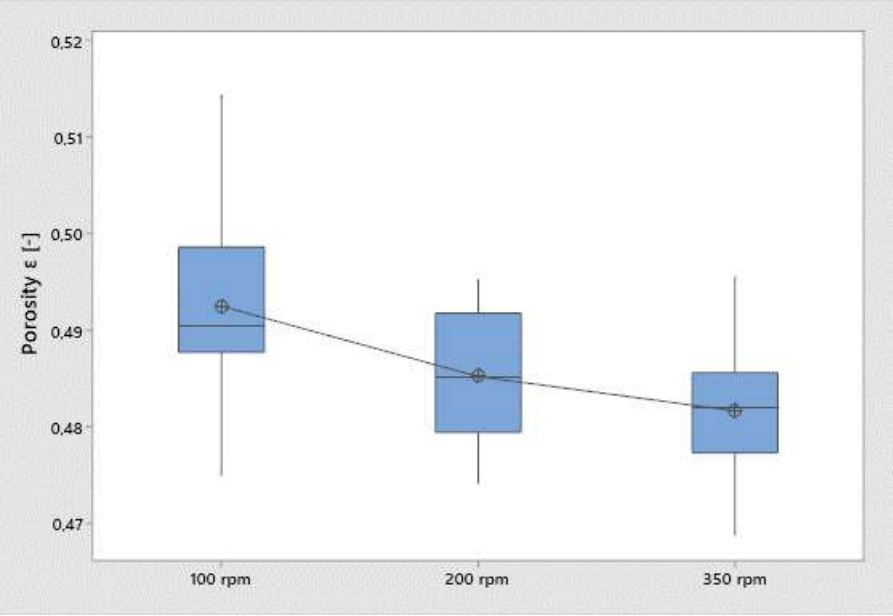

Figure 3.5 *- Boxplot of the batches of all the ribbons of 1 g of mass produced at the compression force equal to 15 kN*

Regarding the batches of ribbons compressed at 15 kN, the variances have been proved to be homogeneous among the three different batches (100, 200, 350 rpm), through the Levene's test. Besides, the samples have been collected casually and the normality of the

distribution has been proved. So, the three conditions necessary to carry out the ANOVA have been verified and the study has been performed. As can be seen qualitatively in Figure 3.5, there is a relevant difference between the 100 rpm and the 200 and 350 ones. The ANOVA shows that there is no statistical difference between 200 and 350 rpm batches, but there are differences statistically significant between 100 rpm batch and the other two ones. This means that the results achieved by the analysis could be lacking in reliability in the comparisons among the 100 rpm and the other 48% of porosity batches, although the difference is quite small and should not represent a problem for the analysis of the main effects of porosity and impeller speeds.

Concerning the batches of ribbons produced at 30 kN of compression force, they have a level of porosity which is roughly equal to 36%. The analysis on the variance through the Levene's test shows that the variances are not always homogeneous among the batches. This could be a problem for the application of the ANOVA. Nevertheless, by considering that the samples have the same wideness, the ANOVA results are not so influenced by differences among the variances, so it can be applied to this study. However, Welch's ANOVA can be performed to this analysis, because it lets to study the differences of the means of samples with different variances. The first three batches are the ribbons produced with 1 g of mass, while the fourth one has been made at the set thickness equal to 1.60 mm.

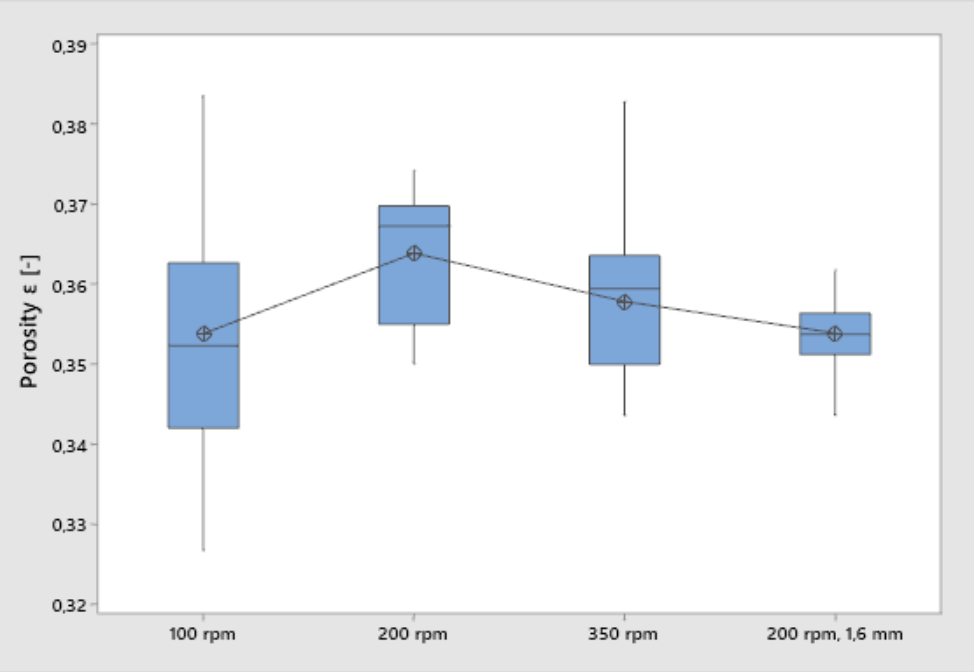

Figure 3.6 *- Boxplot of the batches of all the ribbons of 1 g of mass produced at the compression force equal to 30 kN and the group of ribbons with 1.60 mm of thickness*

The analysis shows a statistical difference only between the means of the batches milled at 200 rpm made by 1 g and the group milled at 200 rpm with a set thickness equal to 1.60 mm. Nevertheless, through the Welch's ANOVA it has been proved that there is no statistical difference among all the other batches of ribbons. The boxplot above highlights a statistical description of the distributions of the four batches of ribbons. The 100 rpm one has got a huge variability, while the 200 rpm, 1.60 mm batch PSD is very narrow. This can be explained by considering that the caliper and the scale used to characterize the dimensions and the weight of each ribbons have a sensitivity equal to 0.01 mm and 0.01 g. Therefore, for thicker and heavier ribbons the impact of a measurement error should be reduced and, so, the variability of the calculated porosity decreases.

The batches of ribbons produced at 45 kN of compression force presents a level of porosity which is roughly equal to 28%. The homogeneity of the variances among all the four batches of ribbons has been verified through the Levene's test. So, the ANOVA can be implemented.

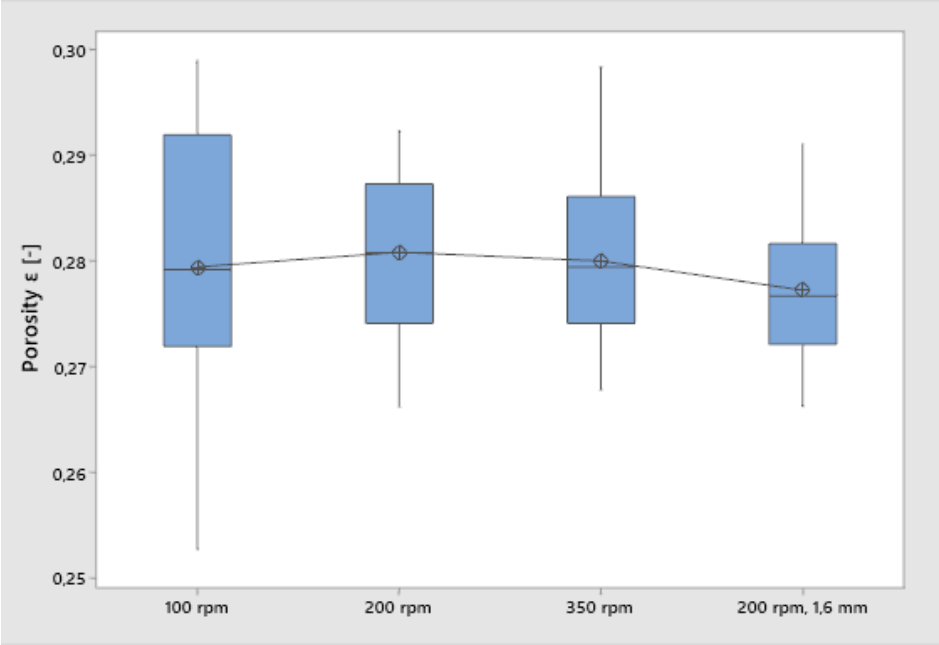

Figure 3.7 *- Boxplot of the batches of all the ribbons of 1 g of mass produced at the compression force equal to 45 kN and the group of ribbons with 1.60 mm of thickness*

The ANOVA test verifies that there are no differences among the means of the four batches of ribbons. Therefore, the porosity achieved is comparable and there are no statistical differences among the ones of the produced groups. This assigns a high reliability to the results achieved and the comparisons carried out among the results of the experimental part. The boxplot shows that even at this level of porosity the batch milled at 100 rpm has the greatest variability of the results.

Regarding the groups of ribbons produced at 60 kN of compression force, a level of porosity roughly equal to 25% has been determined. The homogeneity of the variances among all the four batches of ribbons has not been proved for all the four batches of ribbons analysed. So, the Welch's ANOVA has been implemented.

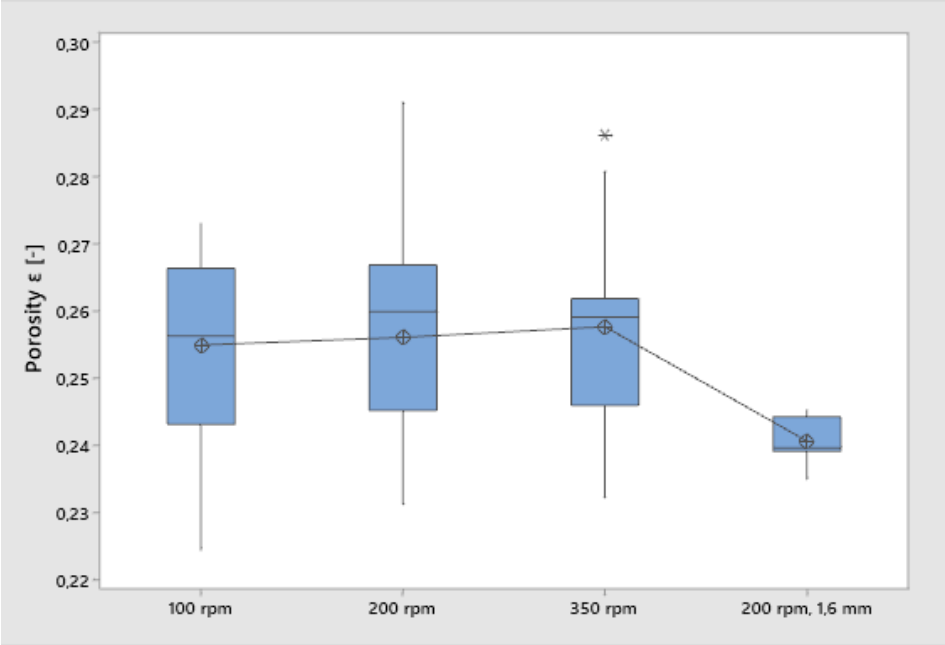

Figure 3.8 *- Boxplot of the batches of all the ribbons of 1 g of mass produced at the compression force equal to 60 kN and the group of ribbons with 1.60 mm of thickness*

The ANOVA test verifies that there are no statistical differences among the means of the first three batches of ribbons. Instead, the fourth batch mean (200 rpm, 1.60 mm) is statistically different with the means of the other three batches of ribbons. This assigns a good reliability to the results achieved and the comparisons carried out among the results of the experimental phase regarding the ribbons produced with 1 g of mass. Nevertheless, by increasing the mass to achieve 1.60 mm of thickness, the porosity of the ribbons is not statistically equal to the ones of the 1 g ribbons. This result can be observed also in the boxplot above, where the means of the fourth batch is clearly different from the other ones. As the previous cases, the batch at 1.60 mm of thickness (200 rpm, 1.60 mm) has the narrowest variability. This can be explained by considering that the production of these ribbons was performed at the end of the experimental phase, so after the gain of a greater experience in the ribbons die compaction. This could have allowed the researcher to produce ribbons with more precision and accuracy. Indeed, it could explain also the fact that the widest variability was achieved in the batches of ribbons produced during the first part of the experimental phase, which are the ones milled at 100 rpm.

3.2 Kinetic of Milling

The milling step has been studied not only for the analysis of the influence of its operating conditions, especially the impeller speeds, on the final PSD of the granules, but also in the effectiveness of the process. This evaluation has been performed by studying the milling time needed to mill the same amount of mass of different groups of ribbons. The purpose is the evaluation of the effect of the porosity and impeller speeds in the time of milling. In all the experiments 18 g of ribbons have been milled, but roughly 15 g of them have been found in the products, as some granules bigger than the sieve holes size were trapped in the bottom of the sieve itself and were not grinded anymore by the impeller. The mass left in the milling chamber is within 15% and 23% of the total mass of the ribbons fed. Besides, the final part of the milling shows a high variability among the experiments in terms of time to end the grinding of ribbon and it does not allow a reliable comparison. Therefore, the evaluation of the milling time has been performed by comparing the time needed to mill the 80% of the total mass found in the product of each experiment. Besides, the trend has been analysed by plotting the milled mass during the time of milling, thanks to the recording of the experiments and the live measurement of the weight of the produced granules. Figure 3.9 shows an example of the mass of ribbons milled during time of process. The trend is roughly the same for all the experiments carried out at different conditions, and it can be always modelled by a four-grade polynomial function with high quality of fitting (R-squared always greater than 0.95). The groups of ribbons reported in Figure 3.9 are the ones produced by 1 g of mass at 45 kN of compression force. Then, they have, then, been milled at a different impeller speeds: 100, 200 and 350 rpm.

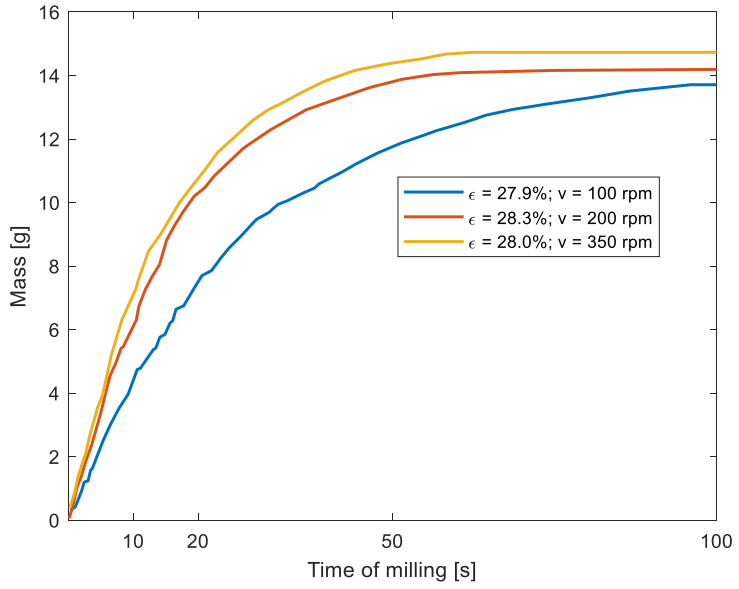

***Figure 3.9** - Milled mass of ribbons during the time of milling for batches of ribbons produced by 1 g of mass at 45 kN of compression force*

The results shown in Figure 3.9 underline that with a higher impeller speed the time of milling decreases, as expected. Besides, this trend can be observed for all the other levels of porosity. Although the charts are not reported in this paragraph, the results are roughly the same of the ones in Figure 3.9. The amount of mass fed to the conical mill has been always kept constant at the value equal to 18 g, although the mass milled has been found to change by changing the operating conditions. Indeed, Table 3.2 clearly shows that the weight of the milled granules decreases by decreasing the impeller speed and the level of porosity. This result proves that for stronger ribbons and for lower impeller speeds more granules with a size higher than the diameters of the holes of the sieve are trapped in the small dead-space between the bottom of the sieve itself and the lower tip of the impeller. As this is related to the milling time, the experiments underline that if the milling requires more time, the total amount of granules produced is lower and so a faster grinding process seems to produce more granules smaller than the screen holes size. This result will be further discussed in §3.5, where the analysis will focus on the production of fines, instead of the mass of trapped granules.

Table 3.2 *- Milled mass in g achieved from 18 g of ribbons during the experiments with batches of ribbons produced by 1 g of powder at different levels of porosity and, then, milled at different impeller speeds*

Porosity	**48%**	**40%**	**36%**	**28%**	**25%**	**21%**
100 rpm	15.27 g	-	14.64 g	13.71 g	13.80 g	-
200 rpm	15.30 g	15.18 g	15.14 g	14.42 g	14.24 g	14.07 g
350 rpm	15.30 g	-	15.26 g	14.75 g	14.89 g	-

Regarding the time of milling, the analysis focuses now on the comparisons of the different times achieved at different operating conditions. The times determined in order to perform a comparison of the effectiveness of the process are two: t_{80} and t_{40}. The first one represents the time (s) required in order to mill the 80% of the total weight of granules effectively produced, while the second one is the time (s) to mill the 40% of the granules. The choice of the t_{80} is led by the observation of a high variability in the final part of the milling among the experiments performed, which does not ensure reliability of the results in terms of kinetic comparisons. Indeed, some experiments needs more time just to mill the last centigrams of mass and this behaviour has been found to be random during all the experiments carried out. Therefore, the final time chosen is the t_{80}, while the mid-time considered is the t_{40}.

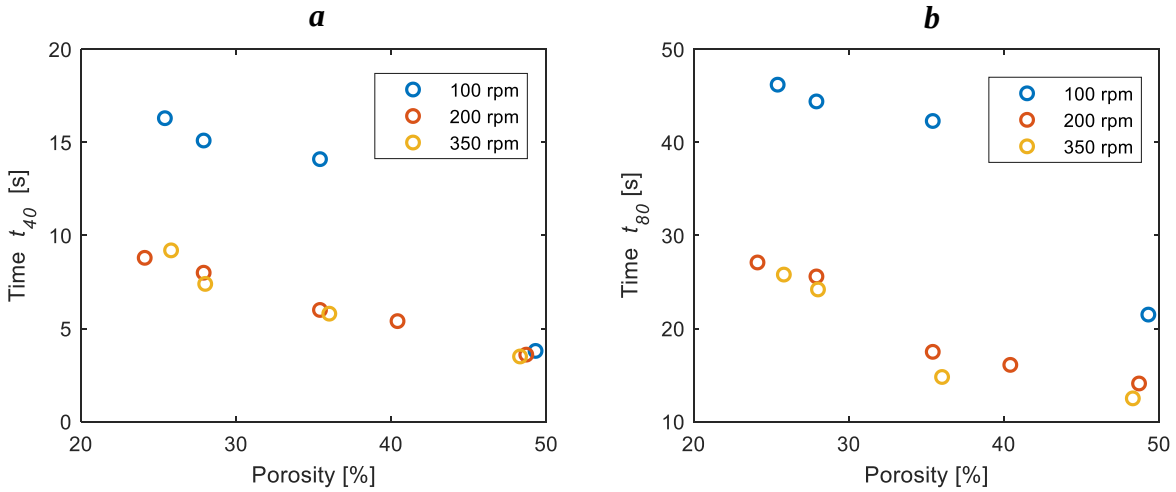

Figure 3.10 *- Milling times t_{40} (a) and t_{80} (b) as function of the porosity and impeller speed for the batches of ribbons made by 1 g of MCC 102*

Figure 3.10 shows the t_{80} and t_{40} of the different batches of ribbons made by 1 g of MCC 102. The results achieved underlines that the milling time increases by decreasing the level of porosity of the ribbons and by decreasing the impeller speed of the mill. This holds true for both the milling times analysed. The result is reasonable and expected, as strong ribbons are more difficult to be broken and faster impeller speeds should ensure a faster process. The differences observed are more relevant between the ribbons processed at 100 rpm and the other two velocities, than the ones between the 200 rpm and 350 rpm batches. Nevertheless, the trend of porosity and impeller speeds is clear and the small differences between these points can be explained by the fact that also the average of the ribbons' porosities is not perfectly homogeneous and that some random errors during the performing of the experiments can be involved especially during the collection of the data of the weight measured live.

Besides, the kinetic of the milling has been also analysed, by comparing the times t_{40} and t_{80} between the groups of ribbons at the same thicknesses (1.60 mm and 2.00 mm) milled at 200 rpm and the batch of ribbons made by 1 g of powder and milled at 200 rpm. The result is reported in Figure 3.11. The relationships among the different groups of ribbons are not so marked as in Figure 3.10, but some observations can be made. Indeed, it is quite homogeneous for all the levels of porosity that the milling time seems to be just a bit greater for the thicker ribbons, while it seems to decrease for the thinner groups of ribbons, which are the ones made by 1 g of powder. The points are not enough to ensure more reliability to this study, especially for the groups of ribbons with 2.00 mm of thickness. Besides, the trend is not sharp, and it is affected by a change in the levels of porosity, so no clear relationships can be established between the thickness and the milling time. As already seen in

Figure 3.10, the porosity affects the milling time. Indeed, the time decreases for the weaker ribbons. However, these results cannot imply a clear relationship between the thickness of ribbons and the milling time, which is related with the strength of the ribbons. So, this consideration will be discussed more in depth in §3.5, which regards the analysis of fines.

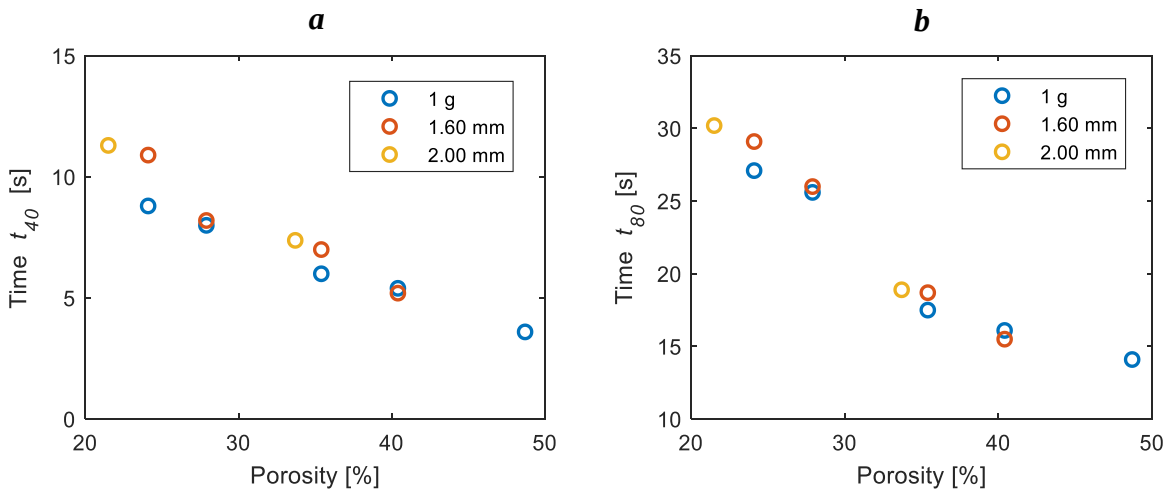

Figure 3.11 *- Milling times t_{40} (a) and t_{80} (b) as function of the porosity and thicknesses for the batches of ribbons produced at fixed mass (1 g) or thickness (1.6 mm and 2.0 mm)*

The kinetic of milling has been studied also for the groups of ribbons with different moisture contents in order to find how the water trapped within the compressed powder can affect the time and performances of the milling. Figure 3.12 shows the two times t_{80} and t_{40} for the six batches of ribbons stored at three different environmental humidity levels (20%, 50% and 80%) and then compressed at two different forces (30 kN and 60 kN). Besides, in the chart

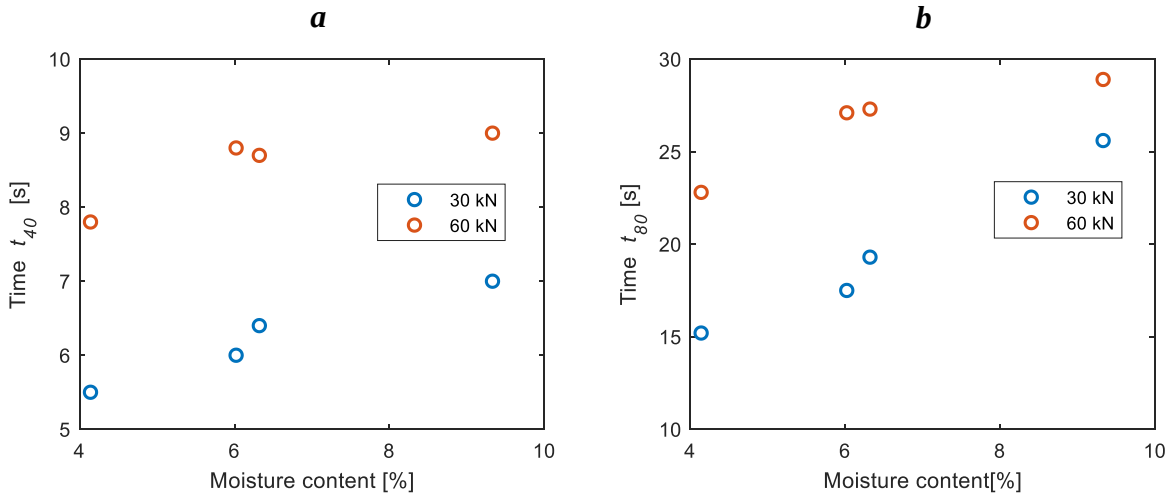

Figure 3.12 *- Milling times t40 (a) and t80 (b) as function of the moisture content and the compression forces set for the batches of ribbons produced at fixed mass (1 g) and different environmental humidity levels*

the times for the corresponding groups of ribbons made with 1 g of powder stored at environmental conditions are reported. All these batches of ribbons were milled at the same impeller speed, equal to 200 rpm. The different groups can be identified thanks to the moisture content and Table 3.1. Figure 3.12 shows that the porosity level of the ribbons, which is related to the strength of the ribbons themselves, affects directly the milling time, as the 30 kN and 60 kN batches presents a wide difference for both t_{80} and t_{40}. Besides, the moisture content seems to increase the milling times for the two compression forces. The increase is more relevant for the t_{80} than the t_{40}. The powder stored at the environmental conditions presents a low difference with that one stored at 50% of relative humidity. The difference is greater for the lower level of porosity, while for the ribbons compressed at 30 kN the time values are comparable. Therefore, the kinetic of milling has been studied and the influence of porosity, impeller speed, thickness of ribbons and moisture content have been analysed and proved. Indeed, tough in different ways and with different intensity, each of them affects the time of milling and so the performances of the process.

3.3 PSD from QicPic

The PSD of each sample collected during all the experiments has been outlined through the QicPic and it has been studied in order to understand the profile of the granules produced by the conical mill chosen. Besides, the comparison of the distributions allows to analyse the effect of the set operating conditions and to define qualitative relationships among the different parameters and factors of the process. The results of each experiments will not be reported in this work, directly, to avoid weighing down the text. Nevertheless, all the PSD will be reported in different charts of comparison among the operating conditions and properties of the ribbons in the following sections.

3.3.1 Final PSD

The samples collected and analysed from the conical mill are then computed in Excel™ in order to find the final distribution of the particle size. Figure 3.13 shows the normalized frequency and the cumulative distribution of the group of ribbons made by 1 g of powder at 30 kN of compression forces and, then, milled at 200 rpm, which represents the example used to analyse the feature of the distribution. The first characteristic that can be observed is the presence of two peaks in the frequency, which underlines that the PSD is bimodal. This represents a difference with the PSD of the original MCC 102, which is unimodal. The first peak has the same position of the original powder (Figure 2.1), which is about 170 µm. Indeed, it corresponds to the fines produced, as the particles have not developed strong

bridges at the contact points during the compression step and during the milling, they have returned to the original size of the MCC 102. Instead, the second peak is located roughly at 1800 µm and it is related to the larger granules produced, which represent the target in order to achieve better mechanical and performance properties in the final pharmaceutical tablet. The position of this peak is linked with the aperture of the holes of the sieve, which determines the size of the larger granules produced, as these ones can pass through the sieve as soon as their sizes are smaller than the holes' ones. The frequency of the medium granules is less than the sizes of the larger and smaller ones, and this is reasonable, by considering that no driving phenomena can manage directly their production, like the original powder size or the one of the holes of the sieve. The slope of the cumulative distribution proves all these observations, as it is sharper in the sizes related to the two peaks. Almost all the granules milled have a size lower than 2500 µm, although the largest ones have a diameter equal roughly 2700 µm, which is a bit larger than the maximum dimension measured of the sieve's holes (2600 µm). This can be explained by considering that a granule with a low aspect ratio and a large elongation can pass through the holes if oriented with its smaller dimension and, then, the diameter average measured by the QicPic could be larger than the 2600 µm. However, these granules are very few and rare. The same considerations are valid for all the other experiments, although the ratio between the height of the two peaks can vary by changing the operating conditions of each test. Besides, the second peak position can move just a bit at a smaller or larger size, in relation to the conditions of the experiment.

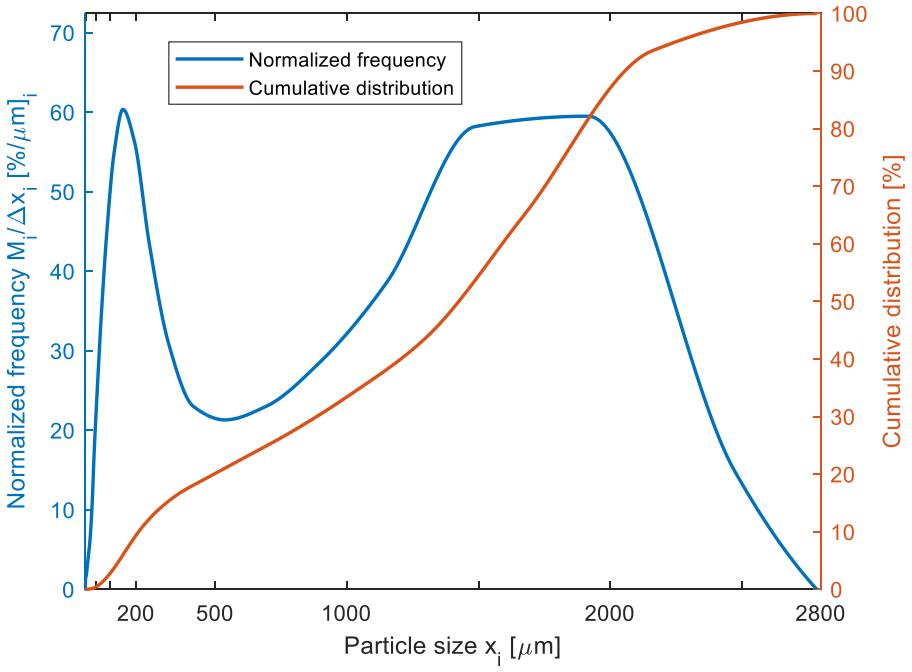

Figure 3.13 *- Normalized frequency and cumulative distribution of the PSD of the group of ribbon made by 1 g of powder compressed at 30 kN and milled at 200 rpm*

3.3.2 Time Comparisons

By considering that during the experiments two different samples have been collected, the first part of the analysis will concern the comparison of the PSD between the sample collected during the first 10 s of the milling and the other ones collected at the end of the process. This allows to understand how the distribution could change during time and if more fines are produced in one moment of the milling.

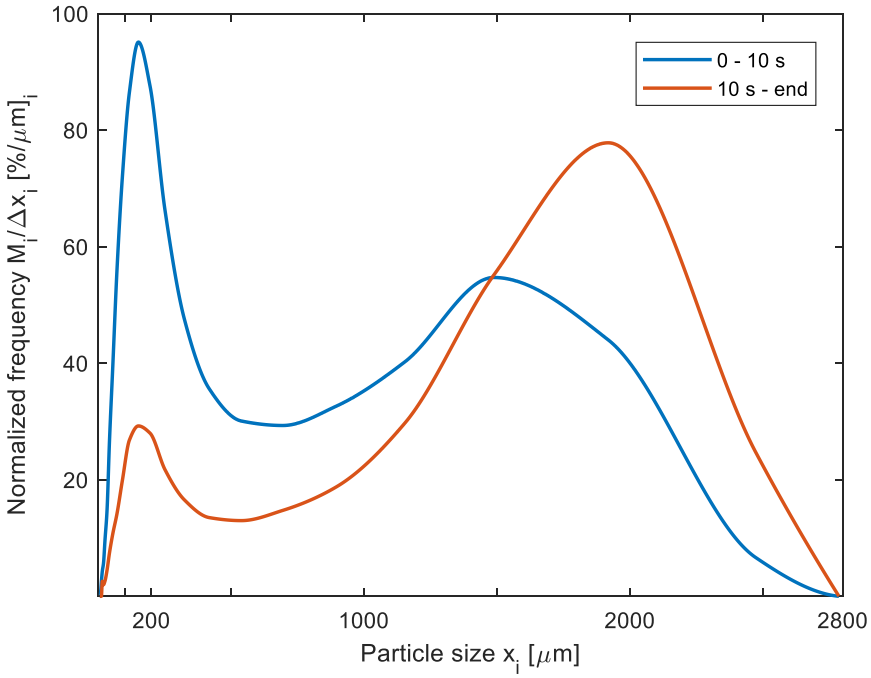

Figure 3.14 *– Normalized frequency of the PSD of the two samples collected at different times for the group of ribbon made by 1 g of powder compressed at 30 kN and milled at 200 rpm*

Figure 3.14 outlines the normalized frequency of the PSD of the group of ribbons made by 1 g of powder at 30 kN of compression forces and, then, milled at 200 rpm. The chart shows clearly that there is a relevant difference among the two samples collected. Indeed, during the first seconds more smaller particles are produced, while for the second sample, so during the last part of the experiment, more larger granules are milled. Therefore, when the milling chamber is full of almost intact ribbons there is a greater contribution of the abrasion and attrition phenomena, responsible to produce more small particles. Indeed, a huge number of fines can be observed in the first moments of milling. Besides, each breakage is responsible to produce smaller particles and a portion of fines. As in the first part of the milling there are more breakages, more fines are produced, while they decrease over time, because the breakage rate decreases and the residual fragments inside the chamber are smaller and stronger. This result is valid for all the other test performed, although the figures are not directly reported in this paragraph. Besides, Figure 3.14 shows that the peak positions change

during time. Indeed, the first one is the same for both the samples, but the second peak position is quite different between the two moments of collection. During the experiment the peak seems to move to larger sizes, starting from 1.5 mm and then going to 1.8 mm. The same phenomena are observed in the other experiments.

3.4 Effect of the Operating Conditions

The main part of the experimental study regards the analysis of the influence of the operating conditions in the modification of the PSD of the milled granules. The conditions analysed involve the porosity and the thickness of the ribbons, the impeller speed set and the moisture content of the powder before the compression step. These four factors have been already studied in §3.2 in order to find the effect in the kinetic of the milling process, but now the understanding of their contribution in the achievement of a better PSD is the main target, in order to discover the best conditions to produce granules suitable for the manufacturing of high-quality pharmaceutical tablets. For all the studies regarding different parameters, the description and comparison of the results will be performed through one homogenous group of batches of ribbons while the other groups of comparison will be just reported in other figures. Indeed, the explanation of the effects can be carried out once time for all the experiments, as the results are comparable. All the studies concern the entire process of milling of the 18 g of powder, therefore just the final PSD of each experiments will be considered, instead of analysing the two samples collected at different times, separately.

3.4.1 Porosity

The effect of the porosity is studied by comparing the PSD of the batches of ribbons made by 1 g of powder and, then, milled at the same impeller speed, to avoid the pollution of the analysis with the effect of another parameter, such as the rotational velocity. Figure 3.15 reports the comparisons of the normalized frequency of all the batches of ribbons milled at 200 rpm. Figure 3.15 shows the main results achieved at different levels of porosity. By analysing the height of the two peaks of each batch’s distribution, the evaluation of the amount of small and large granules can be performed. Besides, the comparisons can be done by observing these heights. The chart highlights that the granules are larger for the lower levels of porosity. Indeed, the first peak, which represent the fines and, so, the smaller granules is taller for the batches with 48% of porosity, while it is smaller for the one at 21.5% and the peak decreases, by decreasing the porosity. Besides, the height of the second peak, at a size almost equal to 1800 µm, presents the opposite behaviour, as it is greater for the lower levels of porosity and it decreases by increasing the porosity. This means that the

amount of large granules is greater for the strongest ribbons, while more fines are produced for the groups of the weakest ribbons. In particular, there are huge differences between the PSD of 48% of porosity group (the weakest ribbons) and the 40.5% one, and in the lower part of the chart, between the PSD of the 21.5% of porosity group (the strongest ribbons) and the 25.6% one. This great shift of the peak can be affected also by inaccuracies in the measurement or by some random errors. Nevertheless, all the curves highlight the same effect of the porosity of ribbons milled in the conical mill.

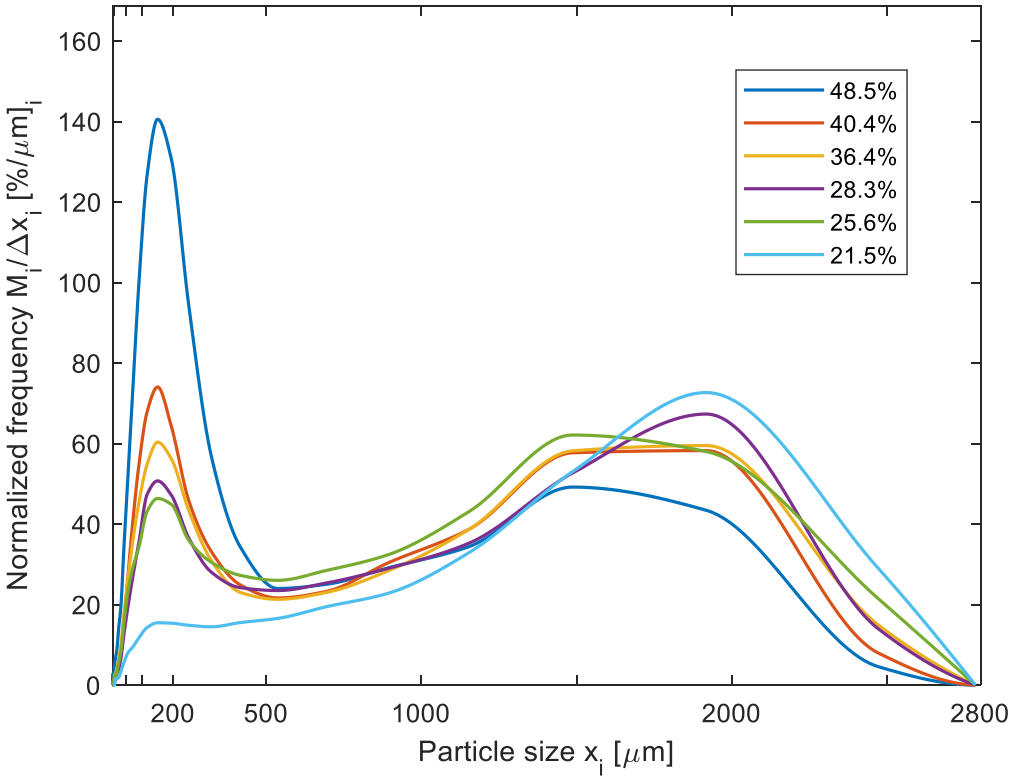

Figure 3.15 *- PSD of the batches of ribbons made by 1 g of powder, with different levels of porosity and milled at 200 rpm*

This behaviour can be explained by considering the strength of the ribbons. Indeed, if the powder is compressed at a greater pressure it will produce strength and small ribbons, as the void space between the particles is reduced and they are linked by a closer bond. So, the bonding forces, like Van Der Waals, are stronger. Hence, through the mill action, the ribbons with a greater porosity (with more void spaces within) are faster reduced into granules, but, mostly, fines. These have the size of the original powder, because the low pressure used does not allow to create strong bonds among the particles, in order to set the agglomerates which can withstand the impeller grinding motion and so, to produce the greater granules, suitable for the following compression into the final tablets.

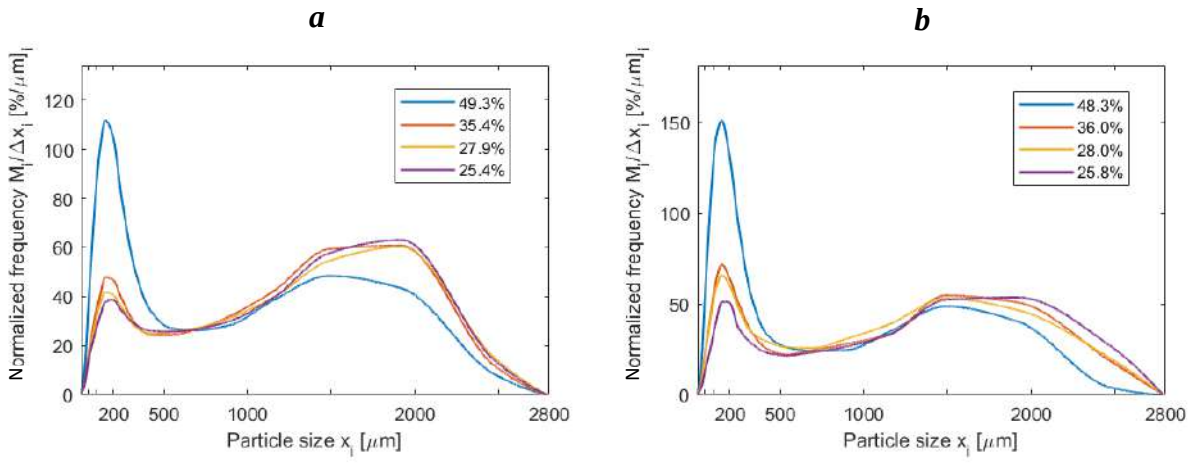

Figure 3.16 *- PSD of the two batches of ribbons made by 1 g of powder, with different levels of porosity and milled at 100 rpm (a) and 350 rpm (b), respectively*

The same effect can be observed in Figure 3.16, which reports the PSD of the corresponding batches of ribbons, which are milled at 100 rpm and 350 rpm. Some different shifts of the peaks and the distribution can be observed among two or more different batches of ribbons of the same chart (so among batches milled at the same impeller speed), but the overall effect is clear and it is proved with more reliability and effectiveness. Figure 3.16-a shows that at 100 rpm, among the batches with a porosity between 36% and 25%, the differences are small, for both the fines and the greater granules, although the trend of the effect of the porosity is the same found in the previous analysis. Instead, the 49.3% porosity batch present a huge difference with the other groups, with a great production of fines, while the number of large granules is very small. This is still valid for the Figure 3.16-b, where also there is a small difference between the PSD of 36% and 28% of porosity. This can be caused by the high speed, which can smooth just a bit the effect of the porosity.

3.4.2 Impeller Speed

The analysis regarding the effect of the impeller speed set in the conical mill is performed by comparing the PSD of the batches of ribbons made by 1 g of powder, as in the porosity study. The study concerns the analysis of the batches with the same level of porosity but milled at different impeller speeds. As explained in §3.1, the porosities are not exactly equal for all the ribbons compressed with the same force, but the differences are minimal and do not affect the main effect produced by a great change of the rotational speed. In Figure 3.17, the normalized frequency of the PSD of the three groups of ribbons compressed at 30 kN is reported. The porosity changes from 35.4% to 36.4% and they were milled at 100, 200 and 350 rpm, respectively. The chart proves the initial hypothesis which regards the influence of

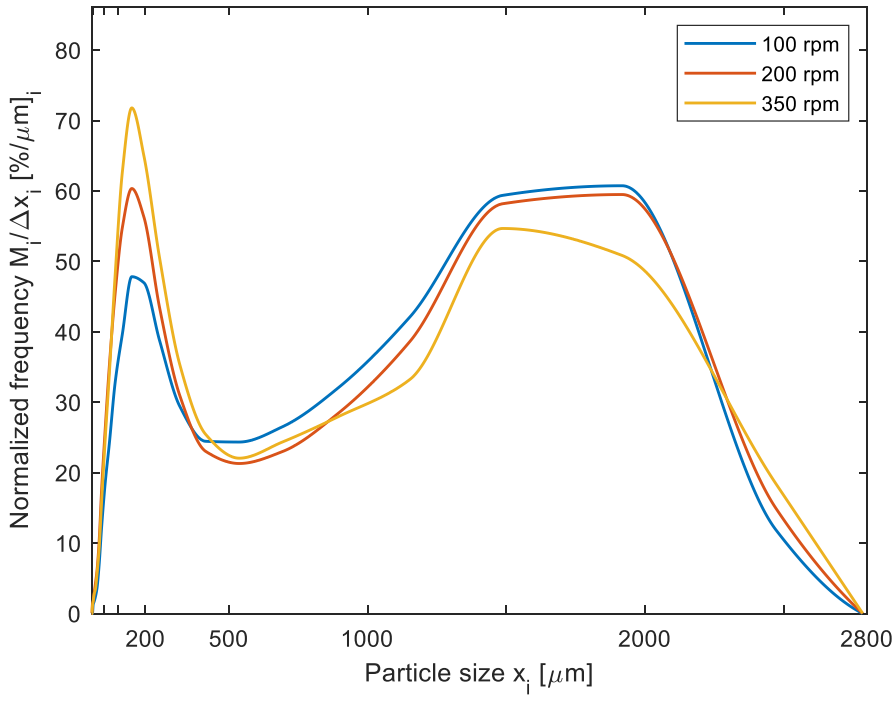

Figure 3.17 *- PSD of the batches of ribbons made by 1 g of powder, with about 36% of porosity and milled at 100, 200 and 350 rpm*

the impeller speed in the production of more fines. Indeed, by increasing the rotational velocity the amount of fines increases, as proved by the taller picks of the group milled at 350 rpm. While the batch milled at 100 rpm, presents the smallest pick of fines and the tallest pick for the larger granules. Therefore, the decrease of the impeller speed allows the production of more large granules and the minimization of the fines, achieving a PSD more suitable to the following manufacturing of the final tablet. The chart also shows that the difference between the first pick of the group milled at 350 rpm and the one of the groups at 200 rpm is quite small, but the trend is visible. A huge difference can be observed between the batch of ribbons milled at 100 rpm and the one milled at 200 rpm, in particular, for the number of fines and the medium-size and larger granules, whose amount is greater for the low speed test. The same evaluations are valid for the other groups of ribbons at different levels of porosity. While the main effect of the impeller speed is relevant, there could be some shifts of the pick in the different distribution, which can be due to the possible variability and inaccuracies that affects the experiments with powders. By evaluating the chart of Figure 3.18-a, it can be observed that the first peak is more significant in the understanding of the effect of the impeller speed. Indeed, observing the amount of fines, the relationships among the production of more small particles and the rotational speed is more clear. The second peak usually shows the same trend, but the difference is less sharp for the groups at 48.5% of porosity. Probably the reason is related to the fact that the porosity effect

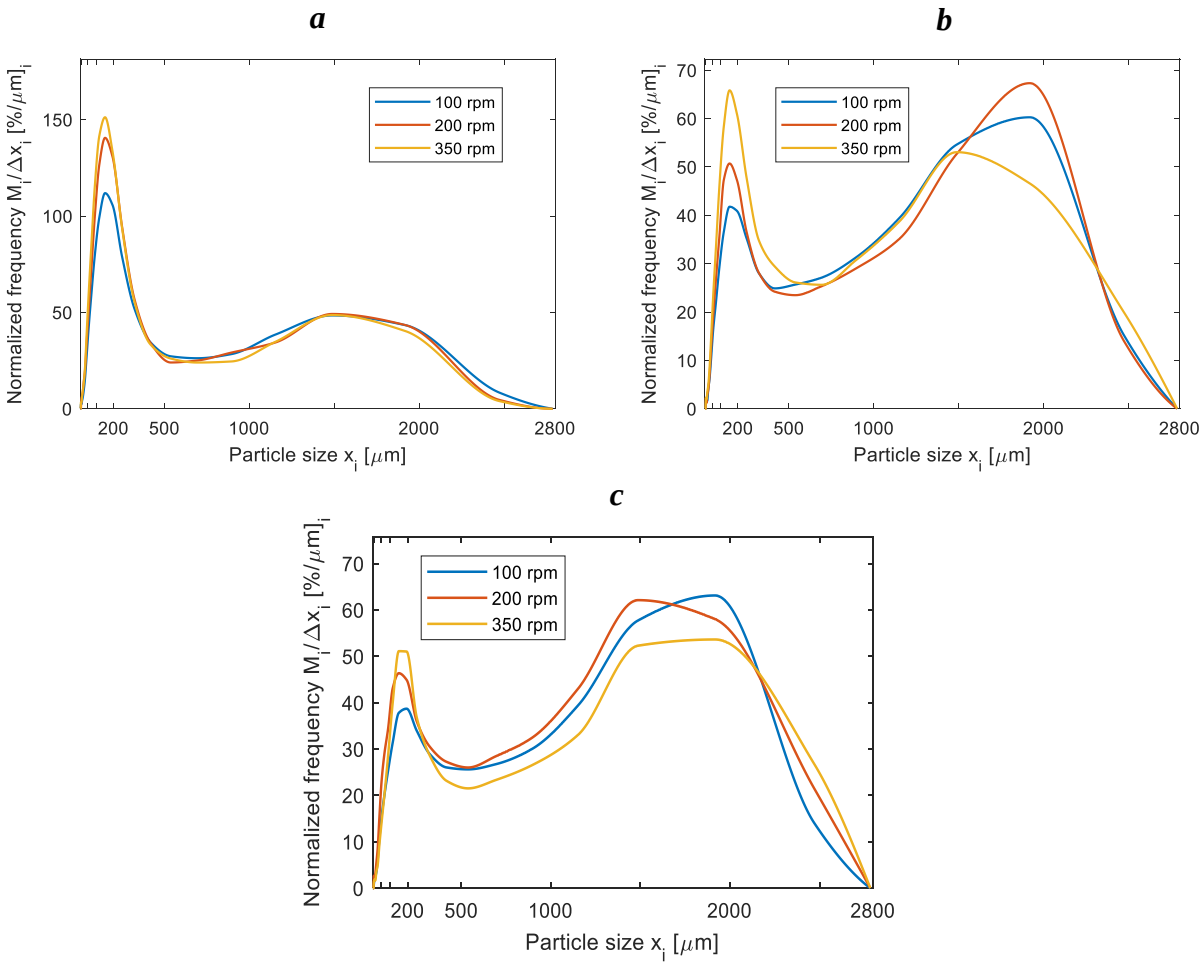

Figure 3.18 *- PSD of the two batches of ribbons made by 1 g of powder, milled at different impeller speeds. Each chart represents groups of ribbons at different porosity: 48.5% (a), 28% (b) and 25.5% (c)*

is dominant in the determination of the larger granules, while for lower porosities the impeller speed covers a more relevant role. However, all the experiments carried out confirm that the faster impeller speed set to the conical mill causes the production of more fines and less large granules. This suggests operating at a low rotational speed in order to achieve a better PSD for the following production of tablets. Nevertheless, the performances of the mill need to be considered, indeed a higher speed represents a greater throughput of milled ribbons in a smaller time of processing. The results achieved corresponds to some results achieved in literature, and already explained in the chapter 1.[9, 30]

3.4.3 Thickness

The effect of the thickness has been analysed in order to understand how it affects the PSD and the production of fines, at the same operating conditions. Literature contains a study of the influence of thickness in fine generation in a dry granulation process.[31] It regards the study of rectangular ribbons made by MCC 101, which has a different PSD, with a small-size

mode. The tests performed in this study aims to mill at two different set thicknesses: 1.60 mm and 2.00 mm. The average porosity and characterization of each group of ribbons have been reported in §2.4.1 and in appendix. It is important to remind that the porosity values change if the compression of more powder is performed at the same force, as the compaction is improved. Nevertheless, the changes are quite small, especially for low compression forces, and the evaluation of the results is still reliable.

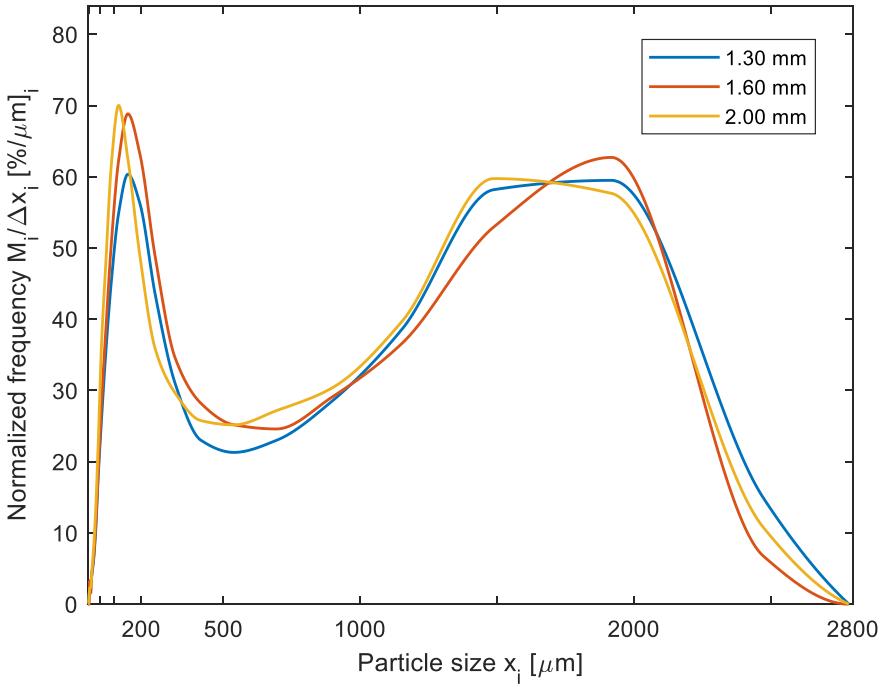

***Figure 3.19** - PSD of the batches of ribbons with different thicknesses, made at 30 kN, with about 36% of porosity and milled at 200 rpm*

Figure 3.19 reports the comparison of the PSD of the three batches of ribbons produced at 30 kN, milled at 200 rpm and with three different thicknesses per ribbon: 1.30, 1.60 and 2.00 mm. The chart suggests that the thickness has a role in the changes of PSD, and it seems to increase the smaller particles and to decrease the medium and larger granules. Indeed, the first peak is taller for the thickest ribbons, while it decreases, by decreasing the thickness. The second mode shows a behaviour more different, as the batch with 1.6 mm of thickness has a peak that shifts to the right, with respect to the other two groups. However, by observing both the medium and large granules distribution the trend of thickness can be proved, as the average of their amount seems to be affected by the effect of thickness. However, a small effect of a change in the porosity could play a role in these experiments, as the values for the groups with thickness of 1.30, 1.60 and 2.00 mm are 36.4%, 35.4% and 33.7%, respectively. Therefore, the last batch, in particular, should be affected by the

opposite effect of the porosity which should decrease the amount of fines and increase the number of large granules. Figure 3.19 shows that this one is still the group with more fines, proves that the thickness effect is dominant, if the change in the porosity values is small. The same results can be observed in Figure 3.20, where the comparisons among the groups with different thicknesses are reported. Each chart of the figure shows two or three PSD, for the group of ribbons compressed at the same force, although the level of porosity could be quite different, as already explained and shown in Table 2.2.

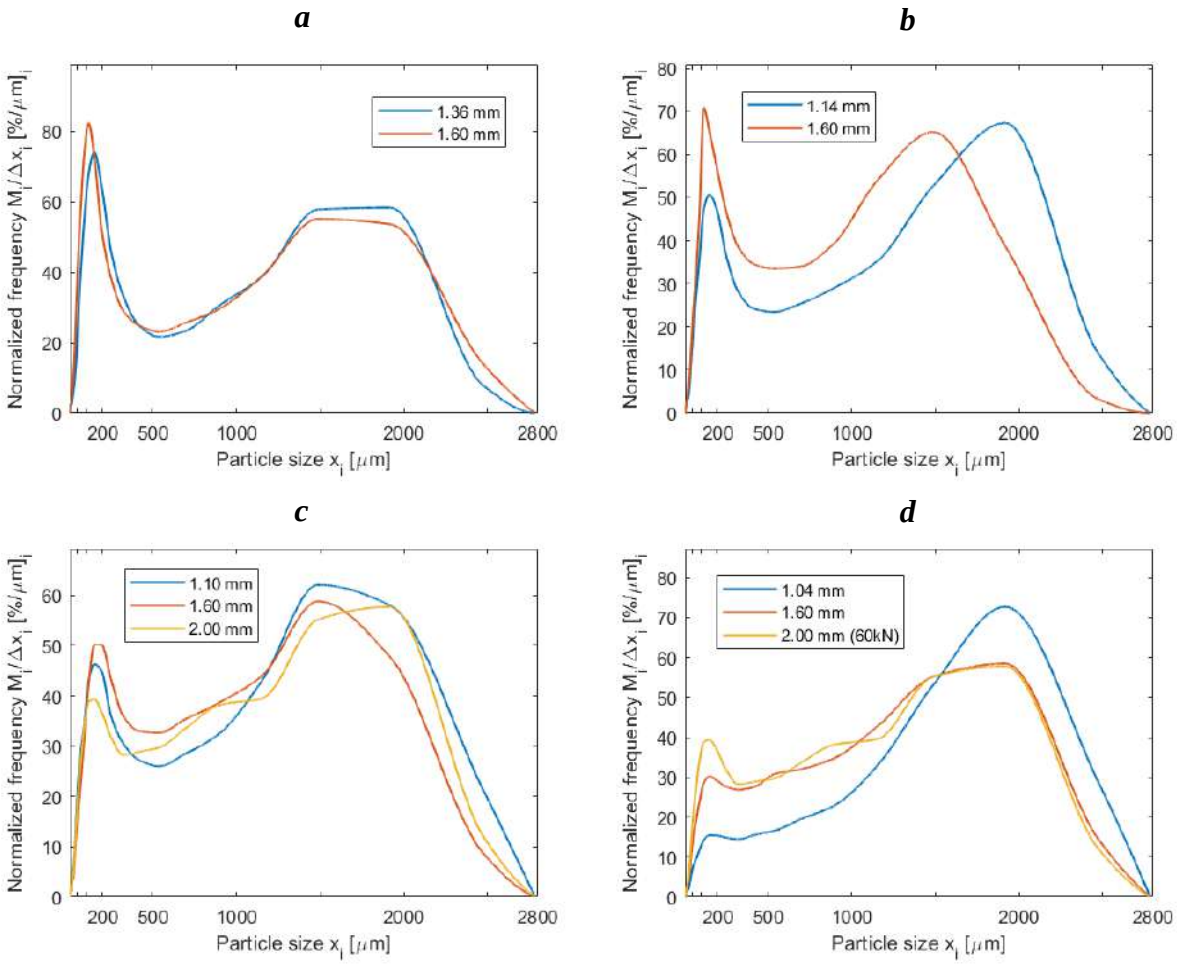

Figure 3.20 *– PSD of the batches of ribbons made at different thicknesses milled. Each chart represents groups of ribbons compressed at different forces: 22.5 kN (a), 45 kN (b), 60 kN (c) and 90 kN (d)*

The charts of Figure 3.20 prove the effect of the thickness, in particular, by observing the first mode of the distributions. The comparisons are clear for the plots *a* and *b*, while for the *c* the groups with 2.00 mm of thickness shows an unexpected PSD. These groups have been compressed at 60 kN and, although the 1.60 mm group presents the same trend of the other batches in relationships with the thinner ribbons, the one with 2.00 mm of thickness has less

fines and more medium and larger granules, with respect to the other two groups of thinner ribbons. This result can be explained by considering the different compaction occurred at the same compression force. Indeed, more mass had to be added to the die in order to achieve 2.00 mm of thickness, and this led to a quite smaller porosity, which is equal to 21.5%. This value is roughly 16% smaller than the 1.10 mm group (its porosity is equal to 25.6%). Therefore, the porosity effect could have had a dominant role in the PSD of this group, with respect to the thickness effect. In order to prove this hypothesis, the same group is compared in the chart *d*, where the batches of ribbons compressed at 90 kN are outlined. This choice is driven by the comparable porosity values that the 2.00 mm batch (compressed at 60 kN) and the batches compressed at 90 kN have (see Table 2.2 for the porosity value of each group). The analysis on the chart *d* confirms the hypothesis, as the thicker ribbons present more fines and less larger granules, and they decrease and increase, respectively, by decreasing the thickness of the ribbons. Between the 1.60 mm group and the 2.00 mm group there is no difference regarding the part of larger sizes, but this can be explained by considering that the influence of the porosity affects the first group and it is in contrast with the opposite effect of the thickness, as it has been already seen. The results achieved agrees with literature.[31] Nevertheless, the explanation given in literature does not describe properly the effect of thickness found in the experimental part of this work. Indeed, the more fines produced were attributed to the longer retention time of the thicker ribbons in the milling chamber. Indeed, the fines are produced due to the action of the attrition/abrasion mechanism, which mostly affects the milling during the last part of the process, while the first part is dominated by the breakage of ribbons into smaller parts. Therefore, if time is longer, ribbons should be more influenced by the attrition and so the production of fines should be greater. Nevertheless, by studying the PSD of the first sample it has been found that more fines are produced in the first part of the experiment and that the milling process is not so much faster for the thicker ribbons (see §3.2). Therefore, another explanation has been proposed in this study. As the experiments have been performed in order to keep the total mass inside the milling chamber constant and equal to 18 g, the tests with thicker ribbons use less tablets, because each ribbon is made by more than 1 g of mass. So, less ribbons are fed to the conical mill. This takes to a low contribution of the impact mechanism in the breakage, because there are less fragments to impact against each other at the beginning of the process. Therefore, the shear and abrasion/attrition mechanism role is more dominant and it leads to a greater production of fines, which can be observed in the experimental analysis performed.

3.4.4 Moisture Content

The effect of the moisture content has been deepened in the last part of the experimental phase, where the milling of ribbons made by powder stored at different environmental humidity levels have been performed. The purpose is to understand how the water content can affect the PSD and the production of fines. Literature reports another study which analyses the effect of environmental humidity in the determination of the final PSD in a dry granulation process for a Lactose powder.[34] Nevertheless, this study differs from the analysis carried out in this work for the structure of the raw powder used. Indeed, the moisture content of the lactose powder strictly depends on the micro-structure of the particles. The moisture content changes, due to the crystallization phenomena which desorbs water when the structure moves from amorphous to crystalline, by changing the environmental relative humidity. This phenomenon does not affect the MCC 102 which remains crystalline and shows a quite linear increase in the moisture content, by rising the storage environmental humidity. Therefore, the results searched and the effects should be quite different and independent from the ones of literature (for lactose powder). The analysis performed highlights two charts, where the PSD of six groups of ribbons are reported (three groups per plot). In Figure 3.21 the distribution for the three batches of ribbons compressed at 30 kN and stored at 20%, 50% and 80%, respectively, are reported. In the moisture analysis all the milling tests have been performed at 200 rpm.

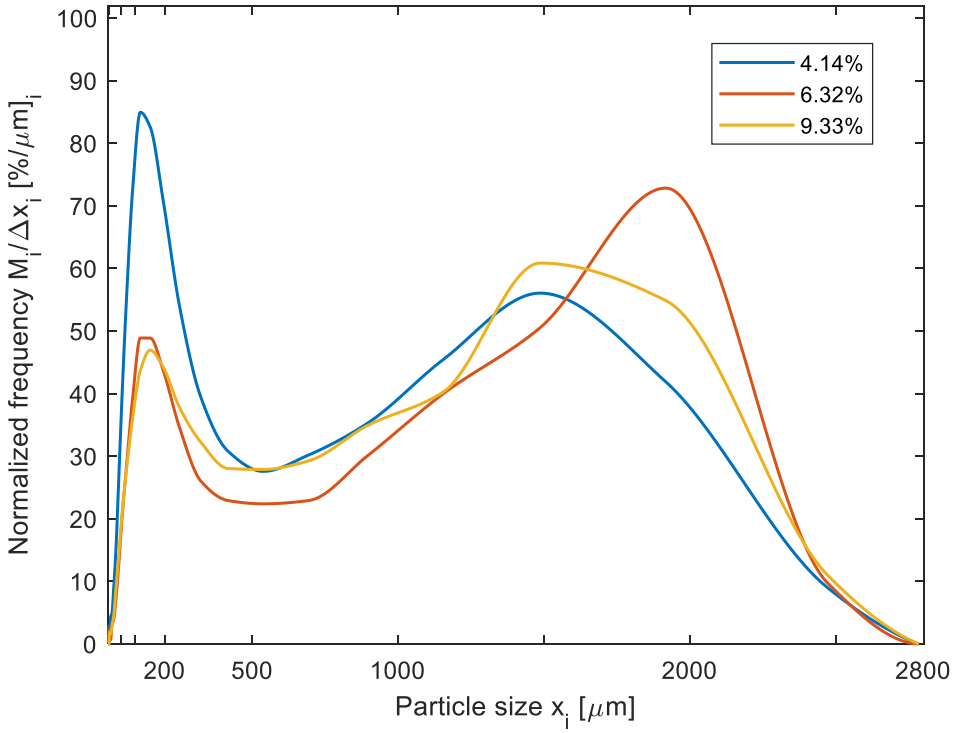

Figure 3.21 *- PSD of the batches of ribbons made by powder stored at three different environmental humidity levels: 20%, 50% and 80%. The compression force set is 30 kN*

Figure 3.21 shows that at lower moisture content the PSD presents more fines and less large granules. Instead, by increasing the water content the height of the first mode decreases, while the one of the second pick increases. For the most wet powder there can be observed more medium-size granules, with respect to the second group, which has the highest second mode. By looking to the different porosity values achieved from powder with different water contents (table 2.2), the effect of the porosity needs to be considered, as it decreases a lot from the group of 20% to the one of 80% of environmental relative humidity. Therefore, the group with 4.14% of moisture content should be compared to the one from powder stored in uncontrolled environmental conditions, compressed at 22.5 kN and then milled at 200 rpm, as they have roughly the same levels of porosity: 40.1% and 40.5%, respectively. The same approach is applied to the group made by powder at 9.33% of moisture content, which is, then, compared with the batch produced at 45 kN and milled at 200 rpm. They have levels of porosity equal to 27.6% and 28.3%, respectively. The two charts are reported in Figure 3.22. The moisture content of the powder stored under normal conditions (6.02%) is reported in the legend.

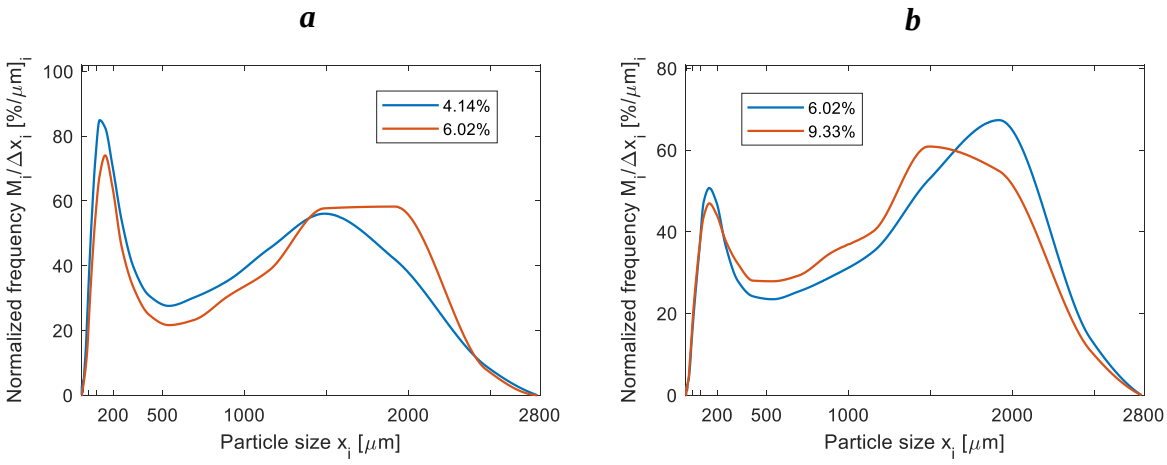

Figure 3.22 *- PSD of the groups of ribbons made from powder at different moisture content (reported in legends) with roughly 40% (a) and 28% (b) of porosity. All groups are milled at 200 rpm*

Figure 3.22 shows the moisture content effect, by avoiding the competing effect of the porosity. Both the two plots (3.22-a and 3.22-b) highlights that the lower the moisture content is and the greater is the production of fines, while the large granules are less if the moisture content is smaller, and they increase for wetter powder. This result is proved especially by the first mode of the distributions, while the second one shows the same trend for Figure 3.22-a. In Figure 3.22-b the second pick seems to be smaller for the wetter powder, but it can be observed that there are more medium-large granules for a wide range of sizes, while the first mode underlines that ore fines are produced if the powder is drier. Therefore,

the effect found in Figure 3.21 is proved, although the PSD are also affected by the porosity contribution. The same analysis is carried out for the same powder kept in the humidity chamber, which has been compressed at 60 kN.

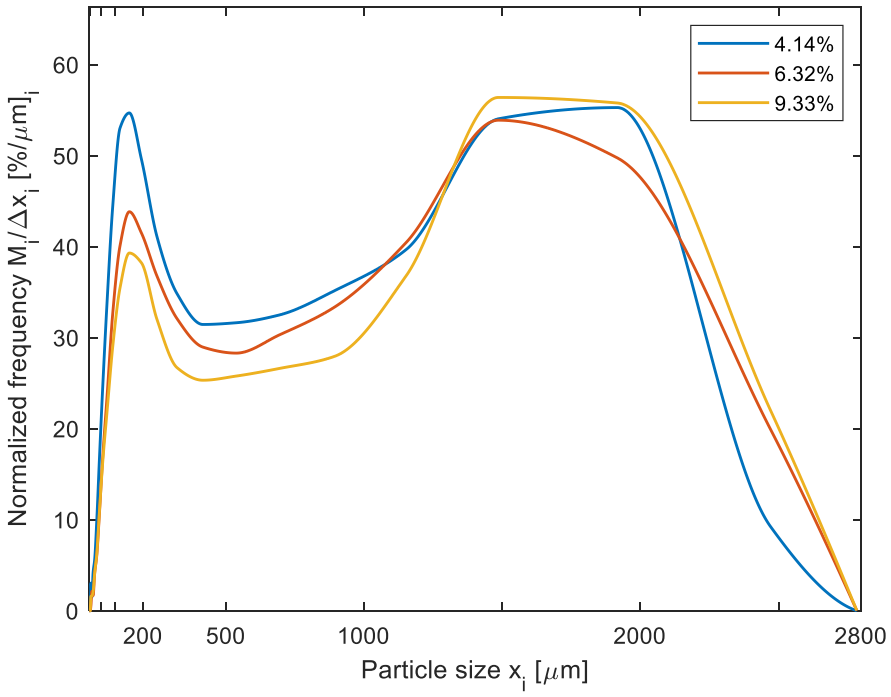

Figure 3.23 *- PSD of the batches of ribbons made by powder stored at three different environmental humidity levels: 20%, 50% and 80%. The compression force set is 60 kN*

Figure 3.23 shows the PSD of the granules milled at 200 rpm from the three groups of ribbons with different moisture contents. It shows the same trend already explained. Indeed, for the drier ribbons the generation of fines is larger, and it decreases by milling wetter ribbons. This can be observed especially in the first mode. Nevertheless, the second pick does not seem to confirm directly this trend, but the greatest number of large granules are the one generated from the wet powder, by observing the largest sizes of the particles (the rightest part of the plot). The reason behind this phenomenon can be related to the strength of the ribbons, which changes by changing the moisture content of the powder. Indeed, according to literature, the ribbons produced with a drier powder are weaker, so the milling will produce more fines. If the moisture content of the powder increases the ribbons are stronger, due to the bonding mechanism favoured by the water and a better deformability of the powder itself.[34] In the industrial dry granulation process another factor affects the process. It is the flowability of the powder, which decreases if the water content increases. So, it does not flow properly in the hopper which takes to the roll compactor, bringing to thinner and weaker ribbons. Therefore, the effect of the moisture content is related to the influence of the water in the strength of the compressed powder, which also depends on the

force set in the compaction step. The experiments performed clearly prove this mechanism. A higher environmental relative humidity is suggested, in order to minimize the generation of fines, although the analysis needs to be applied also to the industrial dry granulation plant, where the effect of the decrease in the flowability plays an important role especially in the compaction step, which affects all the following manufacturing phases, from the milling to the final compression of granules into tablets.

3.5 Determination of Fines

An important role in the study of the dry granulation process is covered by the generation of fines during the milling. The problems related to the presence of fines in the PSD of the granules compressed into tablets have been already explained in the chapter 1. In this section a quantitative analysis regarding the number of fines produced during the milling experiments is performed in order to understand how different operating conditions affect this undesired production. A qualitative analysis has been carried out in the previous section, but, now, quantitative values will be presented and described more in depth. The fines can be represented as the particles with a size mostly equal to the one of the original powder, as the compaction step is not able to agglomerate them into larger granules. The fines are, then, defined as the particles smaller than 240 μm, which represents, roughly, the 80% of the cumulative mass distribution of the original powder (MCC 102), as shown in Figure 2.1. Table 3.3 reports the percentage mass fraction of the fines of the batches of ribbons made by 1 g of MCC 102 and normal environmental conditions of the storage room. The fractions of the other groups are reported in the appendix.

***Table 3.3** - Mass fraction (%) of the fines (<240 μm) for the groups of ribbons made by 1 g of MCC 102*

Porosity	**48%**	**40%**	**36%**	**28%**	**25%**	**21%**
100 rpm	18.01%	-	7.41%	6.95%	5.20%	-
200 rpm	22.42%	11.01%	8.37%	7.68%	5.31%	2.78%
350 rpm	24.05%	-	10.91%	10.38%	7.14%	-

Table 3.3 confirms the initial hypotheses and the qualitative analysis carried out in the previous paragraphs. Indeed, the amount of fines depends clearly on the level of porosity of the ribbons produced and on the operating conditions of the milling step, such as the impeller speed. The fines decrease by slowing down the impeller speed. Instead, they increase if the

porosity levels increase, so, if the ribbons are weaker. The trend can be observed more clearly in Figure 3.24, where the points are plotted into a chart, as function of the impeller speed and the porosity.

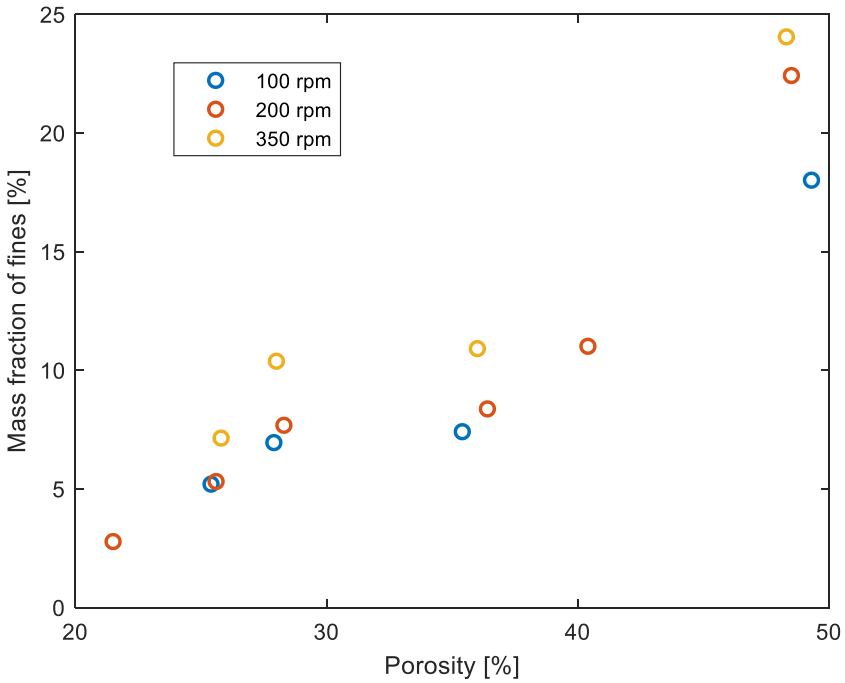

Figure 3.24 *- Mass fraction of fines (in %) as function of the impeller speed and the porosity of the groups of ribbon made by 1 g of MCC 102*

Figure 3.24 proves one more time the trend explained. Nevertheless, the difference among the groups of ribbons are more visible and the quantitative comparisons can be better evaluated. Indeed, the difference of the number of fines at different milling impeller speeds seems to increase, by increasing the level of porosity. This suggests that the impeller speed contribution to the process is more relevant if the ribbons are weaker. Instead, for stronger ribbons the rotational speed role seems to decrease. Besides, it can be observed that for all the three speeds performed, the difference among the fines of the groups at 28% of porosity and the one of the batches at 36% of porosity do not change a lot. A plateau can be observed between these levels of porosity. The explanation is non-trivial and the possibility of experimental errors should be quite low, as the same phenomena at the same intensity can be observed for all the three impeller speeds, between the two porosities. More tests on the strength of the ribbons could enlighten the singularity. The same analysis has been carried out to compare the fines generated at different thickness of ribbons. The batches made by 1 g of powder and at 1.60 mm and 2.00 mm of thickness are reported in Figure 3.25.

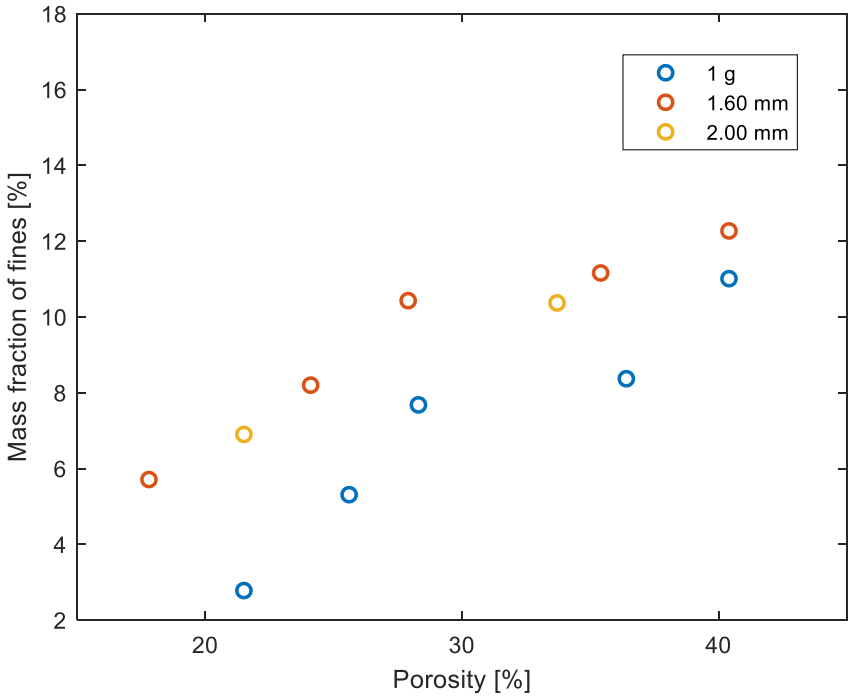

Figure 3.25 *- Mass fraction of fines (in %) as function of the thickness and the porosity of the groups of ribbon made by 1 g of MCC 102 or at 1.60 mm and 2.00 mm of thickness*

Figure 3.25 shows that by increasing the thickness of ribbons at the same level of porosity the amount of fines increases. The rise trend seems to be roughly the same of the group made by 1 g of MCC 102. Besides, a similar plateau can be observed between the batches at 28% and the 36% of porosity, respectively. The two groups at 2.00 mm do not have batches of ribbons at the same level of porosity for a proper comparison, but they confirm the trend. However, the one at 33.7% of porosity shows just a bit less fines than expected. Nevertheless, it could be due to some small experimental inaccuracies. After the thickness analysis the quantitative effect of the moisture content in the production of fines has been deepened. The main results are reported in Figure 3.26, where the mass fraction of fines is outlined as function of the moisture content of the powder used and the porosity of each group of ribbons milled. The impeller speed set for all these experiments is 200 rpm. Figure 3.26 highlights the differences among the batches in terms of porosity. Indeed, they have been compressed at the same forces (30 kN and 60 kN), but the porosity is highly affected by the moisture content of the powder, as it has been already discussed about. The main observation that can be done regards the points in the central part of the chart. Indeed, the number of fines increases if the moisture content decreases. Although the effect of the porosity is still relevant and dominant, the water trapped among the particles disadvantages the generation of fines. Therefore, the storage at a high environmental relative humidity could improve the process performances, thanks to the minimization of the undesired

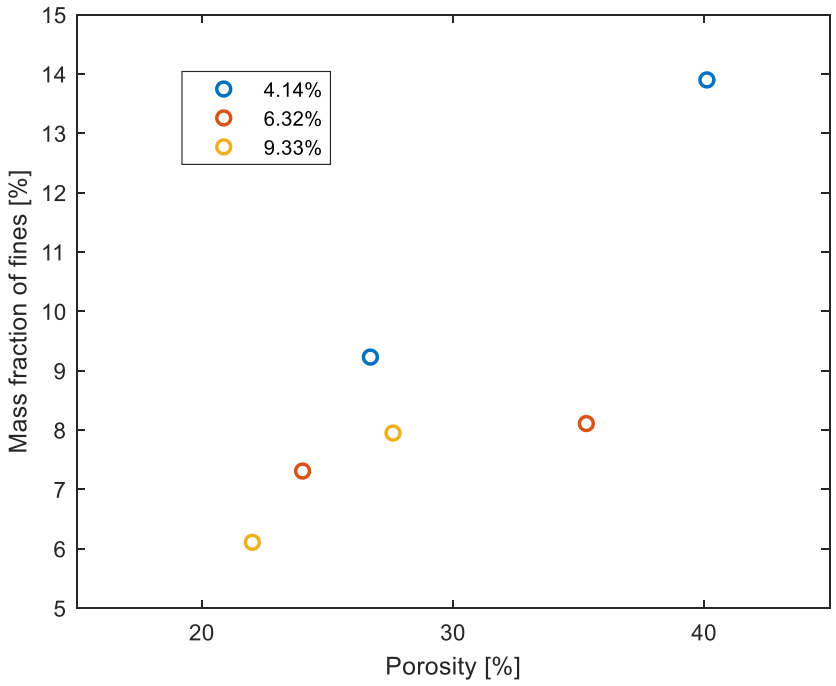

Figure 3.26 *- Mass fraction of fines (in %) as function of the moisture content and the porosity of the groups of ribbon made by 1 g of MCC 102 and powder stored at different environmental humidity*

production of fines. Nevertheless, this analysis does not consider the effects that the decrease on the flowability of the powder, due to a higher moisture content, can affect the flow of particles from the funnel to the two rollers of the compaction steps.

3.6 Shape Analysis

The last part of the experimental phase regards the shape analysis of the granules milled. The main purpose of this kind of work concerns the research of the influences of the porosity of the batches in the production of particles with different shape. Besides, the effects of the impeller speeds will be deepened. This analysis considers both the aspect ratio and the circularity of the groups of milled granules. They are determined through the analysis at the QicPic. In Figure 3.27 the aspect ratio distribution of the groups milled at 200 rpm and made by 1 g of MCC 102 is reported, in order to evaluate the influence of the porosity. It can be observed that the aspect ratio is the same for the sizes of particles which belongs to the original powder, so for sizes lower than about 250 µm. Then, for larger granules, the aspect ratio changes as function of the porosity. Indeed, although there is a high variability in the experimental points calculated by the QicPic, it decreases if the porosity value is lower. This suggests that more irregularities affect the shape of the strongest particles. The explanation of this difference can be found in the strength itself of the ribbons at lower porosity. Indeed, they need more time to be milled and so they are more affected by the breakage action of the

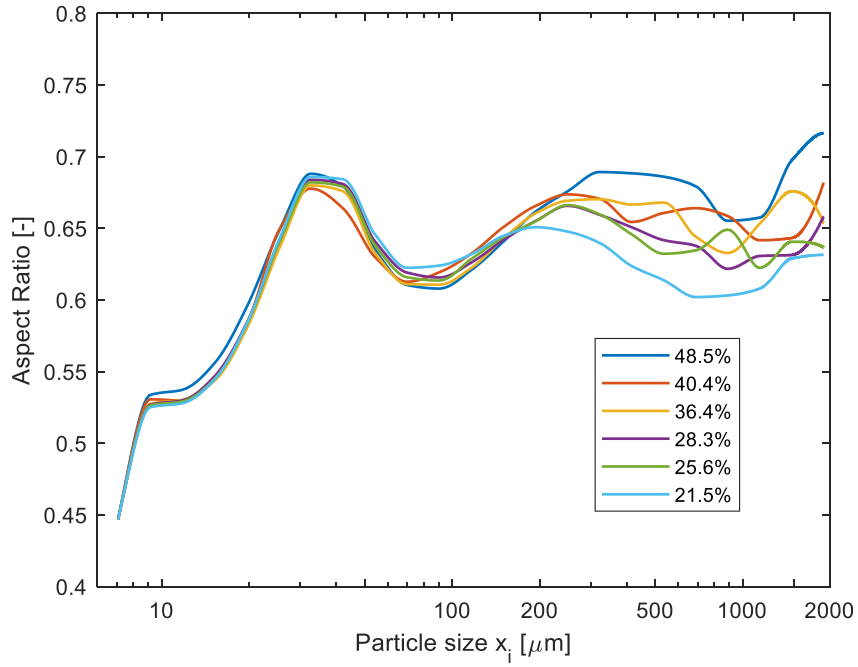

Figure 3.27 *- Aspect ratio of the groups of ribbons milled at 200 rpm and made by 1 g of MCC 102*

impeller, which also contributes to create more irregularities in the surface shape. However, the aspect ratio of all the batches is quite low for the smallest fines, while it increases sharply, to decrease and increase again for the sizes corresponding the first mode of the PSD of each group. A deeper analysis of the shape involves also the study of the circularity, which is outlined in Figure 3.28, for the same groups reported in Figure 3.27. The evaluation on the

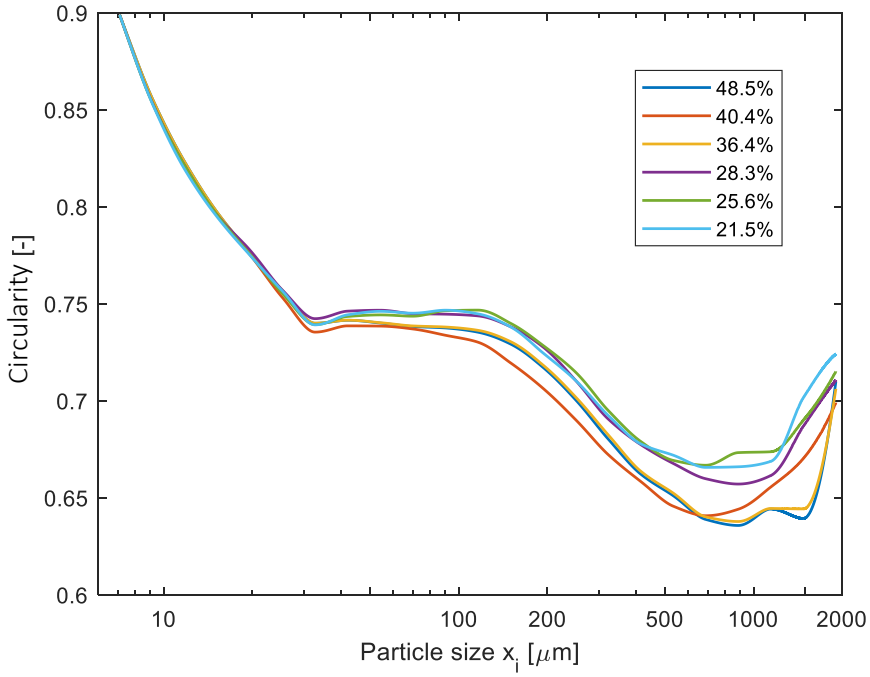

Figure 3.28 *- Circularity of the groups of ribbons milled at 200 rpm and made by 1 g of MCC 102*

circularity highlights that it remains roughly the same for all the batches until about 200 µm. Then, it seems to be smaller for the groups with greater levels of porosities, while it increases, if the ribbons are stronger. This means that the perimeter of the projected area of the particles, determined by the QicPic, is more similar to the perimeter of the circumference with the same area for the batches of ribbons with a lower porosity. By observing Figure 3.28, the minimum value of circularity is set between 500 µm and 1000 µm. For larger granules, the circularity increases again, highlighting that the largest particles, which correspond to the ones of the second mode of the PSD, are more spherical, with values of circularity roughly equal to the particles of the first mode of the PSD.

The same analysis is performed in order to study the effect of the impeller speed on the shape distribution. This is carried out by studying the batches of ribbons made by 1 g of powder compressed at 30 kN and milled at the three different impeller speeds: 100, 200 and 350 rpm. The results for both the aspect ratio and the circularity are reported in Figure 3.29. This shows the same results of the previous analysis regarding the particles which correspond to the PSD of the original powder. However, by looking to the circularity, Figure 3.29-b, it can be observed a kind of relationship between it and the impeller speed for the largest particles. Indeed, the largest particles from a slowest milling seem to have a greater value of circularity, compared to the ones milled at 200 and 350 rpm. The same considerations can be done for the aspect ratio, Figure 3.29-a, regarding the largest granules of the distribution (with a size larger than 1000 µm), although the trend is not so clear, as the AR changes a lot from 300 µm to 1000 µm. A possible explanation of the increase in the irregularities on the shape of the particles can be the same presented in the analysis concerning the effect of the porosity. Indeed, a faster rotational speed improves the breakage action of the impeller, leading to fragments more irregular.

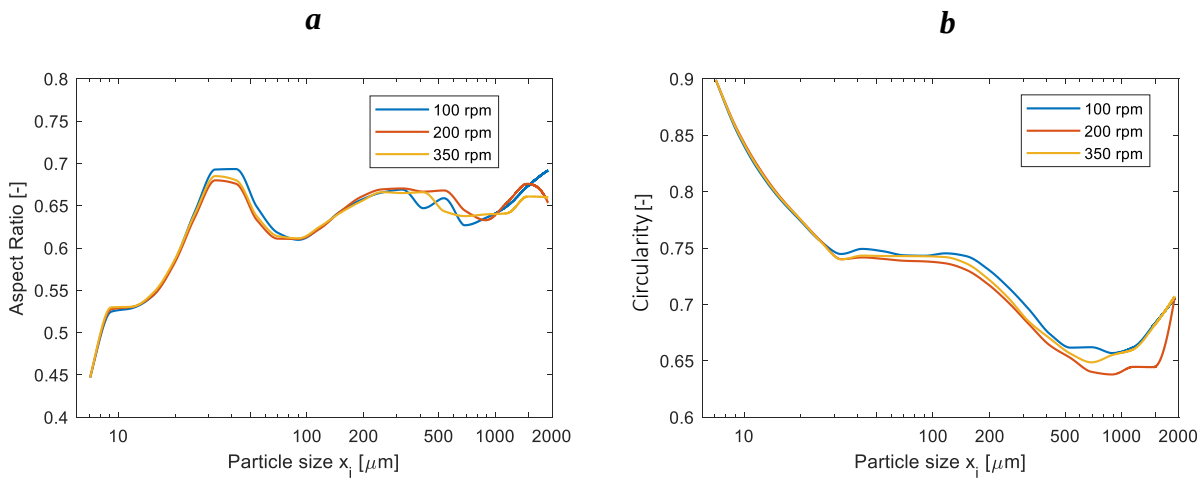

Figure 3.29 *- Aspect ratio (a) and circularity (b) of the groups of ribbons milled at 100, 200 and 350 rpm and with a 36% of porosity*

The same analysis is still valid for the other levels of porosity. In conclusion, the impeller speed does not cover such a relevant role in the determination of the shape of granules, although it seems to affect the distribution. Instead, the porosity has been found to hold a clearer influence in the distribution of the shape of the granules.

3.7 Experimental Results Considerations

The experimental phase of this work covers the main part of the project and it deepens the first compression step and the milling in order to get a deeper understanding of the properties of the dry granulation process. One of the most widespread excipients, such as the MCC 102, has been studied, in order to determine how different operating conditions affect the process performances, in terms of time, quality of the PSD of the granules and amount of fines generated. The main targets achieved can be summarized in the following list:

- 27 groups of 18 ribbons each have been produced at different compression forces, different amount of powder used and different storage conditions set for the original powder of MCC 102.
- The characterization of each batch of ribbons has been performed and a statistical analysis has helped to determine the quality of the uniaxial compression step in the production of ribbons at consistent levels of porosity.
- The kinetic of milling has been studied in order to find how the impeller speed, the porosity and the environmental storage conditions affect the time performances of the milling step.
- The PSD of all the batches of ribbons have been analysed, by focusing on the bimodal distribution produced by the conical mill coupled with the set screen.
- The influences of four factors (porosity, impeller speed, thickness and moisture content of the powder) have been studied in depth.
- The quantitative determination of fines has been performed, in order to find the best operating conditions suitable to minimize the generation of these undesired small particles.
- The shape analysis has been carried out, studying the influence of the porosity and impeller speed.

The porosity and the impeller speed have been found to have an opposite effect in the profiling of the PSD, as their increases lead to a greater generation of fines and a smaller production of the largest granules, which are more suitable for the following compression

into quality pharmaceutical tablets. Besides, the moisture content, related to the environmental relative humidity set in the storage room of the raw powder, plays an important role, together with the thickness set for the ribbons. Therefore, the best operating conditions suggests compressing at large pressures the powder stored at high environmental relative humidity. The ribbons should be quite thin in order to minimize the effect of thickness and so, a small but suitable mass flowrate should be sent to the rollers. Then, the impeller speed of the mill must be as smaller as possible, in order to increase the large granules, although the best compromise should be found by considering also the efficiency and throughput of the overall process. These considerations need the validation through a further analysis regarding the tensile strength of the final tablets produced by the compression of the granules achieved in this project, in order to understand if the tablets strength is suitable for the medical use and for the market. Besides, the applicability of the operating conditions suggested in this work needs more studies on an industrial process of dry granulation with roller compactor, in order to validate the good highlighted performances under an industrial manufacturing point of view.

The main results regarding the effects of the porosity and the impeller speed in the change of the PSD of the milled granules will be the basis for the following step of the work, which concerns the modelling of the experimental PSD through a Population Balance Model (PBM). The main target is to build a model suitable to predict the PSD of the milling of ribbons of MCC 102 made at different levels of porosity and milled at different impeller speeds.

Chapter 4

Modelling

This final chapter regards the modelling part of the milling process. It covers the description of the Population Balance Model adopted and its features, focusing on the development of the model and the method of search of the parameters. The procedure adopted in order to find the correlations between the parameters and the operating conditions will be explored. The results and the final model will be achieved using the experimental data already presented in Chapter 3. In the last part, the model will be compared with the validation experiments carried out in order to test the quality of results.

4.1 Purpose

The modelling part aims to predict the milling process through a Population Balance Model. In this step it is fundamental, first, to tune the structure of the model and, then, to prove the capability of the predictive method adopted. As already discussed in chapter 1, the PBM is widely used in granulation because it can describe the evolution of the sizes of particles during time. Indeed, different types of PBM can be adapted to model different phenomena of a population of particles, from the breakage, to the agglomeration and the coalescence. The targets of the modelling part of this work can be summarized as:

- Development of a PBM structure with a newly developed breakage function;
- Search of the parameters of the model through the fitting of the experimental data;
- Search of the dependence of the model parameters on the analysed operating conditions, such as the impeller speeds set in the mill and the levels of porosity of the batches of ribbons;
- Study of the time-predictive capability of the PBM developed;
- Validation of the final PBM developed through the comparison between the simulated results and more experimental data;
- Prediction of PSD of the milled granules as function of the impeller speed and the levels of porosity of the batches of ribbons processed.

4.2 Structure of the Model

The PBM has been already discussed in chapter 1, where the main uses and the structure have been presented in depth. Starting from the general equation 1.1, which represents the entire family of the PBMs, a more practical form is built and reported in the expression 1.7. This one allows the development of the model starting from the size-discretized experimental data. The main feature regarding the PBM described in the chapter 1 is the breakage kernel, which defines the structure of the predictive mechanism of rupture of particles implemented in the model. Besides, another important characteristic is the breakage function which determines the fraction of particles broken inside the mill. This one is related to two sizes of particles: the intact one and the milled one. Therefore, the model implemented in Matlab® is:

$$\frac{dM_i(t)}{dt} = \sum_{j=1}^{i-1} b_{ij} k_j(t) M_j(t) - k_i(t) M_i(t) \tag{1.7}$$

Reminding that k_i is the size-discretized breakage kernel, while the b_{ij} is the breakage function, the model can be correctly developed through the definition of these two factors. The breakage kernel k represents the specific breakage rate of the particles into granules. The form of the function is the same of the equation 1.9 and, so, it can be defined as:

$$k_i = c_1 \left(\frac{x_i}{x_0}\right)^{c_2} \tag{4.1}$$

Where c_1 (s^{-1}) and c_2 represents the first two parameters of the model. The term x_0 is the maximum size of the particle fed into the mill chamber.[49] By considering the average of the ribbons volume and the $\sqrt{2}$ rule used to define the width of each size of particles in powder technology studies, the maximum size x_0 has been estimated to be equal to 7872 µm. Moreover, the breakage kernel is modified through the classification function, which involves the selective effect of the size of the sieve used in the conical mill. Indeed, the model needs to represent the real behaviour of the breakage mechanism, which continues to mill the particles that are trapped into the mill chamber, as they have sizes greater than the holes of the sieve set. Therefore, by considering the equation 1.10, the classification function H_c is more properly defined as follows:[33]

$$H_c(x_i) = \begin{cases} 0 & for\ x_i < (1-\sigma)\, d_s \\ \dfrac{d_s - x_i}{d_s \sigma} & for\ (1-\sigma)\, d_s < x_i < d_s \\ 1 & for\ x_i > d_s \end{cases} \tag{4.2}$$

Where d_s is the size of the aperture of the screen holes and it is assumed to be equal to 2800 µm, by considering the geometry of the sieve and the experimental data regarding the class sizes. The σ is another parameter of the model, while x_i represents the size of the class *i*. The classification function is used in the model by multiplying the breakage kernel k_i in order to select the sizes smaller than the screen aperture, for which the breakage mechanism has stopped, as in the experiments they exit from the mill chamber, passing through the holes of the sieve. There are medium class sizes, which represent the granules smaller than the screen aperture, but greater than a critical size, which depends on the model parameter σ. Although these particles could theoretically pass through the holes, they stay in the chamber longer and they are involved in a breakage kernel modulated by a classification factor which has a value between 1 and 0 that depends on the model parameter σ. This refined classification function form makes the model more reliable to the real behaviour of grinding of the ribbons, because only the particles much smaller than the screen aperture can exit ideally. Indeed, if the size is smaller, but quite close to the one of the holes, they could be held inside the chamber longer and, so, they could be involved in more breakage phenomena, before finding the right orientation to pass through the sieve. Regarding the breakage function b_{ij}, it is related to the difference between the cumulative breakage function $B(x_j)$ and $B(x_i)$ which correspond to the class *j* and *i*, respectively, as already explained in §1.5.2. So, it can be defined as follows:

$$b_{ij} = B(x_j) - B(x_i) \tag{4.3}$$

The definition of the cumulative breakage function represents one of the main factors that difference many kinds of models. It describes the fraction of particles of a *i* size, which is broken into particles of a *j* size. Therefore, the function is an array of values which covers all the sizes involved in the system. According to literature, the P80-m Weibull distribution has usually been used in order to describe the cumulative breakage function.[71] The quality of the prediction for a single modal distribution has been proved.[71] Therefore, by considering the bi-modal distribution of the PSD achieved through the milling experiments, the equation 1.8 and the P80-m Weibull distribution, the following equation is implemented in order to define the cumulative breakage function:

$$B(x_i) = \alpha\left(1 - e^{\ln(0.2)\left(\frac{x_i}{p_1}\right)^{m_1}}\right) + (1 - \alpha)\left(1 - e^{\ln(0.2)\left(\frac{x_i}{p_2}\right)^{m_2}}\right) \tag{4.4}$$

where α, m_1, m_2, p_1 (µm), p_2 (µm) are the other five model parameters. According to the literature discussion on the P80-m Weibull distribution, either p_1 *or* p_2 is the size of particles

at which the 80% of the total cumulative mass has passed through the screen.[71] The other parameter regards the 80% of the total cumulative mass of the cumulative mass related just to the first mode of the bi-modal distribution.

According to literature some restrictions are needed to the functions of the model.[72] They mostly regard the mass conservation. The first assumption concerns the breakage kernel k_i, which must be equal to zero for the smallest size of the process. Indeed, the mass of the smallest particles cannot be dispersed in more breakage phenomena, as the smaller particles are not involved in the model. Besides, the conservation of the total mass requires also two more constraints on the breakage function b_{ij}. Therefore, if the smallest size of the system is the N-size, the three restrictions implemented in the model can be defined as follows:[72]

- k_N is assumed to be equal to zero;
- $\sum_{i=1}^{n} b_{ij} = 1$, where n represents the number of size classes;
- $b_{ii} = 0$.

The model developed represents a time invariant model, where the breakage kernel is assumed to be time independent. The reliability of this kind of hypothesis is based on the fact that some factors, like fines should have a small impact on the process, as the screen aperture is large and they are difficulty trapped into the milling chamber. So, their influence on the process is low and it can be neglected. Besides, the filling grade of ribbons in the milling chamber is low, so the effect of the small granules trapped in the first moments of the milling process could be neglected, with respect to the final steps, as the difference in the filling is not so marked. Nevertheless, the study of a time-variant PBM could be an interesting future work, useful to compare the results with the ones achieved in this model, in order to estimate the quality of the time-invariant assumptions made.

4.3 Method to Determine the Model Parameters

As already explained, the model is defined by eight parameters, which are reported in Table 4.1.

Table 4.1 *- Eight parameters of the PBM developed, with the corresponding units of measure*

m_1	m_2	p_1	p_2	c_1	c_2	α	σ
-	-	μm	μm	s^{-1}	-	-	-

The model analysis concerns the search of the values of these unknowns and the evaluation of possible relationships with the operating conditions, such as the porosity and the impeller speed. The tool used in order to search the values of the parameter and to implement the model is Matlab. The model has been developed and written, setting the constraints imposed above. The search of the parameters has been carried out through the minimization function of the software. The procedure concerns the fitting of the experimental data achieved during the first part of the project. The objective function of the script is the error between the normalized frequencies of the experimental and modelled points. The standardized form reported in the equation 1.12 is implemented in the model, as it is mostly adopted in literature.[49] It can be defined as follows:

$$F_{obj} = \sqrt{\frac{\sum_{i=1}^{N}\left(\frac{M_i^{Exp}}{\Delta x_i} - \frac{M_i^{Mod}}{\Delta x_i}\right)^2}{N-8}} \tag{4.5}$$

Where N is the number of the experimental points, while i is the size and Δx_i (μm) is the interval of each class size. M_i^{Exp} and M_i^{Mod} are the experimental and modelled frequencies (%), respectively. So, the software works to find the minimum of F_{obj} by changing the values of the parameters.

$$F_{obj}^{min} = \min|_{par}\{F_{obj}\} \tag{4.6}$$

The two commands used by the software in the fitting are `fminsearch` and `fmincon`. The first one finds the minimum of an unconstrained multivariable function using a derivative-free method, while the second one is used for constrained multivariable functions. `fminsearch` is used mostly in the first part of the fitting procedure, in order to study the possible values and to understand the order of magnitude and the sign of each parameter. Instead, the `fmincon` is used in the final steps, when some intervals and constraints to the values of the parameters can be set, in order to refine the search and concentrate the computational effort only within the values intervals more relevant. This allows to achieve quite precise values of parameters, with minimum F_{obj}.

The procedure of search of parameters is non-trivial, because the software tools are affected by local minimums, that can move the parameters far from a convergence to acceptable values, characterized by very small errors. Besides, the initial values set for the eight parameters affect the quality of the fitting process, because they determine if the software is locked in a wrong local minimum where the solver cannot move out from. Therefore, the choice of the initial conditions to set is quite critical in the first part of the search.

Nevertheless, by considering the structure of the model and the principles and hypotheses on which it is based, some preliminary conditions can be set and they regard the intervals of the reasonable values of the parameters:

- p_1 and p_2 must have values within the interval 0-2800 µm, as explained in the previous paragraph. Indeed, one of them is related to the size of the 80% of the cumulative mass fraction passed through the screen, which must be below 2800 µm.
- α and σ must have values within the interval 0-1, because they are parameters used to define the proportion among two factors. Regarding α, the proportion concerns the two modes of the distribution, while for σ it is related to the difference between the screen and the critical sizes.

Regarding the other parameters, the set of preliminary constraints is less simple. Nevertheless, thanks to literature, the initial conditions can be estimated, starting from values used in other similar PBMs. Indeed, according to a study performed in a hammer mill the values of the m_1, m_2, c_1 and c_2 can be set in the order of magnitude between tenths and units. [71] Besides, literature reports the main features that mostly affect each parameter. Indeed, m_1 and m_2 are related with the distribution of the particles in the two modes. Therefore, they could be affected by the porosity and the impeller speeds.[73] Instead p_1 and p_2 are related with the position of the two modes, as they belong to the P80-m Weibull distribution. And these positions should not change if the same raw materials (same PSD of the original powder) and the same screen are used. α and σ need to be determined by fitting, but they may be affected by operating conditions. At last, c_1 depends mostly on the operating conditions, while c_2 depends on the properties of the material, according to literature.[73] The numerical method set uses the command `ode45` in order to solve the differential balance represented by the PBM. The interval of time used goes from time of zero seconds to the time corresponding to the milling end-time, already discussed in the previous chapter. Moreover, by considering that in the experimental phase a sample at 10 s has been collected during each experiment, the model can be studied also at this intermediate time, in order to compare the PSDs outlined in the experiments with the ones achieved through the model. This kind of analysis will be discussed more in depth in §4.4.2.

The procedure set in order to achieve the parameters and the influences of the operating conditions is divided in different phases. First, a general search through the minimization function `fminsearch` is performed mostly thanks to a trial and error method. This allows to reach a first rough estimation of the possible values of the parameters and the relationships with some conditions. Then, the constraints to each parameter are set and a more specific analysis is carried out through the solver `fmincon`. A deeper analysis is performed by

changing each parameter with many values within the interval set as constraint. The computational effort of this kind of analysis is relevant, but it allows to understand much narrower intervals of values per parameter suitable to minimize the objective function. At this point, the relationships between the parameters and the operating conditions can be highlighted. In this work, only the levels of porosity and the impeller speed have been considered. Indeed, the modelling part concerns all the batches made by 1 g of powder stored at normal environmental condition. Therefore, the values of the parameters independent by the two factors are set constant and the possible relationships of the other ones are investigated one by one. The final target is the definition of all the parameters and the relationships between them and the operating conditions through a mathematical function. The final development of these relationships is performed through the fitting of the parameters as function of the porosity and/or the impeller speed. At the end, the model developed will be compared with the validation experiments, in order to assess the quality of the results and the effectiveness of the model itself.

4.4 Model Results

This section concerns the analysis of the model, focusing on its predictive quality of the PSD and the parameters values. The first paragraph regards the most part of the analysis, covering the preliminary one and the tests performed through the set of constraints to the parameter. Hence, the quality of the results will be described through the comparison with the experimental data. In the second paragraph the implementation of the model to the intermediate sample, collected at 10 s, is performed.

4.4.1 Model for the Prediction of the Final PSD

The prediction of the final PSD, achieved at the end of the milling process, is the main target of the modelling part. The first studies of the parameters' values have been performed to the group of ribbons compressed at 30 kN and milled at 200 rpm. This group is assumed as the reference group to report the main results achieved. In the first part of the preliminary search, the analysis of the minimization of the F_{obj} by changing the parameters' values in wide intervals has been performed. The intervals have been set by considering the constraints reported in §4.3, derived from literature. Roughly 1000 values have been evaluated per parameter. The results of the analysis allow to set the intervals reported in Table 4.2, in order to perform the following refinement of the model, through the `fmincon` software tool.

Table 4.2 *- Intervals of the possible values of the model parameters set after the first analysis*

m_1	m_2	p_1	p_2	c_1	c_2	α	σ
1-3	*1-3*	*200-400*	*1500-2500*	*0-5*	*0-5*	*0-0.4*	*0.2-0.4*

The following study allows to determine the best parameters' values that minimize the objective function of each group of ribbons. The PSD achieved for the reference group is reported in Figure 4.1. Both the normalized mass distribution and the cumulative distribution, fitted from the experimental ones, are presented in the chart.

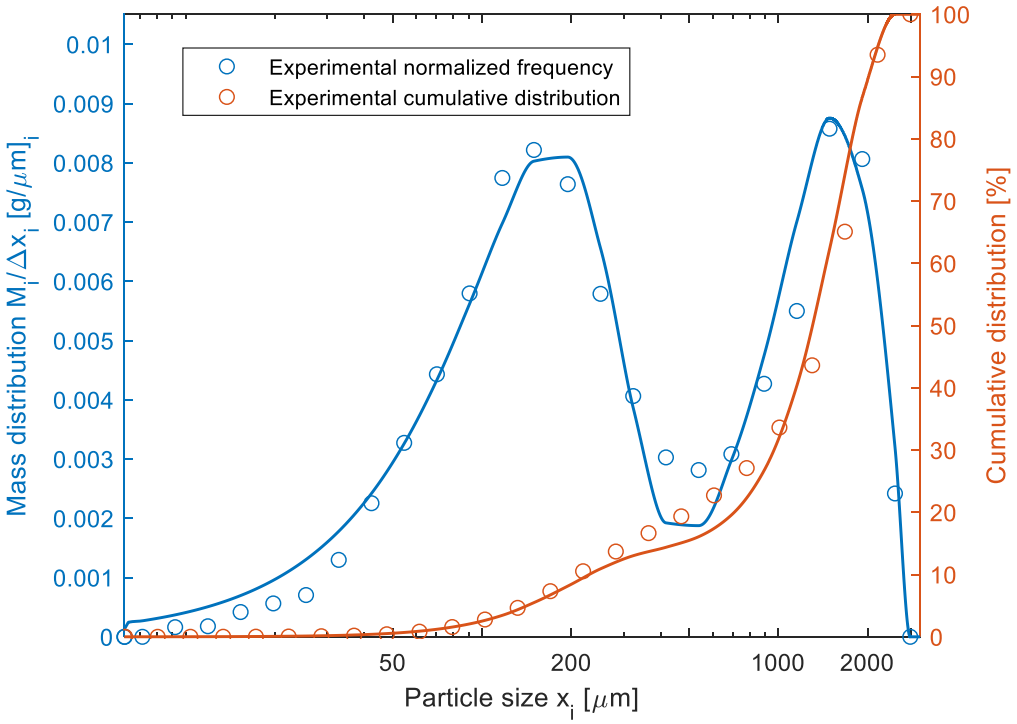

Figure 4.1 *- Experimental and modelled normalized frequency and cumulative distribution of the reference batch of ribbons (at 36.4% of porosity and milled at 200 rpm)*

Figure 4.1 shows the high quality of the results, as the model fits the experimental data with a high accuracy. Both the two modes of the distribution are fitted properly and the particles with larger sizes are predicted accurately, although the first peak seems to be shifted just a bit to larger sizes. The F_{obj} achieved is equal to 0.00063, which is quite low, especially by considering that there are a lot of points to be fitted, which may be affected by experimental inaccuracies. The same good results are achieved for the other groups of ribbons. Nevertheless, all the other charts are not reported in order not to weigh the text. The parameters achieved for all the model runs are presented in the following eight charts reported in Figure 4.2. Each plot shows the value of one parameter as function of the averaged porosity of each group of ribbons and it is parametric on the impeller speed.

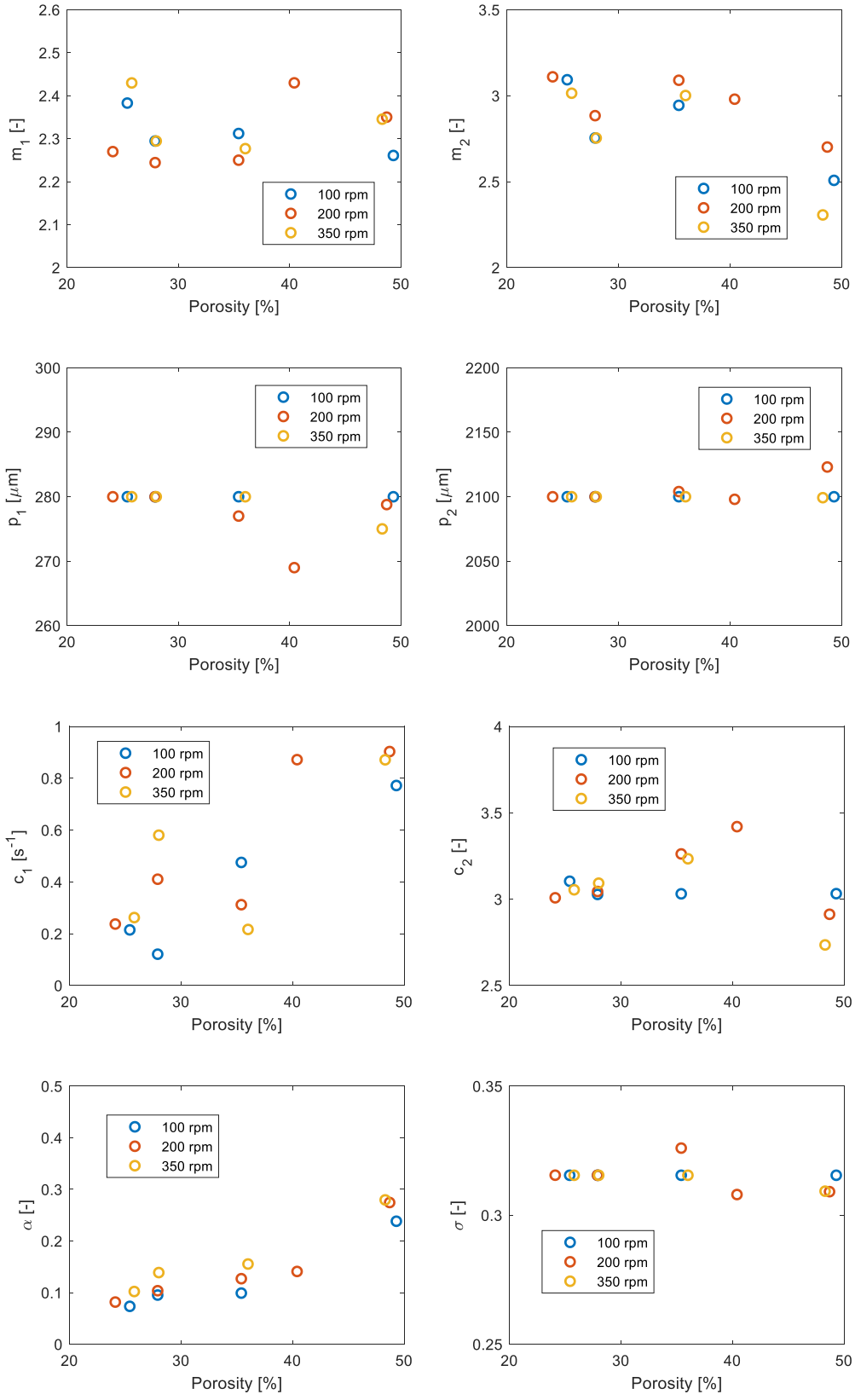

Figure 4.2 *- First step of search of the eight parameters of the model. Each chart reports the values of one of the eight parameters as function of the ribbon porosity and the impeller speed*

These charts show the parameters of each group of ribbons and they represent the best values achieved in order to minimize the F_{obj} and to reach the best fitting of the experimental data. The constraints used are the same for all the runs of the model and they are reported in Table 4.2. This result is important to highlight the possible influences of the porosity and the impeller speed on each parameter of the model. Besides, possible qualitative relationships can be observed between some parameters and the operating conditions. The parameters that can be assumed constant clearly are p_1, p_2 and σ. Indeed, their values are very stable among the batches of ribbons and no relationships with the porosity and the impeller speed are observed. Therefore, their values may be at: 280 µm, 2100 µm and 0.315, respectively. Besides, the parameters m_1 and c_2 do not present clear relationships among the different batches with respect to both the impeller speed and the porosity. Nevertheless, they show a high variability, so, in the first next steps of the analysis of their values are not constrained, but they are strictly monitored. Instead, the other three parameters, m_2, c_1 and α show dependences on the operating conditions, so, they are studied in depth during the following modelling part, in order to catch more precise influences.

Starting from these considerations, the following steps concern the refinement of the process, through the search of the quantitative relationships between parameters and the porosity and impeller speed. In order to perform this kind of analysis, some hypotheses have been considered. Therefore, the parameters found to be constant among the model runs have been kept constant in the following analysis. Then, other runs of the model have been processed in order to achieve the new values of the parameters. As already reported, the p_1, p_2 and σ have been set to the values of 280, 2100, 0.315, respectively. This assumption is based on the results of the fitting of the model, but also on the theoretical principles that characterize these parameters. Indeed, they should not depend on the porosity of the ribbons and the impeller speed, as already explained in §4.3. After the following model runs, the parameters that do not show clear relationships with the operating conditions and that seem to have roughly constant values are assumed to be constant, as already done in the previous simulations. Then, the analysis has been deepened through more model runs, until the final steps which can divide the parameters into two distinct groups, the one that can be kept constant at different operating conditions and the one involving parameters affected by the porosity and/or the impeller speed. At the end of these steps, also m_1 and c_2 do not show dependence on those factors and they have been assumed to be constant for all the batches and equal to 2.32 and 3.1, respectively. Therefore, just three parameters have been found to be dependent by the two conditions analysed: m_2, k_1 and α. The results regarding the values of all the parameters and their relationships with the porosity and impeller speed are reported and discussed in §4.5.

4.4.2 Model for the Time Prediction

During the project, the first part of the modelling study concerned the development of a PBM suitable to predict both the PSDs of the samples collected at two different times. The collection of the two samples has been already discussed in chapter 3. The purpose was the tuning of the model at 10 s of milling and at the end of the process. The procedure followed was the same described in the previous paragraph. The main difference is the research of the parameter aiming to minimize the F_{obj} both for the PSD at 10 s and at the end of the process. This target was implemented in the software through the minimization of the sum of the errors at two times. Then the steps followed aimed to determine the values of all the parameters and the relationships of some of those with the operating conditions. Concerning the parameters, the results are slightly different with the ones reached by analysing just the end of the milling process. This can be explained by considering that the fitting step involves double set of parameters, with respect of the previous analysis. So, in order to get the lowest errors, the model is highly affected by the new set of data used. Nevertheless, a good model should be suitable to predict the PSD during time, so this kind of analysis is of larger interest and the possible positive results are more relevant. However, the model achieved had poor predictive quality and was not able to fit the experimental data properly at the two times considered and for all the data sets used. The main observed problem concerned the fitting of the 10 s of milling for the ribbons at the lowest porosity values (45 kN and 60 kN). An example of this discrepancy between the experimental and modelled results is reported in Figure 4.3.

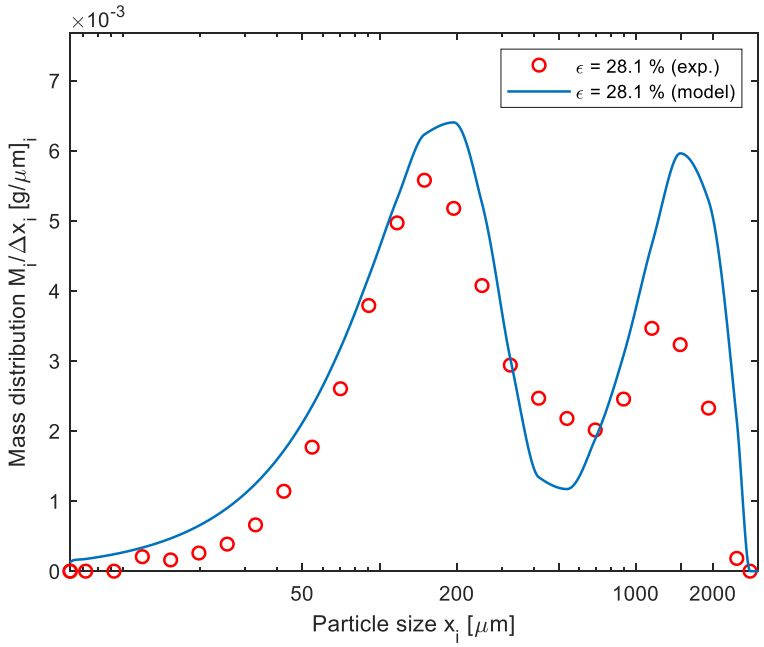

Figure 4.3 *- Experimental and modelled PSD of the first sample, collected at 10 s for the batch of ribbons with 28.1% of porosity and milled at 350 rpm*

It can be shown how the second peak and its ratio with the first one are not predicted properly by the model. More runs and studies of the parameters have been deepened, but the model has never been suitable to predict properly the first 10 s of milling for all the tests. The first possible cause was given to possible random experimental errors, although this did not explain why they concerned only the groups of ribbons at lower levels of porosity, instead of all the batches, randomly. The reason was found to be related to a phenomenon occurred during the first part of the experiment for the strongest ribbons. Indeed, more experiments were made at lower and higher levels of porosity and the particles trapped into the milling chamber at 10 s were analysed in order to determine the distributions of the particles into the different class sizes. By considering the screen size equal to roughly 2600 µm, the sizes of the particles held inside the mill were expected to be larger than the holes' diameters. Nevertheless, the results achieved showed a difference among the groups of ribbons and it seemed to be related to the porosity of the ribbons milled. Indeed, for the ribbons at higher porosity values the distribution of the particles was located at sizes larger than 2600 µm, while some small granules were found trapped in the chamber when the ribbons milled were stronger (with a higher level of porosity). The percentage of particles at different sizes which did not pass the screen for a batch of ribbons of porosity of 25% and milled at 200 rpm is reported in the Table 4.3. The mass percentage is calculated from the milled mass of each size interval collected in the test and measured through the scale.

Table 4.3 *- Mass percentage of the milled granules smaller than screen size and trapped into the mill chamber*

0 – 280 µm	*0.7%*
280 – 500 µm	*1.2%*
500 – 1400 µm	*2.1%*
1400 – 2000 µm	*9.8%*
2000 – 2800 µm	*12.8%*

The results reported in Table 4.3 show that there are a few granules smaller than 2800 µm which do not pass through the sieve. Although the amounts are not great enough to affect the results and the relationships observed in the chapter 3, they can affect the fitting of the parameters and so, the entire procedure of search of parameters. Hence, the model developed is not reliable, as it is based on experimental data with some inaccuracies, though they are quite small. The same analysis was carried out for the particles collected from groups of

ribbons at 48% of porosity, but it showed a very low amount of small granules trapped. This phenomenon can be explained by considering that if the granules milled are stronger the milling process is slower, and the milled mass is less at the same time. So, in the first part of the process some granules of medium sizes are trapped inside the screen by the great amount of mass still held into the chamber after 10 s. Therefore, the first sample collected is not reliable enough to tune a PBM, although the experimental results and the considerations done are still valid, due to the small differences. In order to predict this complex phenomenon a future study should regard the development of suitable classification function and breakage kernel dependent on time and on the filling grade of the milling chamber, which is fundamental to model the initial part of the test.

4.5 Final Model

This section concerns the outline of the final PBM developed and, first, the study of the relationships achieved between the operating conditions of the process and the parameters. Besides, the prediction of the PSD at different impeller speeds set and different levels of porosity will be presented.

4.5.1 Influence of the Operating Conditions of the PBM Parameters

The final model developed during the procedure already explained in §4.4.2 is characterized by some parameters that are constant at different operating conditions and other ones that depends on the impeller speeds and the porosity of the milled ribbons. Table 4.4 reports the constant parameters and their values for the final PBM developed.

Table 4.4 *- Values of the five parameters that are constant with respect to the operating conditions*

m_1	p_1	p_2	c_2	σ
2.32	*280*	*2100*	*3.1*	*0.315*

It can be noticed that the values are widely included within the intervals already discussed in §4.3. In particular, the p_1 and p_2 corresponds physically to almost the 80% of each mode of the distribution, and this can be noticed also through the comparisons with the chart of the PSD. Regarding the other three parameters, they have been found to have a dependence on the operating conditions. The final relationships have been studied after more runs of the model for all the experiments considered in the modelling part, by keeping the previous five

parameters constant. The quality of the prediction is still high and the values of the three parameters affected by the porosity and impeller speed are reported in the three charts of the Figure 4.4.

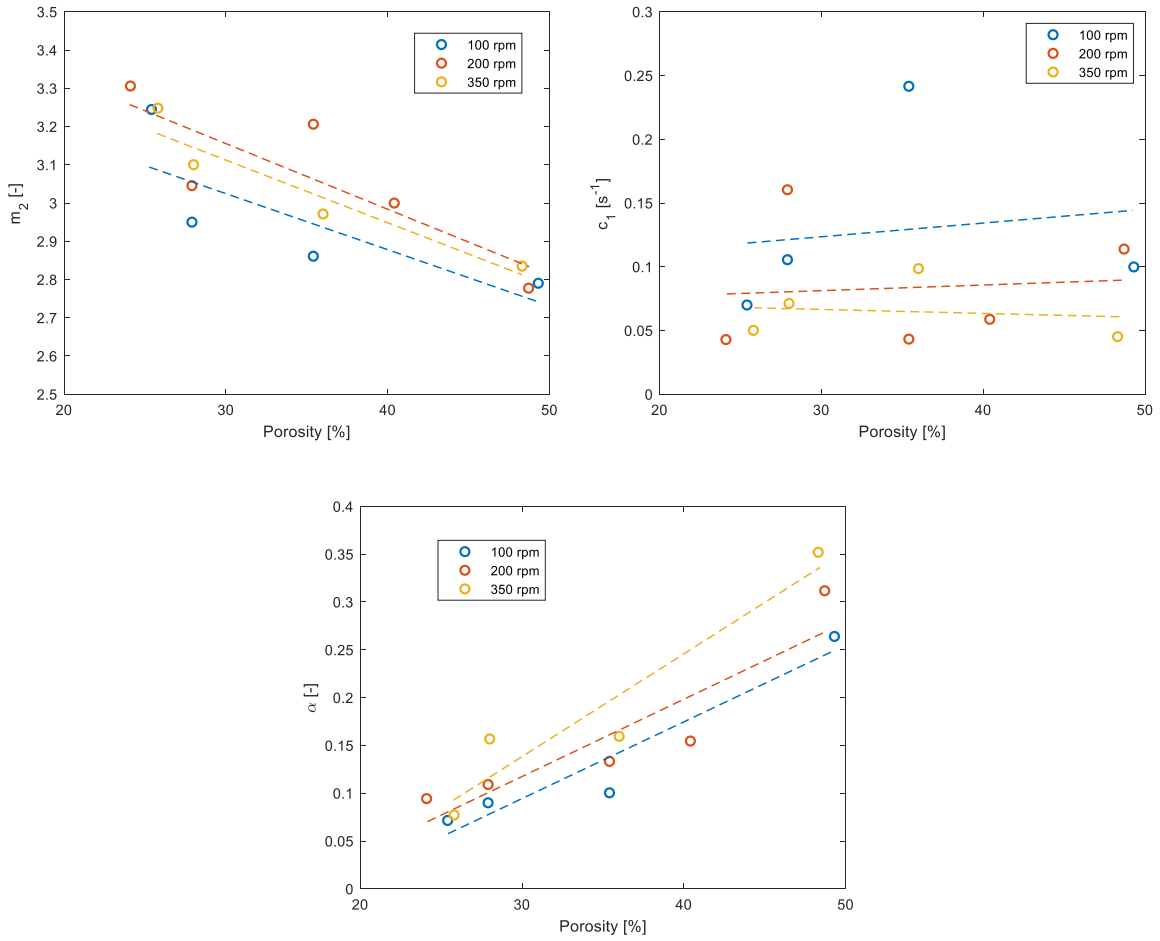

Figure 4.4 *- Values of the three parameters found to be dependent on the operating conditions, for all the batches of ribbons modelled. Linear regressions of the values parametric on the impeller speeds are highlighted by the dashed lines*

It can be observed in Figure 4.4 that the three parameters are affected by the operating conditions. The m_2 is influenced mainly by the level of porosity, as its value decreases when it increases. Instead, the impeller speed does not seem to have an impact on this parameter, as there is no clear trend of variation by changing it. Regarding the c_1 it seems to be affected mainly by the impeller speed, as by observing the average of the groups of batches milled at the same velocity (highlighted by the dashed line), the value increases if the impeller speed decreases, while it does not change with a clear trend if the porosity varies. The last parameter evaluated is α, which is the only one to be affected by both the impeller speed and the level of porosity. This trend is clear by observing the linear regression trend parametric on the velocity and the single points. Indeed, the third chart shows that α increases, by

increasing the level of porosity of the ribbons, while it decreases if the impeller speed is slower. All these trends represent the hypothesis the following analysis is based on. In fact, the next modelling phases aim to refine the search of the relationships between these parameters and the operating conditions, in order to develop the final form of the PBM and to reach a suitable prediction of the PSD of the milled granules. Therefore, by starting from the hypotheses just made, their fittings as function of the levels of porosity and impeller speed are performed. The first parameter to be studied is the c_1, while the m_2 and, at last, the α will be evaluated in order to understand also how the determination of the relationships of the other parameters can affect the remaining ones. Through the analysis performed, the final form of the model has been developed and good relationships between the last three parameters and the operating conditions have been determined. The hypotheses regarding the influence of the porosity and/or the impeller speed on m_2, c_1 and α have been proved and the relationships developed are reported in the following equations:

$$m_2 = -0.023\,\varepsilon + 3.8 \tag{4.7}$$

$$c_1 = -0.051 \ln v + 0.36 \tag{4.8}$$

$$\alpha = -1.35 + 0.13\,\varepsilon - 0.00396\,\varepsilon^2 + 4.02e^{-5}\,\varepsilon^3 + 0.00027\,v^{0.498} \tag{4.9}$$

where ε (%) is the percentage of the porosity level of the batch of ribbons and v (rpm) is the impeller speed.

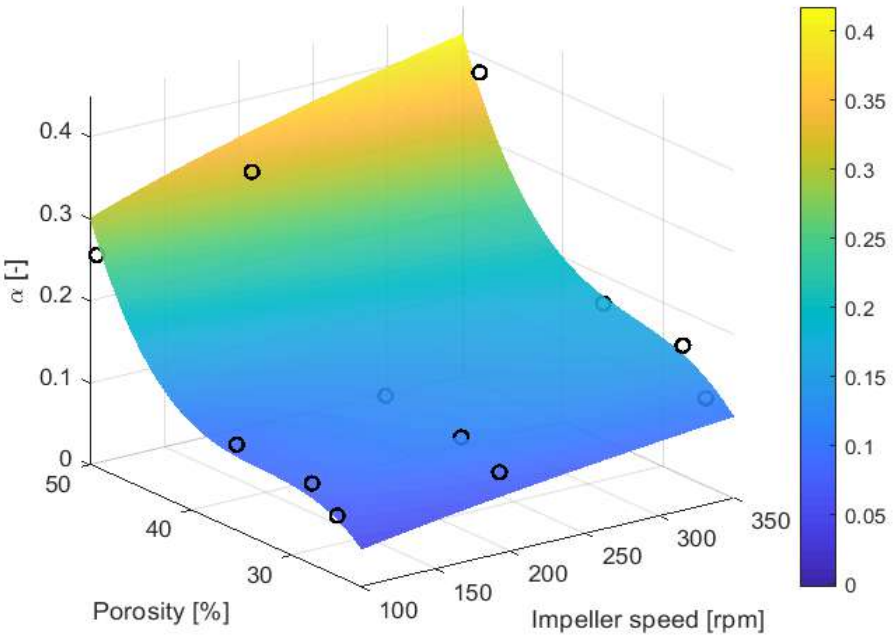

Figure 4.5 *- Values of the parameter α and the fitted surface which describes the α as function of the porosity and the impeller speed*

The first equation shows that the m_2 has a linear dependence on the porosity level, while c_1 can be determined through a logarithmic function based on the impeller speed. The last parameter α is affected by both the two conditions and the dependence is not trivial. It can be observed in Figure 4.5 which reports the surface described by the equation 4.8 and the singular values achieved during the modelling of the PBM. The influence shows that the porosity has a great impact in the determination of the parameters for higher levels, and it decreases if the ribbons are stronger. Besides, the role of the impeller speed is relevant, but non-linear, as it leads to a larger increase of α if the impeller speed is greater, while for lower velocities this difference seems to be a bit smaller. Nevertheless, this particular trend can be well described by the 2-variables equation 4.8, as highlighted in Figure 4.5.

In conclusion, the final PBM can be outlined by the equation 4.1 and five parameters values are reported in Table 4.4 while the last three are described by the equations 4.7-4.9 Regarding the quality of the final PBM developed, it will be deepened in the next paragraph. Nevertheless, an example of the predictive performance of the model is highlighted through the reference group of ribbons in Figure 4.6, which shows the normalized frequency and the cumulative distribution of the PSD of the granules milled at 200 rpm from ribbons with 36.4% of porosity. By comparing the result with the same one achieved in the first part of the model analysis, reported in Figure 4.1, the prediction is still very good, and the refinement of the parameters does not lack the quality of the model.

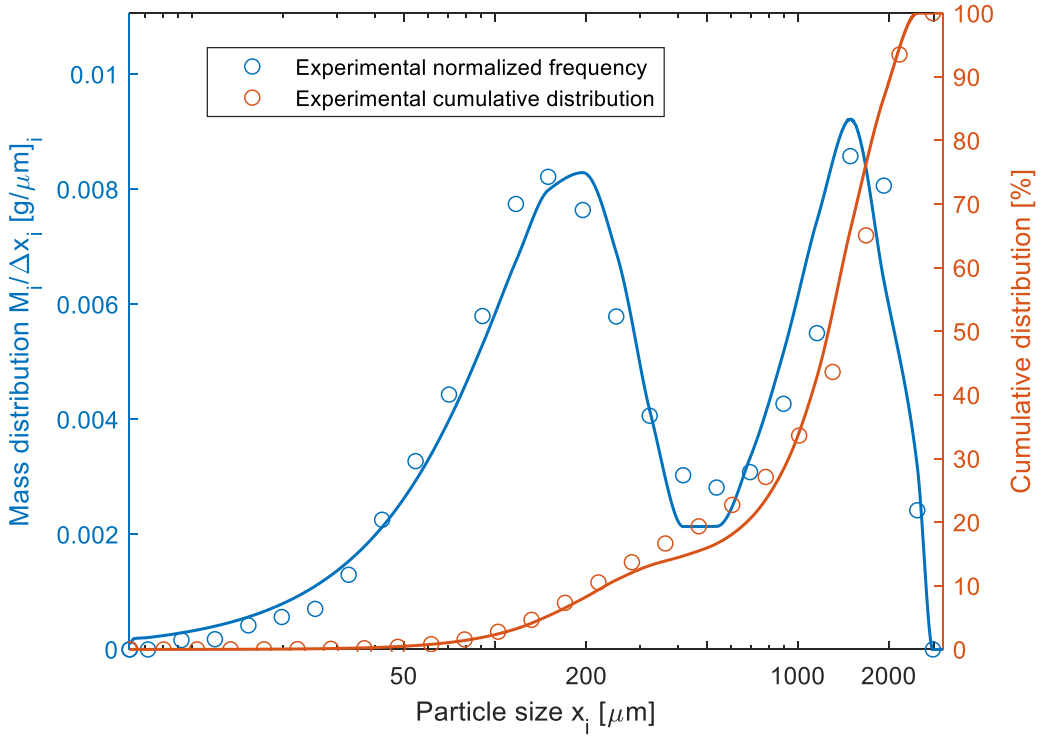

Figure 4.6 *- Experimental and modelled normalized frequency and cumulative distribution of the reference batch of ribbons (at 36.4% of porosity and milled at 200 rpm) achieved with the final PBM*

4.5.2 Prediction at Different Conditions

The final PBM developed in the previous paragraph allows to determine the PSD after milling in a conical mill of ribbons made by MCC 102, with a bulk porosity included in the range of 24% - 50%. The impeller speed set valid for the model goes from 100 rpm to 350 rpm. Higher or lower velocities and porosities of the ribbons concern the extrapolations of the values of some parameters, whose predictability quality needs to be explored through some more experiments. The reliability of the model is ensured only within the limits of each interval studied. More experiments performed in order to validate the model for different conditions involved within the intervals will be described in §4.6. Therefore, once the PBM has been developed the prediction of the PSD of the milled granules at different impeller speeds and different levels of ribbons porosities is carried out. Through the suitable script some 3-D charts are outlined in order to show the PSD as function of the levels of porosity and the impeller speeds. The first one is reported in the Figure 4.7.

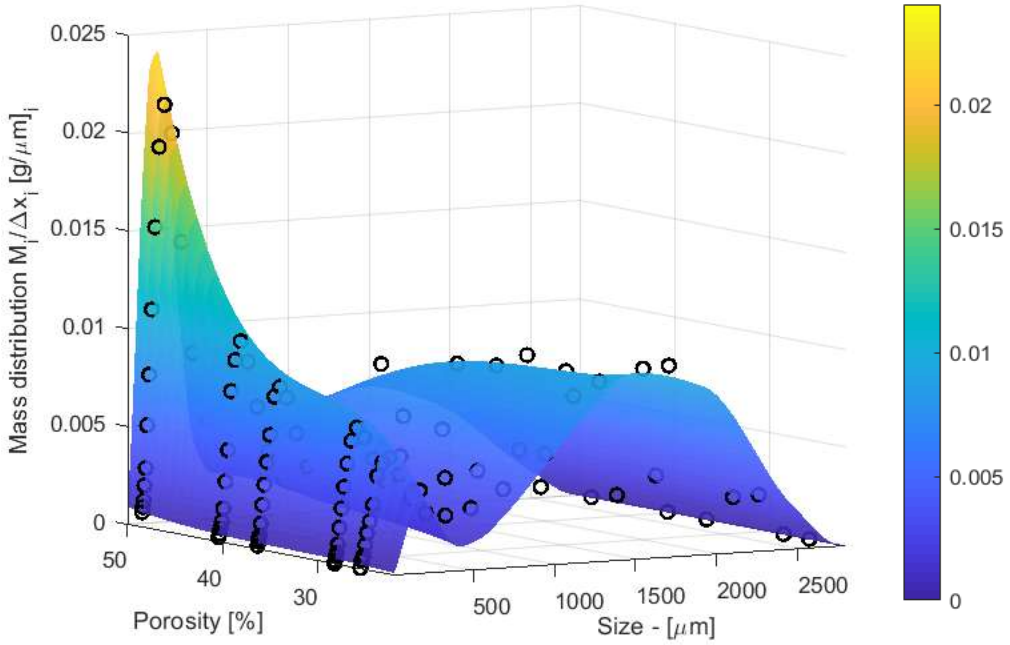

***Figure 4.7** - Modelled PSD of the granules milled at 200 rpm with ribbon porosities within the interval 50%-20%. Black points highlight the experimental distributions achieved for the five batches of ribbons milled at 200 rpm*

Figure 4.7 shows the experimental results already achieved in chapter 3, which the model is based on. Indeed, by increasing the levels of porosity of the ribbons, which is practically made with a smaller pressure force applied during the roller compaction step, the PSD changes, as the second mode decreases, while the first mode increases, meaning that the amount of fines produced is greater. The impeller speed set in the model is 200 rpm and the

experimental points of the PSD are highlighted by the black marks, in order to show the high quality of the PBM prediction. In particular, the first mode is predicted perfectly, while the second peak prediction is still good, although it lacks just a bit in quality for some batches of ribbons. This result is due to the model trend, which is fixed by the parameters, while the experimental data could be affected by some measurement or experimental inaccuracies. The same approach has been used to model the PSD as function of the impeller speed. A porosity value equal to 36% is set and the distribution is reported in Figure 4.8 along velocities which goes from 100 rpm to 350 rpm, which represents the lower and upper limit of conditions studied during the experimental phase. The experimental points corresponding to those categories of ribbons are highlighted by the black marks in the chart.

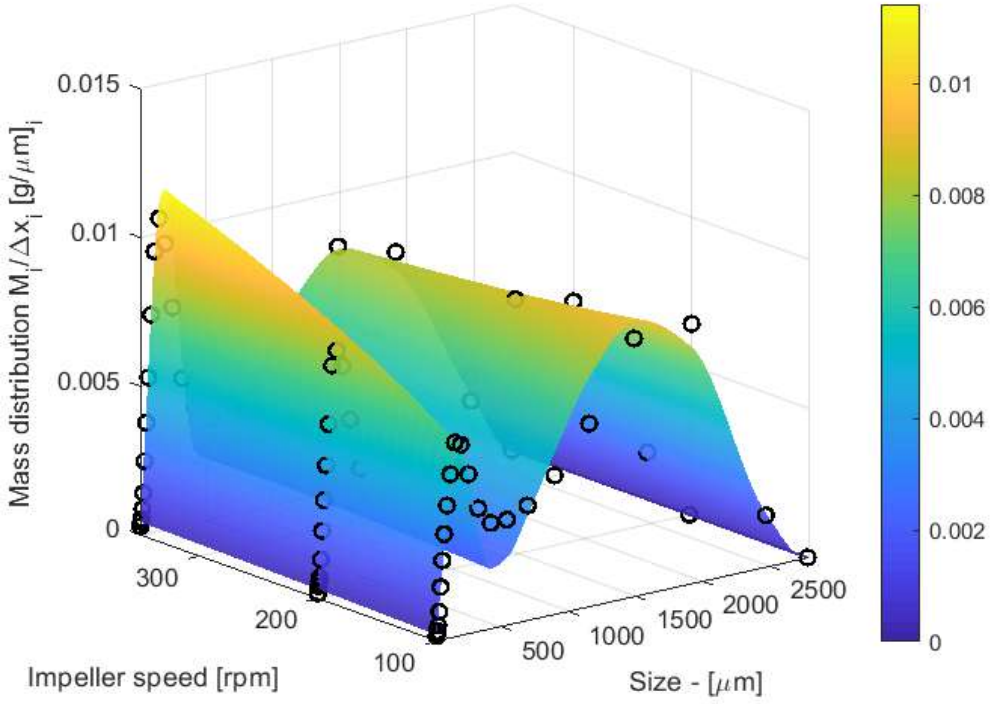

Figure 4.8 *- Modelled PSD of the ribbons with a porosity equal to 36% and milled at different impeller speeds. Black marks highlight the experimental PSD achieved for the three batches of ribbons milled at 100, 200, 350 rpm, respectively*

Figure 4.8 confirms the achievements reached during the experimental phases. It can be seen, how the PSD moves to more large granules if the impeller speed is lower and that more fines are produced at higher velocities. The prediction quality in Figure 4.8 is very high, for both the first and second mode, although it is not optimal for the granules with a size in the middle of the two peaks for the batch of ribbons milled at 100 rpm. This can be explained by some inaccuracies in the experiments, which however do not affect the quality of the results achieved. Therefore, the PBM developed presents a high predictability of the PSD of granules produced through the grinding action of a conical mill.

4.6 Validation of the Model

The final PBM developed and discussed in the previous section needs to be validated through more experiments at different impeller speeds and levels of porosity. Therefore, three more experiments have been performed by setting velocities within the interval analysed, while regarding the level of porosity of the ribbons for two experiments the value has been set within the intervals analysed. Nevertheless, for the last experiments the value has been chosen outside the range studied, in order to understand if the extrapolation of the values of the parameters leads to a poor prediction of the PSD or if the model is still valid and reliable. So, the conditions of the experiments used for the validation are reported in the Table 4.5.

Table 4.5 *- Conditions of the validation experiments performed*

Compression force (kN)		*19*	*37.5*	*90*
Impeller speed (rpm)	*150*	-	31.0 ± 1.6 %	-
	200	-	-	21.5 ± 0.9 %
	300	42.3 ± 0.5 %	-	-

It can be observed that the porosity of the ribbons compressed at 90 kN is lower than the lowest porosity considered during the model development procedure. The corresponding parameters, which depend on the porosity of the ribbons, are calculated through an extrapolation of the values from the interval used to determine the relationships equations.

The results achieved through the comparisons among the simulated PSD and the experimental ones are reported in Figure 4.9. The three charts are outlined in order to show the predictive quality of the model. This figure highlights that for all the three validation experiments the model is still effective, with a good quality of predictability. In particular, the charts *a* and *b* show the comparisons between the modelled and experimental PSD of the milling of ribbons with 42.3% and 31% of porosity, respectively. These plots highlight a quite good effectiveness of the model in the prediction of the PSD of the milled granules, although the results are less precise than the experimental ones used in the development phase of the model. This can be easily explained, by considering that the PSD reported in Figure 3.9 have not been used to tune the parameters of the model, but just to validate it. So, some shifts of the distributions are expected, especially due to the measurement process and experimental type of tests, which may be affected by some inaccuracies.

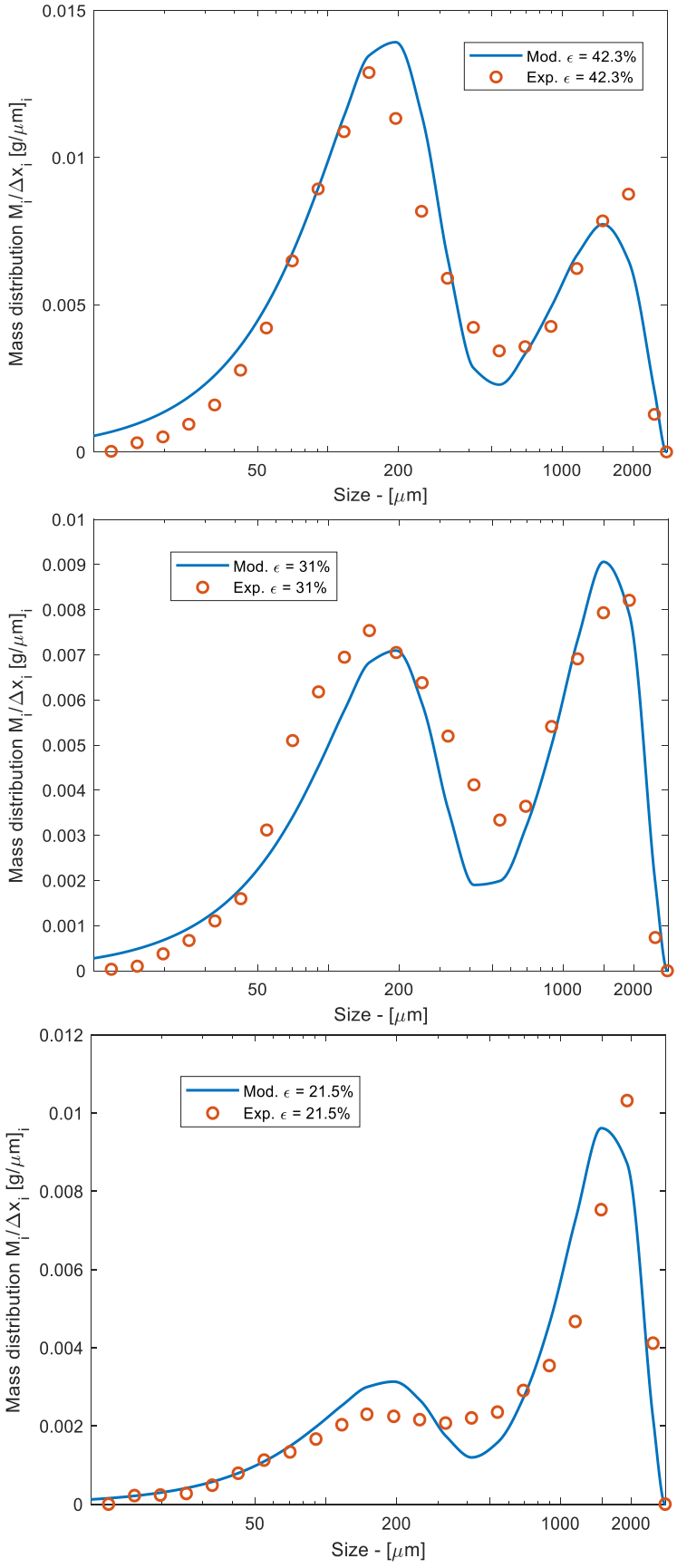

Figure 4.9 *- Modelling of the three validation experiments performed*

Regarding the chart *c* of the model, the result achieved are less accurate and the prediction of the two modes is not as well precise as the previous tests. This result can be explained by considering that the porosity value of that batch of ribbons is lower than the minimum of the interval used in the modelling phase. Therefore, the determination of the three parameters affected by the operating conditions represents an extrapolation of their values and it is not reliable. In particular, the calculation of the parameter α is not reliable outside the interval considered in the modelling analysis, and it is the main cause of the presence of two distinct peaks, which are roughly avoided in the experimental distribution, where the first mode is very flat and much smaller than the peak located at larger sizes. Therefore, Figure 4.9-*c* shows that the model is not suitable for operating conditions outside the intervals used in the development of the PBM.

The good results achieved in the modelling part confirms the high predictability of the PBM developed. The relationships between the parameters and the operating conditions are reliable and effective. Besides, the values of the parameters allow to predict properly the PSD and they are also validated by the experiments performed and the literature. In conclusion, the model can predict effectively the PSD of the granules milled at an impeller speed within the 100-350 rpm interval and from ribbons with a porosity within the 25-50% interval. Therefore, the purposes of the modelling study have been definitely reached and a PBM suitable to predict the PSD of the granules milled in a conical mill has been developed successfully. Moreover, one more time the PBM has been proved to be a suitable and effective tool to model the milling of a dry granulation process.

Conclusions

This project achieved all the targets set in the introduction. The dry granulation of the excipient Microcrystalline Cellulose Avicel® PH-102 (MCC 102) was analysed in depth in order to achieve a better comprehension of the process and of the main features involved. Suitable methods and procedures were adopted to perform a reliable study of the roller compaction of the raw powder and the milling of ribbons in a conical mill. The main purpose of the experimental phase was the understanding of how the operating conditions of these steps could affect the PSD of the milled granules. Indeed, the quality of the final tablets is directly dependent on suitable distributions of the sizes of the granules used for their production. Therefore, the role of four main factors was deepened in order to get their possible influences on the variation of the PSD after the milling step. First, the porosity of the ribbons and the impeller speed were chosen as the main features that could affect the distribution of the granules, as already studied in similar works reported in literature. Besides, the experimental phase was deepened in order to achieve a broader panorama of the process. This was performed through the observation of two more important parameters of the process. The first one concerned the thickness of the ribbons, in order to understand if it could have a possible influence in the change of the PSD, by keeping the other factors constant, while the second parameter was represented by the environmental humidity of the warehouse of the MCC 102, which affects the water content of the powder. The study of the impact of the moisture content was chosen due to its remarkable relevance under an industrial point of view, as the setting of the proper level of humidity of the warehouse can help to achieve a better PSD of the granules, and so higher quality pharmaceutical tablets.

The results of the experimental phase were satisfactory and the dependences of the PSD on the different factors studied were gained from the data analysed through the QicPic. Indeed, the porosity of the ribbons and the impeller speed showed the same trend already found in literature for other kinds of dry granulations and other types of powder. Therefore, the porosity of the ribbons and the impeller speed showed the same trend, and, so, by increasing their values the amount of fines after milling increases, while the bimodal distribution of the granules population is unbalanced towards smaller sizes. Regarding the effect of the thickness, it is less relevant than the first two factors studied, although it seems to increase the amount of fines and the smaller granules in the PSD. Last but not the least, a higher environmental humidity of the warehouse of MCC 102 highlighted a better PSD, with more large granules and less fines. The difference in the water content was small, going from 6% at normal conditions to 9% in a wet environment, and, so, it should not affect the APIs

processed in the dry granulation, which usually are moisture sensitive. This feature needs more studies, related to the specific chemical properties of the drugs. The experimental part deepened also the kinetic of milling, by studying the time required at different impeller speeds and for ribbons at different levels of porosity. Besides, the PSD of the granules milled in the first part of the process was studied, showing the greater production of fines and smaller particles during the initial part of the milling. Moreover, the shape analysis of the granules was performed, showing that the stronger ribbons produce more spherical granules during the milling.

The second main part of the project concerned the development of a PBM suitable to model the milling of the ribbons and to predict the PSD of the granules produced from the ribbons made by 1 g of MCC 102. The results achieved highlighted the high predictive capability of the model, within the range of operating conditions considered which goes from 100 to 350 rpm for the impeller speed of the mill and from 25% to 50% for the level of porosity of the ribbons. The validation experiments performed at the end of the project confirmed the good achievements and the validity of the PBM. The structure of the model was developed starting from some literature studies. The PBM set involved eight parameters which were assumed to be time-independent. The final results reported the values of all the parameters and the dependences of three of them with the porosity and/or the impeller speed. Besides, the time-independent structure of the PBM successfully predict the final PSD of the granules after the milling process. Therefore, the modelling part achieved the set targets and a high-quality PBM was developed.

The future works recommended concern both the experimental part and the improvement of the modelling achievements. In particular, the following possible research are suggested:

- The same experimental study of the dry granulation process, by analysing different types of mills and different excipients.
- The implementation of the PBM developed to the batches of ribbons made by the powder stored at different environmental humidity levels and with different thicknesses.
- The study of a time-dependent PBM where some of the parameters are described by time-dependent equations and comparison with the PBM developed in this project, by observing the effectiveness and the capability to predict the PSD during the milling process.
- The combination of the PBM developed with the DEM approach, which is used as a methodology to model the milling in particle technology.

List of Figures

Fig. 1.1 Ranking of industrial sectors distinguished by the overall R&D contribute as percentage of the net sales in 2016. [4]

Fig. 1.2 Illustration of a direct compression process. [10]

Fig. 1.3 Steps of wetting of powder mixture with the liquid binder. [3-W]

Fig. 1.4 Schemes of the tablets manufacturing processes by wet granulation and dry granulation. [4-W]

Fig. 1.5 Dry Granulation process using roller compaction. [5-W]

Fig. 1.6 Different regions of the roll compactor. [18]

Fig. 1.7 Illustration of the principles of the three main DEM models regarding the breakage of particles. [54]

Fig. 2.1 Normalized frequency and cumulative distribution of the PSD of MCC 102.

Fig. 2.2 Shape analysis of the PSD of MCC 102.

Fig. 2.3 Instron 1175 with highlighted details of the compression platform, of the die compactor (Specac™) and the ribbon produced.

Fig. 2.4 ERWEKA® conical mill and marks of the most important components of its structure. [66]

Fig. 2.5 These figures highlight the vertical section of the milling chamber and the structure of the impeller (a) and the Glatt® sieve inserted in the milling chamber (b) with the detail of its holes dimensions (c).

Fig. 2.6 QicPic SYMPATEC™ machine and detail of the feed hopper. [67]

Fig. 2.7 Scheme of the camera and the images capture of the QicPic. [67]

Fig. 2.8 Humidity chamber CLIMACEL™ used to perform the experimental study of the humidity effect in the powder behaviour. [9-W]

Fig. 2.9 OHAUS® MB 35 Moisture analyser used to determine the moisture content of the powder. [68]

Fig. 2.10 Scheme of the procedure of study followed in this work.

Fig. 2.11 Scheme of the procedure followed and main parameters studied during each step of this work.

Fig. 2.12 Scheme of the procedure for the production of ribbons.

Fig. 2.13 Granules produced after the milling of a test batch of ribbons with an average porosity equal to 36.2%.

Fig. 3.1 Porosity value with the standard deviation interval of the ribbon batches produced at the set compression force. Each ribbon has been made with 1 g of MCC 102.

Fig. 3.2 Thickness of the ribbon batches as function of the porosity. Each ribbon has been made with 1 g of MCC 102.

Fig. 3.3 Mass of each ribbons used to produce tablets of a set thickness equal to 1.60 mm and different levels of porosity.

Fig. 3.4 Thickness of the ribbons produced by powder with different moisture content at two different compression forces: 30 kN and 60 kN.

Fig. 3.5 Boxplot of the batches of all the ribbons of 1 g of mass produced at the compression force equal to 15 kN.

Fig. 3.6 Boxplot of the batches of all the ribbons of 1 g of mass produced at the compression force equal to 30 kN and the group of ribbons with 1.60 mm of thickness.

Fig. 3.7 Boxplot of the batches of all the ribbons of 1 g of mass produced at the compression force equal to 45 kN and the group of ribbons with 1.60 mm of thickness.

Fig. 3.8 Boxplot of the batches of all the ribbons of 1 g of mass produced at the compression force equal to 60 kN and the group of ribbons with 1.60 mm of thickness.

Fig. 3.9 Milled mass of ribbons during the time of milling for batches of ribbons produced by 1 g of mass at 45 kN of compression force.

Fig. 3.10 Milling times t_{40} (a) and t_{80} (b) as function of the porosity and impeller speed for the batches of ribbons made by 1 g of MCC 102.

Fig. 3.11 Milling times t_{40} (a) and t_{80} (b) as function of the porosity and thicknesses for the batches of ribbons produced at fixed mass (1 g) or thickness (1.6 mm and 2.0 mm).

Fig. 3.12 Milling times t40 (a) and t80 (b) as function of the moisture content and the compression forces set for the batches of ribbons produced at fixed mass (1 g) and different environmental humidity levels.

Fig. 3.13 Normalized frequency and cumulative distribution of the PSD of the group of ribbon made by 1 g of powder compressed at 30 kN and milled at 200 rpm.

Fig. 3.14 Normalized frequency of the PSD of the two samples collected at different times for the group of ribbon made by 1 g of powder compressed at 30 kN and milled at 200 rpm.

Fig. 3.15 PSD of the batches of ribbons made by 1 g of powder, with different levels of porosity and milled at 200 rpm.

Fig. 3.16 PSD of the two batches of ribbons made by 1 g of powder, with different levels of porosity and milled at 100 rpm (a) and 350 rpm (b), respectively.

Fig. 3.17 PSD of the batches of ribbons made by 1 g of powder, with about 36% of porosity and milled at 100, 200 and 350 rpm.

Fig. 3.18 PSD of the two batches of ribbons made by 1 g of powder, milled at different impeller speeds. Each chart represents groups of ribbons at different porosity: 48.5% (a), 28% (b) and 25.5% (c).

Fig. 3.19 PSD of the batches of ribbons with different thicknesses, made at 30 kN, with about 36% of porosity and milled at 200 rpm.

Fig. 3.20 PSD of the batches of ribbons made at different thicknesses milled. Each chart represents groups of ribbons compressed at different forces: 22.5 kN (a), 45 kN (b), 60 kN (c) and 90 kN (d).

Fig. 3.21 PSD of the batches of ribbons made by powder stored at three different environmental humidity levels: 20%, 50% and 80%. The compression force set is 30 kN.

Fig. 3.22 PSD of the groups of ribbons made from powder at different moisture content (reported in legends) with roughly 40% (a) and 28% (b) of porosity.

Fig. 3.23 PSD of the batches of ribbons made by powder stored at 3 different environmental humidity levels: 20%, 50% and 80%. The compression force set is 60 kN.

Fig. 3.24 Mass fraction of fines (in %) as function of the impeller speed and the porosity of the groups of ribbon made by 1 g of MCC 102.

Fig. 3.25 Mass fraction of fines (in %) as function of the thickness and the porosity of the groups of ribbon made by 1 g of MCC 102 or at 1.60 mm and 2.00 mm of thickness.

Fig. 3.26 Mass fraction of fines (in %) as function of the moisture content and the porosity of the groups of ribbon made by 1 g of MCC 102 and powder stored at different environmental humidity.

Fig. 3.27 Aspect ratio of the groups of ribbons milled at 200 rpm and made by 1 g of MCC 102.

Fig. 3.28 Circularity of the groups of ribbons milled at 200 rpm and made by 1 g of MCC 102.

Fig. 3.29 Aspect ratio (a) and circularity (b) of the groups of ribbons milled at 100, 200 and 350 rpm and with a 36% of porosity.

Fig. 4.1 Experimental and modelled normalized frequency and cumulative distribution of the reference batch of ribbons (at 36.3% of porosity and milled at 200 rpm).

Fig. 4.2 First step of search of the eight parameters of the model. Each chart reports the value of one of the eight parameters as function of the ribbon porosity and the impeller speed.

Fig. 4.3 Experimental and modelled PSD of the first sample, collected at 10 s of the batch of ribbons with 28.1% of porosity and milled at 350 rpm.

Fig. 4.4 Values of the three parameters found to be dependent on the operating conditions, for all the batches of ribbons modelled. Linear regressions of the values parametric on the impeller speeds is highlighted by the dashed lines.

Fig. 4.5 Values of the parameter α and the fitted surface which describes the α as function of the porosity and the impeller speed.

Fig. 4.6 Experimental and modelled normalized frequency and cumulative distribution of the reference batch of ribbons (with 36.4% of porosity and milled at 200 rpm) achieved with the final PBM.

Fig. 4.7 Modelled PSD of the granules milled at 200 rpm with ribbon porosities within the interval 50%-20%. Black points highlight the experimental distributions achieved for the five batches of ribbons milled at 200 rpm.

Fig. 4.8 Modelled PSD of the ribbons with a porosity equal to 36% and milled at different impeller speeds. Black marks highlight the experimental PSD achieved for the three batches of ribbons milled at 100, 200, 350 rpm, respectively.

List of Tables

Tab. 1.1 Problems of dry granulation process.

Tab. 2.1 PSD parameters of the MCC Avicel PH 102.

Tab. 2.2 Summary of all the batches of ribbons produced during the experimental phase. The values reported in the cells represent the mean of the porosity (%) of each batch ± the standard deviation of the group of ribbon.

Tab. 3.1 Moisture contents of the MCC 102 at different humidity levels of the storage environment.

Tab. 3.2 Milled mass in g achieved during the experiments with batches of 1 g of ribbons produced with different levels of porosity and milled at different impeller speeds.

Tab. 3.3 Mass fraction percentage of the fines (<240 μm) for the groups of ribbons made by 1 g of MCC 102.

Tab. 4.1 Eight parameters of the PBM developed.

Tab. 4.2 Intervals of the possible values of model parameters set after the first analysis.

Tab. 4.3 Mass percentage of granules milled at 200 rpm (ribbon porosity equal to 25%) smaller than screen size and trapped into the mill chamber.

Tab. 4.4 Values of the five parameters that are constant with respect to the operating conditions.

Tab. 4.5 Conditions of the validation experiments performed.

Symbols

A	PBM Specific kernel parameter	[-]
A_p	Projected area of the particle	[mm^2]
b	Breakage function	[-]
B_{ij}	PBM cumulative breakage distribution	[-]
b_{ij}	PBM size breakage function from size j to size I	[-]
c_1	PBM breakage kernel parameter	[s^{-1}]
c_2	PBM breakage kernel parameter	[-]
D	Number of experimental data points	[-]
d_{10}	10^{th} percentile of the PSD distribution	[µm]
d_{50}	50^{th} percentile of the PSD distribution	[µm]
d_{90}	90^{th} percentile of the PSD distribution	[µm]
d_s	Size aperture of the screen holes	[µm]
E_e	Effective specific energy	[J/g]
$f(x,t)$	PBM Density function	[-]
F_{max}	Maximum Feret diameter	[µm]
F_{min}	Minimum Feret diameter	[µm]
F_{obj}^{min}	Minimum of the objective function	[-]
$f_N(x)$	Normalized frequency	[%/µm]
F_{obj}	Objective function for the minimization of the error	[-]
H	Classification function	[-]
$h(x,t)$	PBM reaction term	[s^{-1}]
K	Number of model parameters	[-]
k_i	PBM size-discrete specific breakage kernel	[s^{-1}]
l	Dimension of the particle	[µm]

l_c	Critical size	[µm]
m	Mass milled	[g]
m_1	PBM breakage function parameter	[-]
m_2	PBM breakage function parameter	[-]
M_i	PBM mass fraction	[-]
M_j^{Exp}	Experimental frequency	[%]
M_j^{Mod}	Modelled frequency	[%]
N	Number of the experimental point in sizes interval	[-]
n	PBM Specific kernel parameter	[-]
$n(v,t)$	PBM Numerical density function	[-]
P	Performance of milling	[g^2/Js]
p_1	PBM breakage function parameter	[µm]
p_2	PBM breakage function parameter	[µm]
P_p	Perimeter of the projection of the particles	[mm]
Q_{ji}^{Exp}	Experimental cumulative mass undersize distribution	[g]
Q_{ji}^{Cal}	Calculated cumulative mass undersize distribution	[g]
S	Selection kernel	[s^{-1}]
t	Time	[s]
t_{40}	Time required to mill the 40% of the total weight of granules produced	[s]
t_{80}	Time required to mill the 80% of the total weight of granules produced	[s]
v	Impeller speed	[rpm]
x_0	Normalizing particle size	[µm]
x_i	Class size *i* of the particle	[µm]
ΔP_t	Effective power consumption of milling	[W]
Δx_i	Size interval	[µm]
$\dot{X}(x, t)$	PBM continuous growth term	[m/s]

Greek Letters

α	PBM Breakage distribution function parameter	[-]
β	PBM Breakage distribution function parameter	[-]
γ	PBM Breakage distribution function parameter	[-]
ε	Porosity of ribbons	[%]
v	Granule size	[µm]
v_i	Percentage of the class size i	[%]
ρ_b	Bulk density	[g/cm^3]
ρ_t	True density	[g/cm^3]
σ	PBM classification function parameter	[-]
φ_p	Circularity	[-]

Acronyms

API	Active pharmaceutical ingredient	
AR	Aspect ratio	[-]
CFD	Computational fluid dynamic	
DEM	Discrete element method	
EQPC	Equivalent projection area of a circle	[mm^2]
ER	Sum of the square residuals of the error	[-]
FEM	Finite element method	
MCC	Microcrystalline Cellulose	
PBM	Population balance model	
PSD	Particle size distribution	
SER	Standard error of the residuals	[-]
VMD	Volume mean diameter	[µm]

Acknowledgments

I would like to thank and mention all the people that help and support me during the development of this work. Their assistance and advices have been fundamental for the realization of this Thesis. I would like to thank Prof. Lian X. Liu for the cordial hospitality at the University of Surrey, for the supervision of the project and her priceless advices throughout all the six months of the work. I thank also Ph.D. Busayo for the help and the training in the laboratories during the first weeks at the university. Moreover, I would like to mention and thank all the people I met during my stay in England: Matilde, Susana, Cecilia, Silvia, Pietro, Solomon, Anastasia, Panos, Ingram and many others. The lovely time spent together will remain an indelible memory. Besides, the daily work has been delighted by the discussions and talks with the fellows of the office 04BB04, which I heartily thank.

Inoltre, desidero ringraziare il Prof. Andrea Claudio Santomaso per l'opportunità di sviluppare questo progetto di tesi e l'assistenza ed i preziosi consigli durante la stesura di questo elaborato.

Alla conclusione di questo lungo ed arduo percorso, desidero ringraziare tutti coloro che mi hanno sostenuto e che non hanno mai fatto mancare il loro costante appoggio durante questi cinque anni. Con poche parole spero di riuscire ad esprimere tutta la stima che meritano e l'ammirazione che nutro per ognuno di loro. Ringrazio, quindi, i compagni di università, con cui ho condiviso le fatiche e gli impegni di questi ultimi anni. La vostra piacevole compagnia ha senza dubbio alleviato le difficoltà affrontate. Un ringraziamento particolare va ad Enrico, Cesare e Riccardo per aver condiviso il tempo e gli sforzi quotidiani nei tanti progetti e lavori di questi ultimi due anni. Per l'immancabile pazienza, sostegno ed appoggio, ringrazio Marco e Lorenzo, encomiabili compagni di molte avventure nei sei lunghi mesi passati in Inghilterra e oltre. Desidero poi, ringraziare gli amici di una vita con i quali ho condiviso infiniti momenti, gioie e traguardi, nei molti anni passati.

Un ringraziamento speciale va alla mia famiglia, a Lorella, Alessandro e Francesco per avermi incoraggiato, consigliato ed accompagnato in tutti questi anni. Il vostro sostegno mi ha permesso di diventare la persona che sono oggi.

Infine, ringrazio di cuore Marianna per l'amorevole supporto in questi anni. La tua pazienza ed il tuo appoggio sono stati fonte di ispirazione per affrontare le sfide e le difficoltà di ogni giorno. Grazie per essermi sempre vicina.

Appendix

In this appendix some useful data and achievements are reported in order to complete the experimental results already presented in the chapter 3. The information regarding the characterization of the ribbons and the mass fraction of fines for the remaining tests are reported in the following tables. Then, the normalized frequency of all the experiments performed is presented in different tables. The last part concerns the Matlab script used to implement the PBM and to search the parameters of the model.

Appendix 1. Ribbon Characterization and Fines

Ribbon Characterization

Thickness (mm)

Specification: 1 g of mass per ribbon						
Compression force (kN)		*15*	*22.5*	*30*	*45*	*60*
Impeller speed (rpm)	*100*	1.59 ± 0.01	-	1.28 ± 0.02	1.13 ± 0.02	1.10 ± 0.02
	200	1.59 ± 0.02	1.36 ± 0.02	1.29 ± 0.02	1.14 ± 0.01	1.10 ± 0.02
	350	1.57 ± 0.02	-	1.27 ± 0.02	1.14 ± 0.02	1.10 ± 0.02
Specification: 1.60 mm of thickness per ribbon						
Compression force (kN)		*22.5*	*30*	*45*	*60*	*90*
Impeller speed (rpm)	*200*	1.59 ± 0.02	1.58 ± 0.01	1.59 ± 0.01	1.59 ± 0.01	1.59 ± 0.01
Specification: 2.00 mm of thickness per ribbon						
Compression force (kN)			*30*		*60*	
Impeller speed (rpm)	*200*		2.00 ± 0.02		1.99 ± 0.01	

Specification: 1 g of mass per ribbon from MCC at 20 % of Humidity		
Compression force (kN)	*30*	*60*
200	1.34 ± 0.03	1.12 ± 0.02

Specification: 1 g of mass per ribbon from MCC at 50 % of Humidity		
Compression force (kN)	*30*	*60*
200	1.27 ± 0.01	1.08 ± 0.01

Specification: 1 g of mass per ribbon from MCC at 80 % of Humidity		
Compression force (kN)	*30*	*60*
200	1.13 ± 0.01	1.05 ± 0.01

Specification: Validation of the model, 1 g of mass per ribbon				
Compression force (kN)		*19*	*37.5*	*90*
Impeller speed (rpm)	*150*	-	1.18 ± 0.03	-
	200	-	-	1.04 ± 0.01
	300	1.40 ± 0.01	-	-

Diameter (mm)

Specification: 1 g of mass per ribbon						
Compression force (kN)		*15*	*22.5*	*30*	*45*	*60*
Impeller speed (rpm)	*100*	31.52 ± 0.02	-	31.45 ± 0.01	31.42 ± 0.01	31.40 ± 0.02
	200	31.50 ± 0.01	31.47 ± 0.01	31.46 ± 0.01	31.43 ± 0.01	31.40 ± 0.01
	350	31.50 ± 0.01	-	31.45 ± 0.01	31.43 ± 0.01	31.40 ± 0.01

Specification: 1.60 mm of thickness per ribbon						
Compression force (kN)		*22.5*	*30*	*45*	*60*	*90*
Impeller speed (rpm)	*200*	31.46 ± 0.02	31.45 ± 0.01	31.42 ± 0.01	31.40 ± 0.01	31.39 ± 0.01

Specification: 2.00 mm of thickness per ribbon			
Compression force (kN)		*30*	*60*
Impeller speed (rpm)	*200*	31.43 ± 0.01	31.42 ± 0.01

Specification: 1 g of mass per ribbon from MCC at 20 % of Humidity			
Compression force (kN)		*30*	*60*
	200	31.50 ± 0.01	31.41 ± 0.02

Specification: 1 g of mass per ribbon from MCC at 50 % of Humidity			
Compression force (kN)		*30*	*60*
	200	31.43 ± 0.03	31.40 ± 0.01

Specification: 1 g of mass per ribbon from MCC at 80 % of Humidity			
Compression force (kN)		*30*	*60*
	200	31.40 ± 0.01	31.36 ± 0.01

Specification: Validation of the model, 1 g of mass per ribbon				
Compression force (kN)		*19*	*37.5*	*90*
Impeller speed (rpm)	*150*	-	31.44 ± 0.01	-
	200	-	-	31.39 ± 0.01
	300	31.45 ± 0.01	-	-

Mass (g)

Specification: 1 g of mass per ribbon						
Compression force (kN)		*15*	*22.5*	*30*	*45*	*60*
Impeller speed (rpm)	*100*	0.98 ± 0.01	-	1.00 ± 0.01	1.00 ± 0.01	1.00 ± 0.01
	200	1.00 ± 0.01	0.99 ± 0.01	1.00 ± 0.01	1.00 ± 0.01	0.99 ± 0.01
	350	0.99 ± 0.01	-	1.00 ± 0.01	1.00 ± 0.01	0.99 ± 0.01
Specification: 1.60 mm of thickness per ribbon						
Compression force (kN)		*22.5*	*30*	*45*	*60*	*90*
Impeller speed (rpm)	*200*	1.16 ± 0.01	1.25 ± 0.01	1.40 ± 0.01	1.47 ± 0.01	1.59 ± 0.01
Specification: 2.00 mm of thickness per ribbon						
Compression force (kN)			*30*		*60*	
Impeller speed (rpm)	*200*		1.62 ± 0.01		1.91 ± 0.01	
Specification: 1 g of mass per ribbon from MCC at 20 % of Humidity						
Compression force (kN)			*30*		*60*	
200			0.98 ± 0.02		0.98 ± 0.02	
Specification: 1 g of mass per ribbon from MCC at 50 % of Humidity						
Compression force (kN)			*30*		*60*	
200			1.00 ± 0.02		1.00 ± 0.02	
Specification: 1 g of mass per ribbon from MCC at 80 % of Humidity						
Compression force (kN)			*30*		*60*	
200			0.99 ± 0.01		0.99 ± 0.01	

Specification: Validation of the model, 1 g of mass per ribbon				
Compression force (kN)		*19*	*37.5*	*90*
Impeller speed (rpm)	*150*	-	0.99 ± 0.01	-
	200	-	-	0.99 ± 0.01
	300	0.98 ± 0.01	-	-

Mass fractions of fines (%)

Specification: 1.60 mm of thickness per ribbon						
Compression force (kN)		*22.5*	*30*	*45*	*60*	*90*
Impeller speed (rpm)	*200*	12.27	11.16	10.43	8.20	5.71
Specification: 2.00 mm of thickness per ribbon						
Compression force (kN)			*30*		*60*	
Impeller speed (rpm)	*200*		10.37		6.90	
Specification: 1 g of mass per ribbon from MCC at 20 % of Humidity						
Compression force (kN)			*30*		*60*	
	200		13.90		9.23	
Specification: 1 g of mass per ribbon from MCC at 50 % of Humidity						
Compression force (kN)			*30*		*60*	
	200		8.11		7.31	
Specification: 1 g of mass per ribbon from MCC at 80 % of Humidity						
Compression force (kN)			*30*		*60*	
	200		7.95		6.11	
Specification: Validation of the model, 1 g of mass per ribbon						
Compression force (kN)			*19*	*37.5*		*90*
Impeller speed (rpm)	*150*		-	10.45		-
	200		-	-		2.78
	300		12.45	-		-

Appendix 2. PSD of the Experiments

1 g of MCC 102

	PSD (g), impeller speed = 100 rpm			
Size (μm)	**15 kN**	**30 kN**	**45 kN**	**60 kN**
6.21	0.000	0.000	0.000	0.000
6.23	0.000	0.000	0.000	0.000
7.15	0.000	0.000	0.000	0.000
9.22	2.337	0.000	0.000	0.000
11.89	2.412	1.303	1.774	0.972
15.33	3.991	1.710	1.821	1.861
19.76	5.798	2.356	1.646	2.447
25.48	9.424	3.576	4.043	3.485
32.85	15.401	6.704	6.086	6.069
42.36	26.942	12.325	10.375	10.670
54.61	42.121	18.319	16.332	15.446
70.41	59.264	24.292	21.842	20.029
90.79	79.711	32.737	29.187	25.284
117.06	99.205	39.721	36.600	31.444
150.93	111.867	47.829	41.782	37.809
194.60	105.759	46.970	40.903	38.703
250.92	78.977	38.773	35.240	33.969
323.52	51.987	29.442	28.017	28.923
417.14	34.556	24.459	24.895	26.045
537.85	27.218	24.354	25.685	25.631
693.49	26.222	26.522	27.134	26.754
894.16	28.345	32.043	31.290	30.018
1152.90	38.485	42.130	39.571	39.477
1486.51	48.405	59.377	54.620	57.734
1916.67	43.378	60.744	60.276	63.125
2471.30	8.338	11.856	15.156	14.002
2783.66	0.000	0.000	0.000	0.000

	PSD (g), impeller speed = 200 rpm					
Size (μm)	**15 kN**	**22.5 kN**	**30 kN**	**45 kN**	**60 kN**	**90 kN**
6.21	0.000	0.000	0.000	0.000	0.000	0.000
6.23	0.000	0.000	0.000	0.000	0.000	0.000
7.15	0.000	0.000	0.000	0.000	0.000	0.000
9.22	0.888	0.000	1.387	0.000	0.000	0.000
11.89	5.001	1.961	1.773	2.297	2.699	0.000
15.33	6.674	2.393	2.836	1.203	1.640	1.538
19.76	8.815	3.699	4.210	2.821	3.121	1.639
25.48	13.949	5.842	6.047	3.836	5.413	1.919
32.85	19.706	8.903	9.967	6.713	8.500	3.408
42.36	33.953	14.501	17.701	12.460	15.210	5.562
54.61	50.776	26.332	25.866	19.090	23.023	7.931
70.41	72.486	40.066	35.355	26.569	28.972	9.400
90.79	99.913	54.682	45.389	35.571	34.315	11.722
117.06	126.616	67.841	54.844	47.328	43.145	14.297
150.93	140.550	74.056	60.346	50.719	46.357	15.477
194.60	130.863	64.421	56.285	47.251	44.917	15.392
250.92	94.492	45.921	43.449	36.590	36.011	14.858
323.52	56.992	33.227	30.983	28.084	30.529	14.488
417.14	34.322	24.892	23.027	24.206	27.259	15.527
537.85	24.002	21.650	21.306	23.491	26.026	16.572
693.49	25.035	23.268	23.002	25.359	28.469	19.458
894.16	29.146	30.410	28.426	29.010	32.425	22.836
1152.90	34.385	38.693	38.650	35.248	43.084	32.888
1486.51	49.188	57.704	58.187	52.682	62.118	53.017
1916.67	43.430	58.249	59.496	67.329	58.024	72.661
2471.30	4.570	7.953	14.912	13.960	21.434	28.954
2783.66	0.000	0.000	0.000	0.000	0.000	0.000

	PSD (g), impeller speed = 350 rpm			
Size (µm)	**15 kN**	**30 kN**	**45 kN**	**60 kN**
6.21	0.000	0.000	0.000	0.000
6.23	0.000	0.000	0.000	0.000
7.15	0.000	0.000	0.000	0.000
9.22	3.296	1.075	0.000	0.000
11.89	3.322	1.790	2.699	1.431
15.33	6.018	2.771	1.640	1.841
19.76	9.259	3.413	3.121	1.699
25.48	13.338	5.538	5.413	3.523
32.85	21.301	9.000	8.500	4.938
42.36	38.465	16.043	15.210	9.306
54.61	59.752	24.411	23.023	14.144
70.41	84.902	34.281	28.972	20.069
90.79	115.550	47.940	39.315	28.451
117.06	141.522	62.747	57.145	40.071
150.93	151.222	71.792	64.357	51.117
194.60	133.640	64.971	59.917	51.032
250.92	93.842	50.509	46.011	36.862
323.52	55.680	35.387	34.529	28.618
417.14	33.449	25.432	27.259	23.163
537.85	26.041	22.060	26.026	21.532
693.49	23.978	24.360	28.469	23.345
894.16	24.544	27.944	32.425	26.519
1152.90	34.727	33.253	43.084	33.118
1486.51	48.622	54.677	56.118	52.297
1916.67	40.315	50.848	48.024	53.635
2471.30	3.949	18.400	21.434	26.714
2783.66	0.000	0.000	0.000	0.000

Ribbons at 1.60 mm of thickness

	PSD (g), impeller speed = 200 rpm				
Size (µm)	**22.5 kN**	**30 kN**	**45 kN**	**60 kN**	**90 kN**
6.21	0.000	0.000	0.000	0.000	0.000
6.23	0.000	0.000	0.000	0.000	0.000
7.15	0.000	0.000	0.000	0.000	0.000
9.22	2.765	0.000	0.000	0.000	0.000
11.89	2.684	3.322	2.763	2.471	1.420
15.33	4.249	1.563	1.446	1.085	1.164
19.76	5.988	4.489	4.060	3.160	2.855
25.48	10.308	6.357	5.871	3.669	4.120
32.85	16.681	10.504	8.736	7.107	6.047
42.36	28.798	18.208	15.623	12.037	10.706
54.61	43.503	27.989	23.767	16.710	15.003
70.41	58.422	38.447	32.092	22.772	18.875
90.79	73.422	50.752	45.862	31.565	23.629
117.06	82.302	62.254	70.832	42.294	28.581
150.93	72.606	68.833	65.233	50.256	30.264
194.60	52.106	63.236	57.071	50.179	29.214
250.92	38.295	48.726	46.711	43.299	27.654
323.52	29.033	34.577	38.518	36.001	26.888
417.14	24.872	28.223	34.554	33.029	27.561
537.85	23.091	25.182	33.508	32.677	30.779
693.49	25.588	24.597	34.005	35.359	32.008
894.16	29.495	29.014	39.348	38.624	34.696
1152.90	38.861	36.651	53.929	44.047	42.709
1486.51	55.051	52.943	65.183	58.829	55.129
1916.67	53.563	62.716	38.777	47.772	58.464
2471.30	14.061	6.750	3.277	8.827	14.626
2783.66	0.000	0.000	0.000	0.000	0.000

Ribbons at 2.00 mm of thickness

	PSD (g), impeller speed = 200 rpm	
Size (µm)	**30 kN**	**60 kN**
6.21	0.000	0.000
6.23	0.000	0.000
7.15	0.000	0.000
9.22	1.147	0.000
11.89	2.291	2.502
15.33	2.360	1.485
19.76	4.795	3.305
25.48	7.719	4.525
32.85	12.787	8.210
42.36	22.220	13.842
54.61	36.364	20.744
70.41	47.908	26.834
90.79	61.794	33.921
117.06	70.017	38.792
150.93	62.511	39.361
194.60	48.970	36.855
250.92	35.812	31.841
323.52	29.646	28.230
417.14	25.777	28.890
537.85	25.170	29.728
693.49	27.170	33.498
894.16	30.307	38.151
1152.90	39.753	39.526
1486.51	59.745	55.181
1916.67	57.668	57.738
2471.30	10.766	12.204
2783.66	0.000	0.000

Moisture experiments

	PSD (g), impeller speed = 200 rpm					
	20 % HU		50 % HU		80 % HU	
Size (µm)	30 kN	60 kN	30 kN	60 kN	30 kN	60 kN
6.21	0.000	0.000	0.000	0.000	0.000	0.000
6.23	0.000	0.000	0.000	0.000	0.000	0.000
7.15	0.000	0.000	0.000	0.000	0.000	0.000
9.22	2.893	0.000	0.000	0.000	0.000	0.000
11.89	0.814	3.046	2.337	0.567	1.910	1.589
15.33	4.326	1.503	0.684	2.143	1.617	1.630
19.76	4.884	4.188	3.068	1.682	2.892	2.100
25.48	8.654	5.641	3.829	4.118	4.359	4.139
32.85	14.502	9.784	6.921	6.015	8.468	6.170
42.36	25.489	16.487	12.229	10.534	13.776	10.769
54.61	39.892	24.605	20.306	16.863	21.019	16.343
70.41	55.949	33.981	28.829	23.611	28.189	21.939
90.79	72.716	44.427	39.326	32.657	36.127	29.003
117.06	84.950	53.020	48.890	40.078	43.713	35.456
150.93	82.589	54.691	48.883	43.836	46.951	39.301
194.60	71.071	49.610	43.840	41.503	44.309	38.228
250.92	54.056	41.103	34.632	36.768	37.817	32.008
323.52	39.530	34.832	26.080	32.091	32.285	26.709
417.14	30.812	31.454	22.925	28.965	28.043	25.327
537.85	27.586	31.643	22.392	28.307	27.890	25.785
693.49	30.199	32.495	22.919	30.302	29.260	26.619
894.16	35.245	35.175	30.036	33.376	34.883	27.958
1152.90	45.390	39.690	39.936	40.468	40.208	36.814
1486.51	56.062	54.045	50.542	53.894	60.864	56.393
1916.67	41.894	55.281	72.838	49.753	54.875	55.782
2471.30	8.976	9.242	9.724	19.921	10.983	22.006
2783.66	0.000	0.000	0.000	0.000	0.000	0.000

Appendix 3. Matlab Code of the PBM Model

The following script and functions were used to implement the PBM in Matlab and to look for the eight parameters of the model. Both the `fminsearch` and `fmincon` commands are reported in the code, although one at a time was used for the search.

Script

```
%%                          Script PBM MCC 102
%%                       Conical Mill - Round Ribbon
%                        --------------------------
%
%                              30 kN, 100 rpm
%                            Porosity = 35.4%
%                             Total granules
%
%                        --------------------------
%                         Fitting of PBM parameters
%
%
%% Initial parameters guess
% Use of bimodal distribution
% Total ---> 8 parameters

m1 = 2;
m2 = 3;
p1 = 300;
p2 = 2000;
c1 = 1;
c2 = 3;
alpha = 0.1;
sigma = 0.3;

par0 = [m1;m2;p1;p2;c1;c2;alpha;sigma];

%% Optimization
% Search of the best values of parameters

% Boundaries of the constraints of each parameter
llim = [0;0;0;0;0;0;0;0];          % m1;m2;p1;p2;c1;c2;alpha;sigma
ulim = [10;10;500;3000;10;10;1;1]; % m1;m2;p1;p2;c1;c2;alpha;sigma

% Parameter vector
par0 = [m1 m2 p1 p2 c1 c2 alpha sigma];

options = optimset('TolCon',1e-1000,'TolX',1e-1000,'MaxFunEvals',18000);

% Searching of the parameters through constraints
A = [];   % factor needed for the implementation of fmincon
Bf = [];  % "
Aeq = []; % "
Beq = []; % "
[par,fval] = fmincon(@ErrorPBM,par0,A,Bf,Aeq,Beq,llim,ulim,[],options);
```

```
% Searching of the parameters without constraints
% [par,fval] = fminsearch(@ErrorPBM,par0,options);

% Function call for the minimization of the error
[F0,Xflip,Mplotexp,mplot]  = ErrorPBM(par);

%% Draw of the chart

semilogx(Xflip,Mplotexp,'or')
hold on
semilogx(Xflip,mplot)

xlabel('Particle size x_i [\mum]');
ylabel('Mass distribution M_i/\Deltax_i [g/\mum]_i');
xticks([0 50 100 200 500 1000 2000 2800])
xticklabels({'0','50',' ','200',' ','1000','2000',' '})
ylim([0 max(mplot)*1.2])
xlim([0 3000])
legend('\epsilon = 36.4 % (exp.)','\epsilon = 36.4 % (model)')
grid on
hold off
```

Function for the minimization of the error

```
%% Function for the minimization of the error
% ErrorPBM

function [Err,Xflip,Mplotexp,mplot] = ErrorPBM(par0)

% Vectors of the sizes
X= [4750;3359;2783;2471;1916.67;1486.51;1152.9;894.16;693.49;...
     537.85;417.14;323.52;250.92;194.6;149.6;117.06;90.785;70.41;...
     54.61;42.36;32.85;25.48;19.76;15.33;11.89;9.22;7.15;6.23;6.21];

Xsize = [7867;5564;3935;2783;2158.93;1674.4;1298.62;1007.17;781.14;...
    605.83;469.86;364.41;282.63;219.2;170;131.85;102.26;79.31;61.51;...
    47.71;37;28.7;22.26;17.26;13.39;10.38;8.05;6.25;6.21];

% Size intervals
IntX = zeros(29,1);
for n = 1:28
    IntX(n) = Xsize(n)-Xsize(n+1);
    IntX(29) = 5;
end

% Total mass of the milled granules collected during the experiment
M0 = 14.64; % g
M0(2:29) = 0;

% PSD from the experiments
Mexp = [0,0,0,0,0.000573994,0.000968739,0.001724378,0.003371237,...
    0.008146265,0.019325211,0.037009932,0.063302352,0.103272654,...
    0.163405772,0.25037443,0.316711991,0.3414826,0.340526759,...
    0.377587886,0.484788564,0.680700791,1.06033764,1.797595934,...
    3.26655599,4.237918133,1.084318748,0,0,0]';
```

```
% Calculation of the breakage function bij
B1=par0(7)*(1-exp((log(0.2))*((Xsize/par0(3)).^par0(1))))+...
    ((1-par0(7))*(1-exp((log(0.2)*((Xsize/par0(4)).^par0(2))))));

B2=[B1(2:29);0];

B=B1-B2;

% Adapting the matrix bij to the two conditions: bii=0 & SUM_i (Bij)=1
for i = 2:28
    B(:,i) = B(:,i-1);
end

Bmat = tril(B);

for l=1:28
    Bmat(l,l) = 0;
end

Bdiv = B1(2:29).';

for j = 2:29
    Bdiv(j,:) = Bdiv(j-1,:);
end

% Building of matrix bij
bij = Bmat./Bdiv;

% Calculation of the breakage kernel ki
Xmax = max(Xsize);

ki = par0(5)*((X./Xmax).^par0(6));

% Calculation of the classification function cl
cl = zeros(29,1);

dholes = 2783; % diameter of the screen holes [µm]
limit = (1-par0(8))*dholes;

for ii= 1:29
    if X(ii) <= limit
        cl(ii,1) = 0; % particles pass through the screen
    elseif X(ii) > dholes
        cl(ii,1) = 1; % particles do not pass through the screen
    else
        cl(ii,1) = (dholes-X(ii))/(dholes*par0(8));
    end
end

%% Solution of the differential equation of the PBM
time = [0,70];
[t,m] = ode45(@EquationPBM,time,M0,[],ki,bij,cl);

Mg = fliplr(m);
Dm = Mg(end,1:29);
```

```
% Error to be minimized during the search of the parameters
Err = (norm(((Mexp./flip(IntX))-(Dm'./flip(IntX)))))/sqrt(29-8); % 2-Norm

disp(Err);

%% Normalized frequency calculation
Xflip = flipud(X);    % reversal of size for calculation

Mplotexp=Mexp./flip(IntX);
PM=[Dm(end,1:29)'];
mplot=PM./flip(IntX); % g/µm

end
```

Function for the solution of the differential equation of the PBM

```
%% Function Equation PBM
% To be used for all the different batches of ribbons

%% Differential Mass Balance

function dMdt = EquationPBM(t,m,Sel,bij,cl)

dMdt(1) = - Sel(1)*m(1)*cl(1);

for n = 2:29
    sum = 0;
    for i = 1:n-1
        sum = bij(n,i)*Sel(i)*m(i)*cl(i) + sum;
    end
    dMdt(n) = sum - (Sel(n)*m(n)*cl(n));
end
dMdt=dMdt';
end
```

References

[1] IFPMA Report. (2017) The pharmaceutical Industry and Global health. 2017. *International Federation of Pharmaceutical Manufacturers & Associations.* **3**: 40-43.

[2] FARMINDUSTRIA Report. (2018). Facts&Figures of the Pharmaceutical industry in Italy. July 2018. *Farmindustria.*

[3] Harbir, K. (2012). Processing Technologies for Pharmaceutical Tablets: A Review. *International Research Journal of Pharmacy.* **3(7)**: 20–23.

[4] Cox Gad, S. (2008). Pharmaceutical Manufacturing Handbook, Production and Processes. *Wiley-Interscience*. Hoboken, New Jersey, USA. **4**: 235-262.

[5] Cox Gad. (2008). Pharmaceutical Manufacturing Handbook, Production and Processes. *Wiley-Interscience*. Hoboken, New Jersey, USA. **6**: 882-1087.

[6] Rana, A., Khokra, S. L., Chandel, A., Prasad, G. N., Ram Kumar, S. (2011). Overview on Roll Compaction / Dry Granulation Process. *Pharmacologyonline.* **3**: 286-298.

[7] Shanmugam, S. (2015). Granulation Techniques and Technologies: Recent Progresses. *BioImpacts.* **5**(1): 55–63.

[8] Yu, X., Yu, X. L., Teng, Y., Gaglani, D. K., Rege, B., D., Rosencrance, S. (2019). Implementation of Pharmaceutical Quality by Design in Wet Granulation. *Handbook of Pharmaceutical Wet Granulation.* Maryland, USA. **21**: 703-731.

[9] Hare, C., Ghadiri, M., Guillard, N. et al. (2016). Analysis of Milling of Dry Compacted Ribbons by Distinct Element Method. *Chemical Engineering Science.* **149**: 204–214.

[10] Leuenberger, H. (1982). The Compressibility and Compactability of Powder Systems. *International Journal of Pharmaceutics*. **12**(1): 41-55.

[11] Ervasti, T., Simonaho, S., Ketolainen, J., Forsberg, P., Fransson et al. (2015). Continuous Manufacturing of Extended via Powder Mixing and Direct Compression. *International Journal of Pharmaceutics.* **495**(1): 290-301.

[12] Gerhardt, A. (2010). Fundamentals of Tablet Compression. *Journal of GXP compliance*. **14**(1): 70-79.

[13] Zhang, Y., Law, Y., Chakrabarti, S. (2003). Physical Properties and Compact Analysis of Commonly Used Direct Compression Binders. *AAPS PharmSciTech*. **4**(4): 1-11.

[14] Jivraj, M., Martini, L. G., Thomson, C. M. (2000). An Overview of the Different Excipients Useful for the Direct Compression of Tablets. *Pharmaceutical Science and Technology Today*. **3**(2): 58-63.

[15] Venkateswara Reddy, B., Navaneetha, K., Sandeep, P., Ujwala, P. Improved Tablet Production by Modified Granulation Techniques – A Review. *International Journal of Research in Pharmacy and Life Sciences.* **2**(2): 224-235.

[16] Mehta, K., Rekhi, G., Parikh, D. (2005). Handbook of Pharmaceutical Granulation Technology. 2nd Edition. *Taylor & Francis*. North Carolina, USA. **2**: 7-79.

[17] Tousey, M. D. (2002). The Granulation Process 101. Basic Technologies for Tablet Making. *Pharmaceutical Technology. Tabletting & Granulation*. South Carolina, USA. 8-13.

[18] Schiano S. (2017). Dry Granulation Using Roll Compaction Process: Powder Characterization and Process Understanding. *Ph.D Thesis.* University of Surrey, UK.

[19] Park, S. Y., Galbraith, S. C., Liu, H., Lee, H., Cha, B., Huang, Z., O'Connor, Lee, S., Yoon, S. (2018). Prediction of Critical Quality Attributes and Optimization of Continuous Dry Granulation Process via Flowsheet Modeling and Experimental Validation. *Powder Technology*. **330**: 461-470.

[20] Kleinebudde, P. (2001). Roll Compaction/Dry Granulation: Pharmaceutical Applications. *European Journal of Pharmaceutics and Biopharmaceutics.* **58(**2): 317-326.

[21] Herting, M. G., Kleinebudde, P. (2008). Studies on the Reduction of Tensile Strenght of Tablets after Roll Compaction/Dry Granulation. *European Journal of Pharmaceutics and Biopharmaceutics.* **70**(1): 372-379.

[22] Perez-Gandarillas, L., Perez-Gago, A., Mazor, A., Kleinebudde P., Lecoq, O., Michrafy, A. (2016). Effect of Roll-Compaction and Milling Conditions on Granules and Tablet Properties. *European Journal of Pharmaceutics and Biopharmaceutics*. **106**: 38-49.

[23] Guigon, P., Simon, O. (2003). Roll Press Design-Influence of Force Feed System on Compaction. *Powder Technology*. **130**(1): 41-48.

[24] Inghelbrecht, S., Remon, J. P. (1998). The Roller Compaction of Different Types of Lactose. *International Journal of Pharmaceutics*. **166**(2): 135-144.

[25] Sun, W. J., Rantanen, J., Sun, C. C. (2018). Ribbon Density and Milling Parameters that Determine Fines Fraction in a Dry Granulation. *Powder Technology*. **338**: 162-167.

[26] Samanta, A. K., Wang, L., Yun Ng, K., Sia Heng, P. W. (2014) Energy-based Analysis of Cone Milling Process for the Comminution of Roller Compacted Flakes. *International Journal of Pharmaceutics*. **462**(1): 108-114.

[27] Naik, S., Chaudhuri, B. (201). Quantifying Dry Milling in Pharmaceutical Processing: A Review on Experimental and Modeling Approaches. *Journal of Pharmaceutical Sciences*. **104**(8): 2401-2413.

[28] Breneman, B. (2011). Effect of Size Reduction Parameters in Pharmaceutical Manufacturing Process. *Global Pharmaceutical Operations. Manufacturing Science & Technology. Abbott Laboratories*. California, USA.

[29] Reynolds, G. K. Modelling of Pharmaceutical Granule Size Reduction in a Conical Screen Mill. *Chemical Engineering Journal*. **164(**2): 383-392.

[30] Loreti, S., Wu, C. Y., Reynolds, G., Mirtic, A., Seville, J. (2009). DEM–PBM Modeling of Impact Dominated Ribbon Milling. *AIChE*. **7**(1): 405-410.

[31] Sun, W. J., Sun, C. C. (2017). Ribbon Thickness Influences Fine Generation during Dry Granulation. *International Journal of Pharmaceutics*. **529**(1): 87-88.

[32] Gamble, J. F., Tobyn, M., Dennis, A. B., Shah, T. (2010). Roller Compaction: Application of an in-gap Ribbon Porosity Calculation for the Optimization of Downstream Granule Flow and Compactability Characteristics. *Pharmaceutical Development and Technology*. **15**(3): 223-229.

[33] Barrasso, D., Oka, S., Muliadi, A., Litster, J. D., Wassgren, C., Ramachandran, R. (2013) Population Balance Model Validation and Prediction of CQAs for Continuous Milling Processes: toward QbD in Pharmaceutical Drug Product Manufacturing. *Journal of Pharmaceutical Innovation*. **8**(3): 147-162.

[34] Omar, C., Al-Asady, R., Salman, A. (2019) Roller Compaction: Improving the Homogeneity of Ribbon Properties along the Roller Width. *Powder Technology*. **342**: 464-474.

[35] Chattoraj, S., Daugherity, P., McDermott, T., Olsofsky, A., Roth, W. J., Tobyn, M. (2018). Sticking and Picking in Pharmaceutical Tablet Compression: An IQ Consortium Review. *Journal of Pharmaceutical Sciences*. **107**(9): 2267-2282.

[36] Kukkar, V., Anand, V., Kataria, M., Gera, M., Choudhury, P. K. (2008). Mixing Formulation of Low Dose Drugs: Underlying Problems and Solutions. *Thai Journal of Pharmaceutical Sciences.* **32**: 43-58.

[37] Perez-Gandarillas, L. (2016). Dry Granulation Process and Compaction Behaviour of Granulated Powders. *Ph.D Thesis.* Chemical and Process Engineering. Ecole des Mines d'Albi-Carmaux. University of Toulouse, France.

[38] Tomar, M., Kumar, S. A., Amir Raj, S. (2017). Effect of Moisture Content of Excipient (Microcrystalline Cellulose) on Direct Compressible Solid Dosage Forms. *International Journal of Pharmaceutical Sciences and Research*. **8**(1): 282-288.

[39] Sahputra, I. H., Alexiadis, A., Adams, M. J. (2019). Effects of Moisture on the Mechanical Properties of Microcrystalline Cellulose and the Mobility of the Water Molecules as Studied by the Hybrid Molecular Mechanics–Molecular Dynamics Simulation Method. *Journal of Polymer Science, Polymer Physics*. **57**(8): 454-464.

[40] Osborne, J. D., Althaus, T., Forny, L., Niederreiter, g., Palzer, S., Hounslow, M. J., Salman, A. D. (2013). Investigating the Influence of Moisture Content and Pressure on the Bonding Mechanism during Roller Compaction of an Amorphous Material. *Chemical Engineering Science*. **86**: 61-69.

[41] Wu, C.-Y., Hung, W.-L., Miguélez-Moran, A. M., Gururajan, B., Seville, J. P. (2010). Roller Compaction of Moist Pharmaceutical Powders. *International Journal of Pharmaceutics*. **391**(1): 90-97.

[42] Nokhodchi, A. (2005). An Overview of the Effect of Moisture on Compaction and Compression. *Pharmaceutical Technology*. **29**(1): 46-66.

[43] Omar, C. S., Dhenge, R. M., Palzer, S., Hounslow, M. J., Salman, A. D. (2016). Roller Compaction: Effect of Relative Humidity of Lactose Powder. *European Journal of Pharmaceutics and Biopharmaceutics*. **106**: 26-37.

[44] Johanson, J. R. (1964). A rolling Theory for Granular Solids. *Journal of Applied Mechanics*. **32**(4): 842-848.

[45] Michrafy, A., Zavaliangos, A., Cunningham, J. C. (2016). Dry Granulation Process Modeling. *Predictive Modeling of Pharmaceutical Unit Operations*. 71-79.

[46] Cunningham, J. C., Winstead, D., Zavaliangos, A. (2010). Understanding Variation in Roller Compaction through Finite Element-based Process Modeling. *Computers and Chemical Engineering*. **34**(7): 1058-1071.

[47] Lecompte, T., Doremus, P., Thomas, G., Perier-Camby, L., Le Thiesse, J.-C., Masteau, J.-C., Debove, L. (2005). *Chemical Engineering Science*. **60**(14): 3933-3940.

[48] Esnault, V., Michrafy, A., Heitzmann, D., Michrafy, M., Oulahna, D. (2015). Processing Fine Powders by Roll Press. *Powder Technology*. **270**: 484-489.

[49] Bilgili, E., Capece, M., Afolabi, A. (2016). Modeling of Milling Processes via DEM, PBM, and Microhydrodynamics. *Predictive Modeling of Pharmaceutical Unit Operations*. 159-203.

[50] Cundall, P. A., Strack, O. D. L. (1979). A Discrete Model for Granular Assemblies. *Geotechnique*. **29**(1): 47-65.

[51] Weerasekara, N. S., Powell, M. S., Cleary, P. W., Tavares, L. M., Evertsson, M., Morrison, R. D., Quist, J., Carvalho, R. M. (2013). The Contribution of DEM to the Science of Comminution. *Powder Technology*. **248**: 3-24.

[52] Kalala, J. T., Bwaly, M. M., Moys, M. H. (2005). Discrete Element Method (DEM) Modelling of Evolving Mill Liner Profile due to Wear. Part I: DEM Validation. *Minerals Engineering*. **18**(15): 1386-1391.

[53] Naik, S., Malla, R., Shaw, M., Chaudhuri, B. (2013). Investigation of Comminution in a Wiley Mill: Experiments and DEM Simulations. *Powder Technology*. **237**: 338-354.

[54] McElroy, L., Bao, J., Jayasundara, C. T., Yang, R. Y., Yu, A. B. (2012). A Soft-sensor Approach to Impact Intensity Prediction in Stirred Mills Guided by DEM Models. *Powder Technology*. **219**: 151-157.

[55] Guo, Y., Curtis, J. S. (2015). Discrete Element Method Simulations for Complex Granular Flows. *Annual Review of Fluid Mechanics*. **47**(1): 21-46.

[56] Ho, Y. (2016). Lecture Notes on Population Balance Modelling. *School of Engineering*. Monash University Malaysia.

[57] Capece, M., Bilgili, E., Davé, R. N. (2009). Formulation of a Physically Motivated Specific Breakage Rate Parameter for Ball Milling via the Discrete Element Method. *AIChE*. **7**(4): 405-410.

[58] Freireich, B., Li, J., Litster, J., Wassgren, C. (2011). Incorporating Particle Flow Information from Discrete Element Simulations in Population Balance Models of Mixer-coaters. *Chemical Engineering Science*. **66**(16): 3592-3604.

[59] Wang, M. H., Yang, R. Y., Yu, A. B. (2012). DEM Investigation of Energy Distribution and Particle Breakage in Tumbling Ball Mills. *Powder Technology*. **223**: 83-91.

[60] Loreti, S. (2017). DEM-PBM Modelling of Pharmaceutical Ribbon Breakage. *Ph.D Thesis.* Chemical and Process Engineering. University of Surrey, UK.

[61] Nopens, I., Torfs, E., Ducoste, J., Vanrolleghem, P. A., Gernaey, K. V. (2015). Population Balance Models: a Useful Complementary Modelling Framework for Future WWTP Modelling. *Water Science & Technology*. **71**(2): 159-167.

[62] Sakthivel, S., Pitchumani, R., Pitchumani, B. (2008). Estimation of Specific Rate of Breakage Parameters to Optimize the Industrial Batch Ball Mill. *Industrial Ceramics*. **28**(1): 11-16.

[63] Metta, N., Ierapetritou, M., Ramachandran, R. (2018). A Multiscale DEM-PBM Approach for a Continuous Comilling Process Using a Mechanistically Developed Breakage Kernel. *Chemical Engineering Science*. **178**: 211-221.

[64] Chaerunisaa, A. Y., Sriwidodo, S., Abdassah, M. (2016). Microcrystalline Cellulose as Pharmaceutical Excipient. *IntechOpen*. 1-13.

[65] Shi, L., Chattoraj, S., Sun, C. C. (2011). Reproducibility of Flow Properties of Microcrystalline Cellulose – Avicel PH102. *Powder Technology*. **212**(1): 253-257.

[66] Krok, A. Mirtic, A., Reynolds, G. K., Schiano, S., Roberts, R., Wu, C.-Y. (2016). An Experimental Investigation of Temperature Rise during Compaction of Pharmaceutical Powders. *International Journal of Pharmaceutics*. **513**(1): 97-108.

[67] ERWEKA GmbH. (2016). All-Purpose Equipment Program Conical Mill Type CM. *Instruction Manual*. https://www.erweka.com/images/downloads/manualsENG/allpurpose ENG/CM_ Manual_ 22947_En_V1.0-web.pdf. Last access: 18/01/20.

[68] Sympatec GmbH. (2017). QicPic Manual. 1-12. https://www.blgkimya.com/assets/upload/services/qicpic-en.pdf. Last access: 19/01/20.

[69] Ohaus Europe GmbH. MB Series Moisture Analysers Manual. 1-4. https://www.dataweigh.com/media/14517/ohaus-mb45-spec-sheet.pdf Last access: 21/01/20.

[70] Litster, J. (2016). Particle Characterization and Particle Property Distributions. *Design and Processing of Particulate Products*. **2**: 9-45.

[71] Yu, P., Xie, W., Liu, L. X., Powell, M. S. (2017). The Development of the Wide-range 4D Appearance Function for Breakage Characterisation in Grinding Mills. *Minerals Engineering*. **110**: 1-11.

[72] Bilgili, E., Scarlett, B. (2005). Population Balance Modeling of Non-linear Effects in Milling Processes. *Powder Technology*. **153**(1): 59-71.

[73] Gotsis, C., Austin, L. G., Luckie, P. T., Shoji, K. (1985). Modeling of a Grinding Circuit with a Swing-hammer Mill and a Twin-cone Classifier. *Powder Technology*. **42**(2): 209-216.

Websites

[1-W] https://www.ibisworld.com/global/market-research-reports/global-pharmaceuticals-medicine-manufacturing-industry/. Last access: 05/12/19.

[2-W] https://pharmlabs.unc.edu/labs/tablets/methods.htm. Last access:08/12/19.

[3-W] https://www.saintytec.com/granulation-process/. Last access: 15/12/19.

[4-W] https://www.epmmagazine.com/opinion/understanding-the-continuous-process/. Last access: 13/01/20.

[5-W] https://ytron-quadro.co.uk/products/chilsonator-roller-compaction/. Last access: 25/01/20.

[6-W] https://medium.com/@anikumar19866/what-is-microcrystalline-cellulose-what-is-it-used-for-8cff484ea5d1. Last access: 27/01/20.

[7-W] https://www.upc.edu/sct/en/equip/33/universal-electromechanical-testing-machine.html. Last access: 25/01/20.

[8-W] https://www.quadro-mpt.com/technology-milling. Last access: 28/01/20.

[9-W] https://www.mmm-medcenter.de/climacell. Last access: 28/01/20.